# A MATHEMATICAL STUDY OF FINITE-AMPLITUDE ROCK-FOLDING

Thesis by

William Massee Chapple

In Partial Fulfillment of the Requirements

For the Degree of

Doctor of Philosophy

California Institute of Technology

Pasadena, California

1964

( Accepted September 10, 1963 )

# ACKNOWLEDGMENTS

I gratefully acknowledge the assistance given to me throughout the course of this study by Professor W. Barclay Kamb of the California Institute of Technology. His aid in the formulation of the problem and the development of the mathematical method was invaluable. I am particularly grateful for the penetrating questions he raised about the meaning of results obtained at all stages of the study.

Professor C. Hewitt Dix gave guidance and assistance during the early portion of the study. Professor C. W. McCormick suggested the method used for the solution of the algebraic equations and pointed out its advantages for machine computation. Numerous discussions of the problem of folding with Dr. James E. Conel are greatly appreciated.

Financial support, both fellowships and research funds, was provided by the National Science Foundation, the Standard Oil Company of California, the Woodrow Wilson Foundation, and the Geological Society of America. I am grateful for this support.

Finally, I would like to thank Janet O. Chapple for valuable aid in the revision and preparation of this manuscript and for welcome encouragement through the entire study.

## ABSTRACT

The problem of the finite-amplitude folding of an isolated, linearly viscous layer under compression and imbedded in a medium of lower viscosity is treated theoretically by using a variational method to derive finite difference equations which are solved on a digital computer. The problem depends on a single physical parameter, the ratio of the fold wavelength, L, to the "dominant wavelength" of the infinitesimal-amplitude treatment, $L_d$. Therefore, the natural range of physical parameters is covered by the computation of three folds, with $L/L_d$ = 0, 1, and 4.6, up to a maximum dip of 90°.

Significant differences in fold shape are found among the three folds; folds with higher $L/L_d$ have sharper crests. Folds with $L/L_d$ = 0 and $L/L_d$ = 1 become fan folds at high amplitude. A description of the shape in terms of a harmonic analysis of inclination as a function of arc length shows this systematic variation with $L/L_d$ and is relatively insensitive to the initial shape of the layer. This method of shape description is proposed as a convenient way of measuring the shape of natural folds.

The infinitesimal-amplitude treatment does not predict fold-shape development satisfactorily beyond a limb-dip of 5°. A proposed extension of the treatment continues the wavelength-selection mechanism of the

infinitesimal treatment up to a limb-dip of 15°; after this stage the wavelength-selection mechanism no longer operates and fold shape is mainly determined by $L/L_d$ and limb-dip.

Strain-rates and finite strains in the medium are calculated for all stages of the $L/L_d = 1$ and $L/L_d = 4.6$ folds. At limb-dips greater than 45° the planes of maximum flattening and maximum flattening rate show the characteristic orientation and fanning of axial-plane cleavage.

# LIST OF FIGURES

# LIST OF TABLES

# CHAPTER I

# INTRODUCTION

## 1. Folding as an example of large geologic strain

Folding of layered rocks is an attractive subject for the study of large geologic deformation because of its importance in structural geology and because it is amenable to a systematic theoretical treatment.

There are three main ways in which detailed information about the mechanism of formation of folds might be used. (1) A knowledge of the way in which the boundary conditions imposed on a folding region determine the nature of the folds produced can aid in the deduction of the external forces that have produced the folds. This use of folds to give information about a larger structural element is employed not only for minor folds on the outcrop scale, but also for major folds where it may help in the understanding of the structural history of a whole mountain range. (2) Information about the folding process may be turned in the other direction: knowledge of the strain history of a small element of the fold provides a framework in which to study the mechanisms of deformation and to interpret petrofabric and finite-strain information. (3) Because of their prevalence, folds are ideally suited to test the applicability of theories of deformation.

Folded rocks in nature show a number of regular features. It is common to find a bed or a group of beds deformed into a train of folds with a relatively constant wavelength and fold shape (1). A fairly elaborate geologic terminology has been developed to describe the shapes of folds (2). The usefulness of this terminology rests on the fact that fold shapes do show certain regularities. Folds in a whole region will sometimes have relatively constant shape characteristics. In other regions there may be two generations of folding with systematic differences between the shapes of the folds of the two ages. Finally, many folds are relatively constant in shape along the direction of the fold axis (3); this property suggests that many of the features of the folding mechanism are appropriate to a two-dimensional analysis.

The present study considers folds in which the relative competencies of the beds have played an important role. Folds do exist where the "beds" are mere colored markers which, though they exhibit the deformation, have had little or no influence on it. This type of folding does not often show the regularities discussed above.

---

(1) H. Ramberg, Strain distribution and geometry of folds: Bull. Geol. Inst. Uppsala, v. XLII, 1963, p. 1-20

(2) E. S. Hills, Outlines of structural geology: London, Methuen and Co., Ltd., 3d ed. rev., 1953, p. 77-89

(3) Ibid., p. 97

2. Theoretical studies

Previous studies which attempt to analyze the geometric properties of geologic structures in terms of the forces that produce them have used either a static or a steady-state approach. In the static approach the stress fields before the onset of deformation are used to predict the geometrical nature of the resulting deformation. In general, when the predicted deformation begins, it modifies the stress fields, so that the course of the deformation cannot be followed beyond the initial stage. In a steady-state situation, the stress field remains constant throughout the deformation, so that, when it is applicable, the steady-state approach is more satisfactory than the static approach.

The static approach has been used to study both faulting and folding. Fault patterns due to either a uniform stress field (4, 5), or the stress field set up in a rectangular region by specified boundary conditions (6, 7), have been analyzed on the basis of linear elasticity and the

---

(4) M. K. Hubbert, Mechanical basis for certain familiar geologic structures: Geol. Soc. America Bull., v. 62, 1951, p. 355-372

(5) E. M. Anderson, The dynamics of faulting and dyke formation with applications to Britain: Edinburgh, Oliver and Boyd, Ltd., 2d ed. rev., 1951

(6) W. Hafner, Stress distributions and faulting: Geol. Soc. America Bull., v. 62, 1951, p. 373-398

(7) A. R. Sanford, Analytical and experimental study of simple geologic structures: Geol. Soc. America Bull., v. 70, 1959, p. 19-52

Mohr fracture criterion. Formation of a fault will alter the stress distribution in the region, so that these studies are limited to the consideration of incipient faulting. Anderson (8) attempts to extend the analysis by considering the stresses in a medium containing a crack, but his approach is essentially a static one, since the predicted subsidiary faults will alter the stress field in an unknown manner. Plasticity theory is not limited to the static approach, but published studies (9, 10) have not considered the changes in the geometry of the region which the predicted deformation would produce. Predicted patterns of dike intrusion (11, 12) are a more valid subject for the static approach, since the intrusion of a dike may not alter the orientation of the prevailing stress system as drastically as the formation of a fault.

Studies of faulting may assume a single homogeneous medium, but consideration of two media of different material properties is essential to a study of the folding process.

---

(8) Anderson, op. cit., p. 160-173

(9) D. J. Varnes, Analysis of plastic deformation according to von Mises' theory, with application to the South Silverton area, San Juan County, Colorado: U. S. Geol. Survey Professional Paper 378-B, 1962

(10) H. Odé, Faulting as a velocity discontinuity in plastic deformation: chap. 11 in Rock deformation (A symposium), Geol. Soc. America Mem. 79, 1960, p. 293-321

(11) H. Odé, Mechanical analysis of the dike pattern of the Spanish Peaks area, Colorado: Geol. Soc. America Bull., v. 68, 1957, p. 567-576

(12) Anderson, op. cit.

The static approach has been applied to both infinitesimal and finite-amplitude folding. If the maximum dip of the folding layer is very small, certain mathematical simplifications can be made in the theoretical treatment. The analysis of folds of infinitesimal amplitude is not strictly a static analysis, since the treatment remains approximately valid for a limited range of fold amplitude. However, the limits of this range of validity are not determined precisely by the infinitesimal analysis itself. Previous studies of infinitesimal amplitude folding and their relation to the present study are discussed in Chapter II.

The static approach has also been applied to folds of finite amplitude (13, 14). The validity of these studies is severely restricted by the need to assume the shape of the finite amplitude fold in advance.

Finally, in certain important geologic situations, the stress field does not change with time. Flow of a glacier in a fixed channel has been studied with the steady-state approach (15). Certain aspects of salt dome formation are

---

(13) J. Goguel, Introduction à l'étude mécanique des déformations de l'écorce terrestre: Service Carte Géol. France Mém., 1948, 530 p.

(14) S. Kienow, Grundzüge einer Theorie der Faltungs- und Schieferungsvorgänge: Berlin, Borntträger, Fortschritte der Geologie und Paleontologie, bd. XIV, h. 46, 1942, 129 p.

(15) J. F. Nye, The flow of glaciers and ice-sheets as a problem in plasticity: Proc. Roy. Soc., series A, v. 207, 1951, p. 554-572; The mechanics of glacier flow: Jour. Glaciology, v. 2, no. 12, 1952, p. 82-93; The distribution of stress and velocity in glaciers and ice-sheets: Proc. Roy. Soc., series A, v. 239, 1957, p. 113-133.

also amenable to a steady-state treatment (16).

Neither the static nor the steady-state approach is truly suitable for a study of the mechanical origin of finite amplitude folds: as folding progresses the stress field and the geometrical relations of the layers show significant changes. The method of the present study deals explicitly with this time dependence. Therefore the method is a more powerful tool for the study of geologic deformation than either the static or the steady-state approach.

3. Objectives

The present study has four main objectives:

1) To define the limit of validity of the infinitesimal treatment. It is clear that the geometrical assumptions of the infinitesimal treatment are only valid over a limited range of fold amplitude. The results of the present study define a limiting maximum dip beyond which the infinitesimal treatment is no longer valid and indicate the factors that determine the further growth of the fold.

2) To investigate the information content of fold shapes. A particular characteristic of the shape of a folded layer may be determined by the physical parameters of the fold system, may be caused by the particular combination of forces exerted on the boundaries of the system, or may be due to essentially chance variations in the original shape. The present study shows the range in variation of fold shape

---

(16) Goguel, op. cit., p. 359-372

which results from certain changes in the physical parameters of the system. A method of describing fold shapes is presented that exhibits these systematic changes and is relatively insensitive to the initial shape.

3) To test the physical assumptions of the infinitesimal treatment. All natural folds that can be studied are of finite amplitude. By retaining the main physical assumptions of the infinitesimal treatment, while relaxing its inherent geometrical restrictions, it is possible to make detailed predictions about the properties of finite amplitude folds. These predictions can then be tested against the properties of naturally occurring folds.

4) To provide a detailed picture of the course of growth of a fold. Even though derived under somewhat idealized assumptions, a complete picture of the course of growth of a fold will add to the understanding of the folding process. The instantaneous strain-rate field and the cumulative finite-strain field at successive stages of folding are derived in this study. These should be valuable for comparison with various geologic indicators of stress orientation and finite strain, such as deformed oolites, rolled garnets, schistosity, grain elongations, and petrofabric orientation data. There are still a number of difficulties involved in the interpretation of some of these indicators, and knowledge of the strain and stress history of a particular region of a fold would be of great value in attacking some of these difficulties.

4. Description of the problem studied

In order to achieve the objectives listed in Section 3, a mathematical analysis of finite amplitude folding must satisfy several requirements: (1) The treatment must be able to treat an arbitrary succession of fold shapes, and the a priori assumptions about the shape should be kept to a minimum. (2) Although the folds considered may be of an idealized type, it must be possible to find natural folds which approach this idealized type. (3) It is desirable to relate the finite-amplitude treatment to the infinitesimal-amplitude theory. (4) Since satisfaction of these three requirements will certainly require a numerical treatment, it must be possible to reduce the variation of the physical parameters of the fold system sufficiently so that this variation can be delineated with a reasonable number of computational examples.

The problem of an isolated, thin, linearly viscous layer imbedded in a medium of lower viscosity and thrown into a symmetric train of folds most nearly satisfies the above requirements and is chosen for investigation here.

The single-layer problem is a natural extension of the most complete of the infinitesimal amplitude treatments (17). Although combinations of multiple layers have been

---

(17) M. A. Biot, Theory of folding of stratified viscoelastic media and its implications in tectonics and orogenesis: Geol. Soc. America Bull., v. 72, 1961, p. 1595-1620

studied by means of the infinitesimal treatment (18), the meaning of the results is not as clear as for the single-layer treatment (Chapter II, Section 3). Even though the single-layer case is less common in nature than the multiple-layer case, it does occur sufficiently often to provide opportunities for verification of the results of the theory.

Newtonian viscosity is probably the simplest reasonable rheological law to use. Since a viscous material has no "memory" of its past strain history, it is relatively simple to follow the deformation up to large strains by computing a series of velocity distributions for the successive shapes. The significance of the assumption of linear viscosity is discussed in more detail in Chapter IV, Section 5. The assumption of a symmetric train of folds is not crucial to the mathematical development, but it does permit a considerable reduction in the number of examples to be treated.

It will be shown that if the problem is properly formulated the fold shape depends only on the ratio of the folding wavelength to the dominant wavelength. The dominant wavelength (19) is the wavelength of the fold which the infinitesimal treatment predicts will grow the fastest (Chapter II, Section 2). Because of this dependence on a single ratio, a set of three calculated examples can cover the

---

(18) H. Ramberg, Fluid dynamics of viscous buckling applicable to folding of layered rocks: Bull. Amer. Assoc. Petr. Geol., v. 47, no. 3, 1963, p. 484-505

(19) Biot, op. cit

range of physical parameters fairly completely. This simple categorization is one of the reasons that the particular mathematical formulation used in this study was used. Relaxation of some of the simplifying assumptions would destroy the dependence on a single physical parameter.

The mathematical formulation of the problem and the probable effects of the simplifying assumptions made are discussed in Chapters III and IV. The following three chapters (V, VI, and VII) deal primarily with the details of the numerical method. A reader who is more interested in the geologic aspects of the study can omit these three chapters, except for Section 2 of Chapter VII, where the Fourier-analysis method of describing the shape of a folded layer is discussed. The infinitesimal theory and its relation to the present study are discussed in Chapter II. The results of the numerical computations are presented and interpreted in Chapter VIII, while their geologic significance is discussed in Chapter IX.

# CHAPTER II

## INFINITESIMAL-AMPLITUDE TREATMENT

The theory of infinitesimal-amplitude folding of layered media (1) provides the starting point for the present study. Wavelengths of folds are determined in the early stages of the folding process, and the infinitesimal treatment deals mainly with the wavelength-selection mechanism.

The energy dissipated in the folding of a competent layer in a less competent medium by compression parallel to the layer can be separated into two portions: (1) the bending dissipation in the layer, and (2) the dissipation in the medium. For a fixed rate of shortening, the bending dissipation in the layer increases as the wavelength of the folds becomes shorter, whereas the dissipation in the medium decreases, since the shorter wavelength folds disturb the medium over a smaller distance from the layer. There is thus a certain wavelength for which the total rate of dissipation for a fixed rate of shortening is minimal. As shown by Biot (2), this wavelength is the one that tends to be realized when a nearly plane competent layer is thrown into

---

(1) M. A. Biot, Theory of folding of stratified viscoelastic media and its implications in tectonics and orogenesis: Geol. Soc. America Bull., v. 72, 1961, p. 1595-1620

(2) Ibid.

folds by compression, and it is therefore called the dominant wavelength.

1. Geometrical assumptions

Certain geometrical assumptions are made in the infinitesimal treatment in order to simplify the mathematical analysis. These assumptions restrict the theory to folds with very low dips, making it essentially a static approach. They are: (1) The boundary between the layer and the medium can be considered as a plane when calculating the stress distribution in the medium. (2) The inclination of the layer, $\theta$, is small so that it can be assumed that:

$$\sin\theta = \tan\theta = \theta$$

(3) The distinction between arc length along the layer and distance parallel to the axis of coordinates may be neglected. In the finite-amplitude treatment none of these assumptions is made.

2. Concept of the dominant wavelength

Expressions for the dominant wavelength have been derived by Biot (3) and Ramberg (4) for viscous media, and by

---

(3) Ibid.

(4) H. Ramberg, Relationships between length of arc and thickness of ptygmatically folded veins: Am. Jour. Sci., v. 258, 1960, p. 36-46

Kienow (5) and Currie et al. (6) for elastic media. The various analyses differ in the method of calculating the resistance of the surrounding medium. Biot uses the proper treatment and arrives at an expression discussed below. Ramberg makes an incorrect assumption about the way the velocity in the medium dies out as distance from the layer increases, and gets an expression which differs by a multiplicative constant from Biot's. Using elasticity theory, Currie et al. arrive at an expression which is equivalent to Biot's when the appropriate elastic constants are replaced by the coefficients of viscosity. This equivalence between the elastic and the viscous theory is a general mathematical property, discussed in more detail below. Kienow uses elastic analysis, but assumes that the resistance of the medium is independent of wavelength, so that he does not arrive at the same result as Currie et al. Goguel (7) analyzes the problem of folding in some detail and considers plastic as well as viscous media, but he does not derive an explicit expression for the dominant wavelength.

Biot's treatment (8) shows that small perturbations

---

(5) S. Kienow, Grundzüge einer Theorie der Faltungs- und Schieferungsvorgänge: Berlin, Bornträger, Fortschritte der Geologie und Paleontologie, bd. XIV, h. 46, 1942, 129 p.

(6) J. B. Currie, H. W. Patnode, and R. P. Trump, Development of folds in sedimentary strata: Geol. Soc. America Bull., v. 73, 1962, p. 655-674

(7) J. Goguel, Introduction à l'étude mécanique des déformations de l'écorce terrestre: Service Carte Géol. France Mém., 1948, 530 p.

(8) Biot, op. cit.

in the initial shape of the competent layer are amplified at a rate which is a function of their wavelength and their initial amplitude. If the initial vertical displacement, $y$, is given by

$$y = y_0 \cos \frac{2\pi}{L} x,$$

the displacement at time $t$ will be

$$y = y_0 e^{pt} \cos \frac{2\pi}{L} x,$$

where $p = p(L, \mu_p, \mu_m, F)$ is a function of the wavelength, the viscosities of plate and medium, and the longitudinal force in the plate, $F$. For a given viscosity ratio, there will be one wavelength for which the exponential growth factor $p$ is the largest. It is the dominant wavelength, given by,

$$L_d = 2\pi h \sqrt[3]{\frac{\mu_p}{6\mu_m}},$$

where $h$ is the thickness of the competent layer.

An expression analogous to this can be developed for the elastic case, but the significance of the dominant wavelength for the elastic case is different from that for the viscous case. The elastic system has no memory of the shapes that it has assumed. It will buckle at a wavelength determined by the physical parameters of the system and the constraints imposed on it, and its shape will contain no

displacement components of other wavelengths. The viscous system, on the other hand, has a complete memory of its past shape history. The physical parameters and constraints on the system will determine the rate at which the various components of the shape grow, but all wavelengths initially present will be amplified to a certain degree. Therefore, the mechanism of fold growth in the viscous system must be analyzed in some detail before it can be said that the dominant wavelength will in fact predominate at finite amplitudes.

Biot (9) presents such an analysis. His principal conclusion is that if the total amplification of the dominant wavelength is large (e.g., amplification by a factor of 1000 or more), the resultant fold train will show a sharply defined wavelength with its value given by the dominant wavelength expression. This will occur whatever the distribution of wavelengths in the initial shape perturbations may have been. This lack of dependence on the initial shape of the layer is an important consequence of the Biot theory; it can be used to explain the observation that trains of folds with a relatively constant wavelength are quite common in nature.

---

(9) Ibid.

3. Multiple layers

Ramberg (10) develops expressions for the dominant wavelength for various combinations of multiple layers, but there is some doubt as to the meaning of the dominant wavelength concept as applied to multiple layers. In particular, Ramberg tacitly assumes that the initial shape perturbations are identical in each of the multiple layers. If this assumption were relaxed it would be necessary to treat the problem of the nature of the interactions between the different layers. Some progress with this problem has been made experimentally by Currie et al. (11), but the problem is far from being solved. An analogous difficulty arises in the finite-amplitude problem, where it would be necessary to make assumptions about the way the fold shape changes with distance up and down from the central layer of the multiple-layer packet.

4. Limitations of the infinitesimal theory

One consequence of the linear viscous analysis is that large amplification factors will occur for any viscosity ratio and any initial shape if the "time" of folding is large enough. The time of folding is determined only for a specified force on the layer, and time is used in this section

---

(10) H. Ramberg, Fluid dynamics of viscous buckling applicable to folding of layered rocks: Bull. Amer. Assoc. Petr. Geol., v. 47, no. 3, 1963, p. 484-505

(11) Currie et al., op. cit.

with this qualification. Biot (12) places a limit on the time of folding by assuming that if the uniform compression of the layer--which will of course continue during the folding process--produces a shortening of 25%, the folding phenomenon will be masked by the shortening. However, this criterion is both physically and geologically unrealistic. When the fold deviates little from a plane, the thickening associated with the shortening will be uniform along the length of the layer. Physically, such a uniform shortening has no effect on the problem except to make all wavelengths shorter. Geologically, such shortening can be recognized only by using indicators of geologic strain such as deformed oolites or fossils in the layer. Geologic use of such indicators has not been frequent enough to rule out large uniform shortening in folded beds.

It seems more realistic to place the limit of the time of folding at the fold amplitude where the wavelength-selection mechanism breaks down. This occurs when the maximum dip of the limb is between $10^{\circ}$ and $20^{\circ}$ (Chapter VIII, Section 5). Even at a $10^{\circ}$ limb-dip the selection mechanism is not that of the infinitesimal analysis.

If the wavelength-selection process operates only at low amplitudes, then the principle factor which determines whether a fold train of the dominant wavelength will develop is the amplitude of the initial shape perturbations. When these perturbations are small enough, the dominant wavelength

---

(12) Biot, op. cit.

will have time enough to assert itself before the finite-amplitude stage is reached; if they are not sufficiently small, the resulting fold train will not exhibit the dominant wavelength--and will not have a regular wavelength at all, unless the initial shape perturbation does.

Uniform compression parallel to the layer may disturb the wavelength-selection process by shortening all wavelengths. It seems possible that uniform compression could operate in such a way as to produce a train of folds with a regular wavelength significantly shorter than the dominant wavelength.

Even if a train of folds develops at the dominant wavelength, it is possible that the viscosity ratio will change during the folding process. As lithification of the rocks proceeds, it is likely that different mechanisms of deformation come into play. Investigations of the effect of temperature on the rheological properties of rocks (13, 14, 15) have shown that, by the time the temperature has reached values consistent with the greenschist facies of metamorphism, significant changes have taken place in the

---

(13) H. C. Heard, Effect of large changes in strain rate in the experimental deformation of Yule marble: Jour. Geology, v. 71, no. 2, 1963, p. 162-195

(14) D. T. Griggs, Experimental flow of rocks under conditions favoring recrystallization: Geol. Soc. America Bull., v. 51, 1940, p. 1001-1022

(15) D. T. Griggs, F. J. Turner, and H. C. Heard, Deformation of rocks at 500° to 800° C., chap. 4 in Rock deformation (A symposium), Geol. Soc. America Mem. 79, 1960, p. 39-104

deformational behavior of rocks. It is likely that a given temperature change will effect rocks of different composition in different ways so that the viscosity ratio may show significant changes with time.

The results of the present study show (Chapter VIII, Section 3) that the shape of finite-amplitude folds varies significantly with variation in the ratio of the fold wavelength to the dominant wavelength. This variation provides an independent measure of the viscosity ratio.

# CHAPTER III

## MATHEMATICAL FORMULATION OF THE PROBLEM

### 1. Choice of region; boundary conditions

The first step in the mathematical formulation of the finite-amplitude development of a fold in a viscous medium is to isolate the region under consideration. Although the method used in this study could be applied to any limited region with an arbitrary distribution of stresses or velocities imposed on its boundary, in most geologic situations these external constraints are unknown. Therefore, rather than starting with assumptions about the boundary conditions, we shall make assumptions about the geometrical properties of the folding system during its development. Natural examples can be found in which these geometrical conditions are fulfilled to a fair degree of approximation; the extent to which they are fulfilled by the final shape as we observe it in the field can be clearly determined in any given example.

Consider an isolated competent layer imbedded in a homogeneous medium of lower competency. This layer is assumed to be folded into a rather long train of waves; individual folds should have the same wave length and amplitude, and the axial plane of each successive anticline and syncline should be a plane of symmetry for the folded shape. By

"isolated" is meant, in practice, that the homogeneous medium extends a few wavelengths above and below the layer. Consider a fold near the center of the train; it is reasonable to assume that the stresses exerted on this portion of the body will be substantially those which would be exerted if the wave train were very long. We shall make the further assumption that velocities do not vary with distance along the axis of the folds; this is the assumption of plane strain (1).

If we assume that the above geometrical properties hold throughout the deformation, we can isolate a portion of the layer+medium system and state the boundary conditions which must be imposed on it. Since each axial plane is a plane of symmetry, the shear stress across it must be zero. In addition, since it is assumed that the folds grow with time, two adjacent axial planes must approach each other with a given horizontal velocity $\underline{u}_B$. ($\underline{u}_B$ may vary with time, but not with $\underline{y}$). At large distances above and below the layer we again assume that there are horizontal planes of zero shear stress which are moving away from each other at a velocity $\underline{V}_B$ such that the total volume of our rectangular region remains constant. These boundary conditions, coupled with the assumption of Newtonian viscosity, provide a completely defined mathematical problem.

An additional consequence of our geometrical

---

(1) I. S. Sokolnikoff, Mathematical theory of elasticity: New York, McGraw-Hill Book Co., Inc., 1956, p. 250

assumptions is that there will be a center of symmetry at the inflection point on the limb of the fold.

The problem as thus defined is pictured in figure 1.

## 2. Equations of Motion

The equations which govern the two-dimensional motion of a slow-moving, linearly viscous fluid are the equations of stress equilibrium:

$$\sum_j \frac{\partial \tau_{ij}}{\partial x_j} + F_i = 0 \quad ; \tag{1a}$$

the stress-strain-rate relations:

$$\tau_{ij} = 2\mu e_{ij} - \delta_{ij} P \quad ; \tag{1b}$$

the condition of incompressibility:

$$\sum_i \frac{\partial u_i}{\partial x_i} = 0 \quad ; \tag{1c}$$

and the compatibility condition:

$$e_{11,22} + e_{22,11} = 2 e_{12,12} \quad . \tag{1d}$$

$P = -\frac{1}{3}(\tau_{11} + \tau_{22} + \tau_{33})$ is the pressure and $\delta_{ij} = \begin{cases} 1 & , i = j \\ 0 & , i \neq j \end{cases}$ is the Kronecker delta. Relation 1d insures that the strain rates are derivable from a velocity field; if the problem is rephrased in terms of the velocities alone, relation 1d is automatically satisfied.

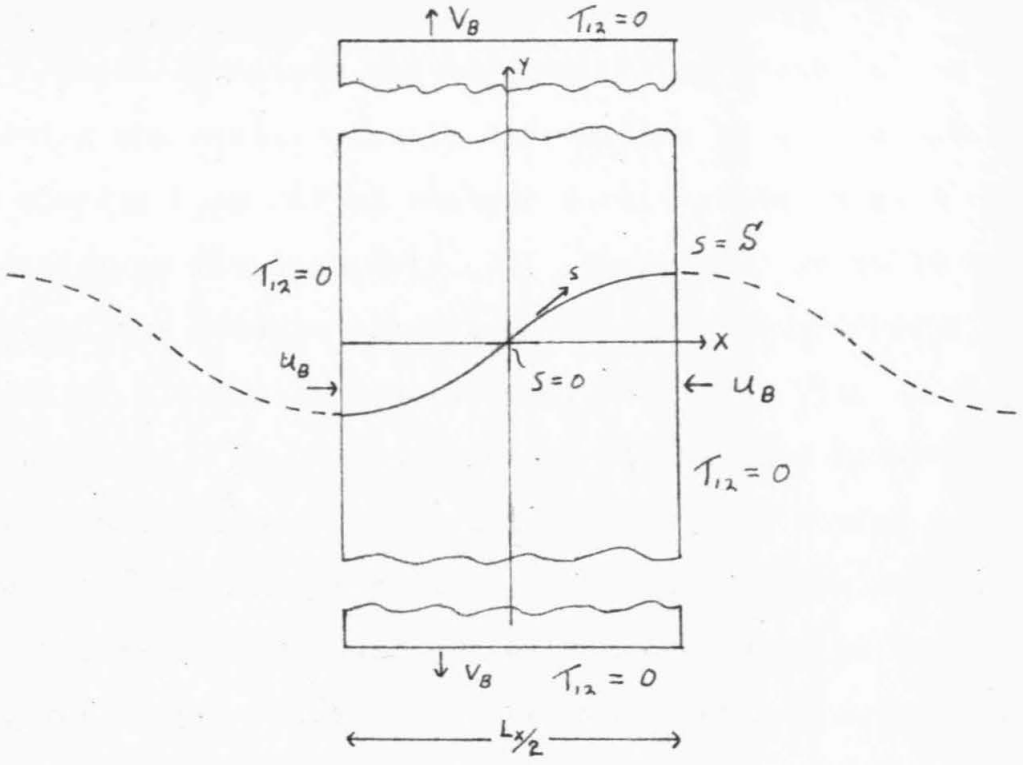


Figure 1.--Folding of an isolated layer: coordinate system and boundary conditions.

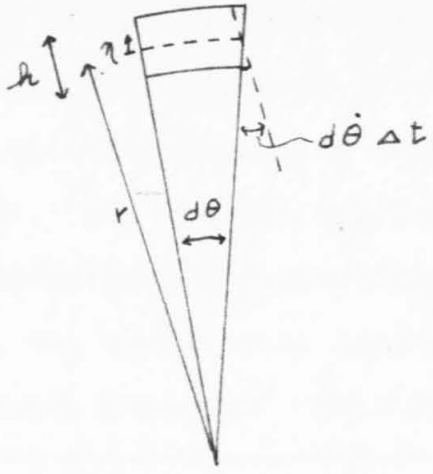


Figure 2.--Dissipation in the layer: coordinate system.

3. Variational Method

These equations are mathematically identical to those governing the static elastic deformation of an incompressible elastic body, if we replace strain-rates by strains and velocities by displacements (2). Therefore, there is a complete analogy between elastic and slow-viscous theory; any results of elasticity theory carry over into viscous deformation theory. In particular, the equivalence between elastic variational methods using the strain energy density and elastic methods using the static equilibrium equations implies a similar equivalence between variational methods using the viscous dissipation rate and methods using the viscous equations of motion. The variational method is particularly convenient in setting up the discrete analogue of the continuous problem defined in this chapter and will therefore be used in this study.

It is convenient to formulate the problem in terms of velocities rather than stresses, since it is the changes in the shape of the plate that are of most direct interest. The variational principle that applies in this case is known in elasticity theory as the Theorem of Minimum Potential Energy. The theorem can be stated thus: "Of all displacements satisfying the given boundary conditions those which satisfy the equilibrium equations make the potential energy an absolute minimum." This theorem and its

---

(2) J. W. S. Rayleigh, The theory of sound: New York, Dover Publications, Inc., v. II, 1945, p. 313

converse are proved by Sokolnikoff (3). The potential energy of the theorem is defined as the strain energy of the body minus the work done on the body by the stresses on those portions of the boundary where stresses are given, and minus the work done by the body forces. In our problem the given stresses are zero shear stress on the outer boundaries of the region, so that the work done by the given stresses is automatically zero. Since normal velocities are specified on the boundary, we shall consider only velocity distributions which have these boundary velocities in seeking the minimum dissipation.

In the particular problem under consideration, the primary advantage of the variational method is the relative freedom of choice that it permits in the choice of a mathematical representation of the velocity distribution. In particular, the problem region may be divided into smaller sub-regions and a different representation of the velocity distribution used in each sub-region. We may also use different methods of calculating the dissipation in accordance with the physical assumptions about the nature of the region. Although we are free to pick the description of the velocity distribution which is most convenient for the particular portion of the region, we must insure that the velocity distributions match at the internal boundaries. This matching introduces additional constraining relations which must be satisfied by any velocity distribution

---

(3) Sokolnikoff, op. cit., p. 382-386

considered in seeking the minimum dissipation.

4. Shape and dissipation of the layer

Let us now consider the specific representation of the velocity distribution and the calculation of the dissipation from this representation. Consider first the plate itself. If the plate is sufficiently thin, it can be assumed that: (1) the central plane of the plate undergoes neither extension nor compression; (2) originally plane cross sections normal to the central plane of the plate remain plane during deformation; (3) the variation of the bending strain across the plate is linear, with extension on the convex side and compression on the concave side of the plate; and (4) the velocity of points on the inner and outer sides of the plate situated on the same normal to the plate is identical. The validity of these assumptions is discussed in the next chapter. Since the length of the plate is fixed, its shape can be described by specifying its inclination $\theta$ as a function of arc length $s$, measured from the center of symmetry, and its velocity can be described by specifying $\dot{\theta}$ as a function of $s$. In order to calculate the dissipation involved in the bending of the plate, we must first calculate the strain rate in the plate; to do this we refer to figure 2, page 23, where the original shape of a small element of the plate and its shape after a small increment of time $\Delta t$ is shown. The change in length per unit length of a longitudinal fiber in the plate at a distance $\eta$ from the central fiber of the plate is then given

by:

$$\dot{e}\,\Delta t = \frac{\eta\, d\dot{\theta}\,\Delta t}{(r-\eta)\,d\theta} \quad .$$

If we neglect $\eta$ in relation to the radius of curvature $r$ of the central fiber of the plate, as the assumption (3) of linear strain variation demands, the resulting strain rate is:

$$\dot{e} = \frac{\eta\, d\dot{\theta}}{r\, d\theta} = \eta \frac{d\dot{\theta}}{ds} \quad .$$

Because of the assumption of plane strain, the corresponding longitudinal stress is given by the stress-strain rate relations as:

$$\sigma = 2\mu_p \dot{e} - P = 2\mu_p \dot{e} + \frac{\sigma}{2} \quad ,$$

$$\sigma = 4\mu_p \dot{e} \quad .$$

Integrating over the thickness of the plate and over the length of the plate, the bending dissipation becomes:

$$\int_{-S}^{S} \left( \int_{-\frac{h}{2}}^{\frac{h}{2}} \frac{1}{2} \sum_{i,j} \tau_{ij} \dot{e}_{ij}\, d\eta \right) ds = \int_{-S}^{S} \left( 2\mu_p \left(\frac{d\dot{\theta}}{ds}\right)^2 \int_{-\frac{h}{2}}^{\frac{h}{2}} \eta^2 d\eta \right) ds = \frac{1}{6}\mu_p h^3 \int_{-S}^{S} \left(\frac{d\dot{\theta}}{ds}\right)^2 ds \, .$$

The horizontal and vertical velocity of a point $S$ on the plate are found by using the relationships between arc length, inclination, and $X$ and $Y$ of the plate:

$$\frac{dx}{ds} = \cos\theta ,$$

$$\frac{dy}{ds} = \sin\theta .$$

Differentiating these relations with respect to time,

$$\frac{du}{ds} = \frac{d}{dt}\left(\frac{dx}{ds}\right) = -\dot{\theta}\sin\theta ,$$

$$\frac{dv}{ds} = \frac{d}{dt}\left(\frac{dy}{ds}\right) = \dot{\theta}\cos\theta ,$$

and finally integrating with respect to $s$, remembering that $u$ and $v$ are zero at the inflection point on the limb ($s = 0$), we have:

$$u = -\int_0^s \dot{\theta}\sin\theta \, ds ,$$

$$v = \int_0^s \dot{\theta}\cos\theta \, ds . \qquad (2)$$

According to assumption 4 above, these velocity components must match the velocity components in the medium adjacent to the plate.

5. Dissipation in the medium

The velocity distribution in the surrounding medium is most conveniently described in terms of a stream function. This stream function is defined so that its derivatives are the horizontal and vertical velocities:

$$u = \frac{\partial\phi}{\partial y} \quad , \quad v = -\frac{\partial\phi}{\partial x} .$$

A velocity distribution defined by such a stream function automatically satisfies the incompressibility relation, equation 1c. It can be shown (4) that the equilibrium equations imply that the stream function is biharmonic:

$$\nabla^4 \phi = 0 .$$

Although this fact is not utilized directly in the present treatment of the problem, it does provide a verification of the difference equations derived in Chapter V. For handling the boundary conditions on the medium, it is convenient to separate the velocity distribution into two parts, that due to a uniform compression, and the remainder, which can be thought of as due to the folding. This separation is represented by:

$$\phi = \phi_c + \phi_f \qquad (3)$$

where $\phi_c = K x y$ gives the contribution due to uniform compression.

The dissipation in the medium may be written in terms of this stream function as follows:

---

(4) J. C. Jaeger, Elasticity, fracture and flow: London, Methuen and Co., Ltd., 1956, p. 140

$$\iint \tfrac{1}{2} \sum_{i,j} \tau_{ij} \dot{e}_{ij}\, dx\, dy = \iint \tfrac{1}{2} \sum_{i,j} (2\mu_m \dot{e}_{ij} - \delta_{ij} p)\dot{e}_{ij}\, dx\, dy$$

$$= \mu_m \iint (\dot{e}_{11}^2 + \dot{e}_{22}^2 + 2\dot{e}_{12}^2)\, dx\, dy$$

$$= \mu_m \iint \left[ 2\phi_{,12}^2 + \tfrac{1}{2}(\phi_{,11} - \phi_{,22})^2 \right] dx\, dy \qquad (4)$$

$$= \mu_m \iint \left[ 2(\phi_{,12} + K)^2 + \tfrac{1}{2}(\phi_{,11} - \phi_{,22})^2 \right] dx\, dy \,.$$

Under the assumption of isolation, the medium extends to $\pm\infty$ in the y-direction, but it is more convenient to deal with a finite rectangular region. Therefore, $\phi$ outside this region is represented as a sum of products of trigonometric functions and exponentials:

$$\phi = Kxy + \sum_{i=1}^{\infty} (A_i + B_i y')\, e^{-(2i-1)\frac{2\pi}{L_x} y'} \cos (2i-1)\frac{2\pi}{L_x} x$$

$$+ \sum_{i=1}^{\infty} (C_i + D_i y')\, e^{-2i\frac{2\pi}{L_x} y'} \sin 2i\frac{2\pi}{L_x} x \,. \qquad (5)$$

$y'$ is measured from the top of the rectangular region, and

the $\underline{A}_i$ , $\underline{B}_i$ , $\underline{C}_i$ , and $\underline{D}_i$ are chosen to match $\phi$ and $\frac{d\phi}{dy}$ at $\underline{y}' = 0$ . Each term of the sum satisfies the boundary conditions on $\phi_t$ at the right and left hand walls, and the exponential dependence on $\underline{y}'$ gives $\phi = \frac{\partial \phi}{\partial y} = 0$ at infinity. The dissipation for this region is calculated with the same expression used for the rectangular region, equation 4.

## 6. Statement of the mathematical problem

When the dissipation expressions and the constraints for the various sub-regions are collected, the mathematical problem of calculating the velocities of deformation of the folding region can be stated as follows. We denote the $\underline{y}$-coordinate of the line on which the mesh point representation of $\phi$ passes into the trigonometric sum representation of $\phi$ by $\underline{y}_t$ , the stream function in the rectangular region by $\phi$ , and the trigonometric stream function by $\Phi$ . The total dissipation rate, $\underline{I}$, is:

$$I = \frac{\mu_p h^3}{6} \int_{-s}^{s} \left(\frac{d\dot{\theta}}{ds}\right)^2 ds + \mu_m \int_{-y_0}^{y_0} \int_{-\frac{L_x}{4}}^{\frac{L_x}{4}} \left[\frac{1}{2}\left(\phi_{f,11} - \phi_{f,22}\right)^2 + 2\left(\phi_{f,12} + K\right)^2\right] dx\, dy$$

$$+ \mu_m \int_{y_t}^{\infty} \int_{-\frac{L_x}{4}}^{\frac{L_x}{4}} \left[\frac{1}{2}\left(\Phi_{,11} - \Phi_{,22}\right)^2 + 2\left(\Phi_{,12} + K\right)^2\right] dx\, dy \qquad (6)$$

$$+ \mu_m \int_{-\infty}^{-y_t} \int_{-\frac{L_x}{4}}^{\frac{L_x}{4}} \left[\frac{1}{2}\left(\Phi_{,11} - \Phi_{,22}\right)^2 + 2\left(\Phi_{,12} + K\right)^2\right] dx\, dy \quad .$$

We seek the velocity distribution which (1) satisfies the internal matching conditions:

$$\frac{\partial \Phi}{\partial y} = -\int_0^s \dot{\theta} \sin\theta \, ds \quad ,$$

$$\frac{\partial \Phi}{\partial x} = -\int_0^s \dot{\theta} \cos\theta \, ds$$

at all points $s$ on the plate and:

$$\Phi = \phi$$

$$\frac{\partial \Phi}{\partial y} = \frac{\partial \phi}{\partial y}$$

on the horizontal lines $y = \pm y_t$ ; (2) satisfies the velocity constraints on the external boundaries:

$$\Phi_f = 0 \quad \text{at} \quad x = \pm L_x/4 \quad ;$$

and (3) makes $I$ a minimum. (The center of symmetry has been ignored in this formulation of the problem; when the discrete analogue of the problem is formulated, the center of symmetry will be taken into account in order to reduce the number of algebraic equations to be solved.)

At the start of the folding, the shape of the layer is taken to be that of a sine wave of low amplitude. The consequences of this assumption are best considered in the light of the computational results of this study; therefore,

they will be discussed in Chapter VIII, Section 5.

7. Parametrization of the problem

As thus formulated, the problem depends on a single physical parameter. To show this we first write the dissipation rate as a sum of two terms, dissipation in the medium and bending dissipation in the plate:

$$I = \frac{\mu_p h^3}{6} \int_{-S}^{S} \left(\frac{d\dot{\theta}}{ds}\right)^2 ds \quad + \mu_m \iint (\dot{e}_{11}^2 + \dot{e}_{22}^2 + 2\dot{e}_{12}^2)\, dx\, dy .$$

The spatial variation of the velocity distribution depends on the relative magnitude of these two terms. Any change in the system which multiplies both terms by a constant, such as a change in the boundary velocities, will change the dissipation of all the possible velocity distributions considered in seeking the minimum by the same factor. Therefore, we need consider only those changes in the physical parameters of the system which change the ratio:

$$\frac{I_p}{I_m} = \frac{h^3}{6}\frac{\mu_p}{\mu_m} \frac{\int_{-S}^{S} \left(\frac{d\dot{\theta}}{ds}\right)^2 ds}{\iint (\dot{e}_{11}^2 + \dot{e}_{22}^2 + 2\dot{e}_{12}^2)\, dx\, dy} .$$

It is seen from this expression that if we keep the shape of

the plate constant and change either the time scale or the distance scale, the spatial variation of the velocity distribution remains unchanged. Since the absolute values of the stresses are not specified in the problem, a change in the magnitudes of the viscosities which leaves $\mu_p/\mu_m$ unchanged will not alter the problem. Also, any change in the viscosity ratio and the thickness of the plate which leaves $\frac{1}{6}\frac{\mu_p}{\mu_m}h^3$ constant does not change the problem. Apart from a factor of $2\pi$ this quantity is just the cube of the dominant wavelength (5):

$$L_d = 2\pi h \sqrt[3]{\frac{\mu_p}{6\mu_m}} \quad .$$

Therefore, under the assumptions of the problem as formulated, the velocity distributions and fold shapes that result from a given initial shape depend on a single physical parameter, the ratio of the fold wavelength to the dominant wavelength, $L/L_d$ .

It should be noted that this "one-parameter" nature of the problem is a result of the assumption that the plate is thin and inextensible. If a more accurate bending-dissipation expression were used, so that changes in the length of the plate were taken into consideration, the total dissipation would include terms multiplied by other powers of the thickness, and the plate thickness and the viscosity

---

(5) M. A. Biot, Theory of folding of stratified viscoelastic media and its implications in tectonics and orogenesis: Geol. Soc. America Bull., v. 72, 1961, p. 1595-1620

ratio would be independent parameters.

The growth of a finite-amplitude fold was computed for three values of $L/L_d$ : (1) $L \ll L_d$ , (2) $L = L_d$ , and (3) $L = 4.6\, L_d$ . In case 1, the free plate, the dissipation in the medium is negligible compared to the bending dissipation of the plate. Case 2, the dominant-wavelength fold, corresponds to an approximate balance between the dissipation in the medium and the plate. In case 3, the weak-plate fold, the dissipation in the medium is large compared to that of the plate.

8. The free plate

One end member of this single-parameter sequence deserves special consideration, since its shape as a function of time is obtained in a simple fashion. When the viscosity ratio is very large, or alternatively, when the wavelength is much shorter than the dominant wavelength, the dissipation in the medium is negligible in comparison to the bending dissipation of the plate. This is the case of the free plate. Its dissipation is:

$$I = \frac{\mu_0 h^3}{6} \int_0^S \left(\frac{d\dot{\theta}}{ds}\right)^2 ds$$

with the constraints:

$$\frac{d\dot{\theta}}{ds} = 0 \qquad at \qquad s = 0$$

$$\dot{\theta} = 0 \qquad at \qquad s = S$$

Rather than constrain the horizontal velocity at $s = S$ , it is simpler for the free plate to specify the force acting on this end of the plate. This introduces a new term in the dissipation expression which takes into account the rate of work done by this external force; the dissipation expression then becomes:

$$I = \frac{\mu_p h^3}{6} \int_0^S \left(\frac{d\dot{\theta}}{ds}\right)^2 ds \; - \; P \int_0^S \dot{\theta} \sin\theta \, ds \; .$$

Using the standard methods of the calculus of variations, the first variation of this expression is:

$$\delta I = \frac{\mu_p h^3}{3} \int_0^S \frac{d\dot{\theta}}{ds} \, \delta \frac{d\theta}{ds} \, ds \; - \; P \int_0^S \delta\dot{\theta} \sin\theta \, ds \; .$$

Integrating the first integral by parts, we have:

$$\delta I = \frac{\mu_p h^3}{3} \left\{ \frac{d\dot{\theta}}{ds} \delta\theta \Big|_0^S - \int_0^S \frac{d^2\dot{\theta}}{ds^2} \, \delta\theta \, ds \right\} - P \int_0^S \delta\dot{\theta} \sin\theta \, ds \; .$$

Now, the integrated parts from the integration by parts vanish due to the boundary conditions and, since $\delta\dot{\theta}$ is arbitrary except at the ends, the vanishing of the first variation implies that:

$$\frac{\mu_p h^3}{3} \frac{d^2\dot{\theta}}{ds^2} + P \sin\theta = 0 \; .$$

Except for the presence of the time derivative of $\theta$ , this

equation is identical to the Euler elastica equation (6); the equation could, of course, have been derived merely by use of the analogy between elastic and viscous problems.

It was not found possible to solve this equation in closed form, but the numerical solution is a very simple one. At any given stage of the deformation $\theta$ is known as a function of $s$, and therefore $\sin\theta$ can be calculated at a series of equally spaced $s$ values. Two numerical integrations of this set of $\sin\theta_i$ give the values of $\dot{\theta}_i$ corresponding to this shape. The new shape after a short interval of time, $\Delta t$, is given by:

$$\theta_i^{(new)} = \theta_i^{(old)} + \dot{\theta}\,\Delta t \quad .$$

The process is then repeated until the fold is of sufficiently large amplitude.

---

(6) J. Prescott, Applied elasticity: New York, Dover Publication, Inc., 1961, p. 100

# CHAPTER IV

## ASSUMPTIONS AND LIMITATIONS OF THE MATHEMATICAL FORMULATION OF THE PROBLEM

In the previous chapter a number of idealizing assumptions were made in order to formulate a well-defined and mathematically tractable problem; in this chapter we shall examine the more important ones and the restrictions which they place on the interpretation of the results of the study. These assumptions can be placed in three general categories: (1) the geometrical assumptions made in defining the specific problems to be solved, (2) the mathematical simplifications needed to reduce the analytical difficulty of the problem, and (3) the assumption of linear viscosity as a rheological law.

### 1. Geometrical assumptions

The geometrical assumptions about the periodicity and the symmetry of the folds are not strictly necessary from a mathematical standpoint. If they were relaxed, only minor changes would be necessary in the discrete formulation of the problem. For example, treatment of a series of asymmetric, but still periodic folds would require no major revision of the mathematical treatment or the computational method. However, at the present stage of knowledge of the folding process it is logical to start with the simplest

geometry that adequately represents a class of natural folds and to study the evolution and the variations in shape in this idealized case.

2. Plane strain

The assumption of two-dimensional deformation is essential to the present formulation of the problem, but this assumption is a common one in most geologic thinking about the folding process. It is clearly justified in a large number of geologic situations. Extension or compression parallel to fold axes which did not alter the cylindrical shape of the fold would not change any of the conclusions of this study. However, fold culminations and folds with curved axes fall outside the scope of the treatment.

3. Thin-plate assumption

The assumption that the competent layer can be treated as a thin plate requires more detailed justification. To be sure, a problem in which the ratio of initial wavelength to dominant wavelength is fixed will correspond to as thin a plate as we care to choose if the viscosity ratio is made high enough. However, in a natural example the viscosity ratio is unknown, and the thickness of the plate is easily observed; therefore, we would like to have some objective measure of the errors involved in the assumption of a thin plate. There are three independent errors which are introduced by this assumption: (1) if the plate has finite thickness, the velocity of the boundary between medium

and plate is not exactly what we have assumed; (2) the assumption of linear strain distribution in the plate is only true for a very thin plate; and (3) the plate will be inextensible only if it is very thin and the viscosity ratio is very high.

The effect of the assumption that we can treat the plate as a surface when matching the velocities of medium and plate is difficult to evaluate precisely. For plate thickness corresponding to a viscosity ratio of 500 to 1000 at the dominant wavelength, the contribution to the velocity of a point on the surface of the plate due to the rotation of the plate will be as large as several per cent of the velocity of the center line of the plate. One way to visualize this error is to consider a certain "overlap" area that would be part of the plate if it had finite thickness. In the thin-plate approximation this overlap area is treated as part of the medium. As a result, shear strain parallel to the layer is permitted, even though this shear strain would not be present in the thick plate. Therefore, the strain distribution in the medium will be incorrect in the overlap area and probably for a short distance further into the medium. It is probable that this error is important only near the plate and that the overall strain distribution in the medium and the shape of the layer are not appreciably affected.

To consider the effects of the assumption of a linear strain distribution in the plate, we examine the next more

complicated approximation: that in which a linear strain distribution is not assumed but in which it is still assumed that transverse cross sections perpendicular to the center line remain plane and perpendicular during bending (1). In this case, the strain rate in the plate is given by the expression:

$$\dot{e} = \frac{R(y+\eta)}{R+y} \frac{d\dot{\theta}}{ds} ,$$

where $R$ is the local radius of curvature of the center line, $y$ is the distance from the center line of the plate, taken as positive on the convex side, and $-\eta$ is the $y$-coordinate of the neutral plane of the plate. $\eta$ is determined by the condition of inextensibility of the plate:

$$\int_{-\frac{h}{2}}^{\frac{h}{2}} \dot{e}(y)\, dy = \int_{-\frac{h}{2}}^{\frac{h}{2}} \frac{R(y+\eta)}{R+y} \frac{d\dot{\theta}}{ds} dy = 0 ,$$

and is given by

$$\eta = R - \frac{h}{\ln \frac{R+h/2}{R-h/2}} \approx \frac{1}{12} \frac{h^2}{R} .$$

Values chosen from a tight fold in this study give: $h = 1$, $R = 10$, and $\eta = 0.0083$.

The bending dissipation in the plate is given by:

---

(1) S. Timoshenko, Strength of materials, Pt. I, Elementary theory and problems: Toronto, D. Van Nostrand Co., Inc., 3d ed., 1955, p. 362

$$I_p = \mu_p \int_{-h/2}^{h/2} \dot{e}^2 dy = \mu_p \left(\frac{d\dot{\theta}}{ds}\right)^2 \int_{-h/2}^{h/2} \frac{R^2(y+n)^2}{(R+y)^2} dy .$$

Substituting the expression for $\dot{e}$ derived above and performing the integration:

$$I_p = \mu_p \left(\frac{d\dot{\theta}}{ds}\right)^2 R^2 h \left[ -1 + \frac{h/2}{R^2 - (h/2)^2} \frac{1}{\ln \frac{R+h/2}{R-h/2}} \right]$$

$$\approx \mu_p \left(\frac{d\dot{\theta}}{ds}\right)^2 R^2 h \left[ -1 + 1 + \frac{1}{3}\left(\frac{h}{2R}\right)^2 + \frac{4}{15}\left(\frac{h}{2R}\right)^4 \right]$$

$$= \mu_p \left(\frac{d\dot{\theta}}{ds}\right)^2 \frac{R^3}{12} \left[ 1 + \frac{4}{5}\left(\frac{h}{2R}\right)^2 \right]$$

Thus, in the example cited above, the first correction to the dissipation would be zero on the limb and 0.4% at the crest of the fold.

4. Inextensibility

The condition of inextensibility is probably the most serious aspect of the thin plate assumption. Most fairly tight natural folds show some thickening in the crestal region (2).

A relative thickening of the crest of the competent layer has two main effects on the resulting shape: (1) The

---

(2) J. G. Ramsay, The geometry and mechanics of formation of "similar" type folds: Jour. Geology, v. 70, no. 3, 1962, p. 309-327

thickening will change the local bending resistance of the plate. This effect will tend to slow the growth of curvature in the crestal region and result in a more open fold. (2) The extra shortening in the crestal region will increase the curvature there, tending to produce a tighter fold. It seems likely that the first effect will be most important and that the folds resulting from the computations of this study will be tighter than those which would result from a more accurate analysis which did not assume inextensibility. These effects will be least important for the free plate and most important for a fold whose wavelength is much longer than the dominant wavelength. The reason for this is that the longitudinal stresses in the plate are increased by the presence of the medium.

5. Linear viscosity

The assumption of linear viscosity as a rheological law is of a different character from the assumptions discussed above. It is better regarded as a working hypothesis than as an assumption. The extent to which the geometrical idealizations and the mathematical simplifications are justified in relation to any particular fold can be determined by observing the shape of the fold, the variations in thickness of the layer, and the radius of curvature at the crest. Consequences of the rheological law are tested by comparing fold characteristics predicted by computations based on the law with those observed in natural folds.

In general, there are three ways of approaching the

problem of determining the rheological law under which rocks deform in nature: (1) measurement of stress-strain and stress-strain-rate relationships on rock samples subjected to stress in the laboratory; (2) study of the detailed mechanisms of deformation of rocks in the field and laboratory and prediction of the rheological laws by theoretical considerations based on these mechanisms; and (3) calculation of predicted patterns of deformation under assumed laws and comparison of these predictions with natural examples.

In terms of experimental results the simplest way to distinguish a viscous material from a plastic one is to observe whether the material shows a threshold stress below which no deformation takes place. In all the experimental work on rocks known to the writer such a threshold is found to exist, but it seems to be lower at lower strain-rates. The experimental work done at the lowest strain-rates (3) was done under conditions of constant strain-rate, so that the simple test of a threshold stress cannot be applied. Heard states (4) that his data neither contradict nor affirm the presence of a threshold stress. The strong non-linear dependence of stress on strain-rate shown in Heard's results does not agree well with either linear viscosity or perfect plasticity.

Consideration of the mechanisms of deformation provides

---

(3) H. C. Heard, Effect of large changes in strain rate in the experimental deformation of Yule marble: Jour. Geology, v. 71, no. 2, 1963, p. 162-195

(4) Ibid., p. 181

clues to the expected rheological behavior of rocks. Single crystal experiments on deformation by twinning and gliding suggest that a minimum resolved shear stress is necessary to produce either twinning or gliding. On the other hand, consideration of the thermodynamic equilibrium of a non-hydrostatically stressed solid in contact with a fluid into which the solid may dissolve (5) indicates that recrystallization may take place under vanishingly small stresses. Microscopic observation of naturally deformed rocks commonly indicates that several mechanisms have operated in producing the observed deformation.

The third method of determining the rheological law, comparison of predicted and naturally observed deformations, is one of the objectives of the present study. If the predictions include the shape of the deformed body, then the mathematical method used must not assume this shape a priori. This restriction greatly complicates the mathematical problem and makes it difficult to consider any but the most simple rheological laws, such as linear viscosity and perfect plasticity.

Although the choice of a rheological law is an important hypothesis, it seems probable that many of the general features of the deformation are fixed by the overall geometry of the problem. In particular, the course of the deformation in the medium would probably be grossly similar whatever

---

(5) J. W. Gibbs, The scientific papers of J. Willard Gibbs: New York, Dover Publications, Inc., v. I, 1961, p. 184ff.

law were chosen, provided that the general succession of fold shapes were similar to that found in this study.

# CHAPTER V

## DISCRETE FORMULATION OF THE PROBLEM

An analytical solution of the problem formulated in Chapter III would be extremely difficult to find, and probably does not exist except in examples with simple geometries. Since the geometry of the folded layer is determined by the solution of the problem, a method applicable to a layer of relatively general shape must be used. We have chosen to set up the discrete analogue of the continuous problem of Chapter III; this discrete analogue leads to a set of linear algebraic equations which can be solved on a high-speed digital computer.

### 1. Outline of the discretization process

A general outline of the method of setting up the difference equations corresponding to a variational problem is found in Forsythe and Wasow (1), and a specific application to the equation of the thin elastic plate is discussed by Engeli et al. (2). An outline of the scheme employed in the present treatment follows.

---

(1) G. E. Forsythe and W. R. Wasow, Finite-difference methods for partial differential equations: New York, John Wiley and Sons, Inc., 1960, p. 182-184

(2) M. Engeli, T. Ginsburg, H. Rutishauser, and E. Stiefel, Refined iterative methods for computation of the solution and the eigenvalues of self-adjoint boundary-value problems: Basle, Birkhäuser, 1959

1) The velocity distribution is represented in terms of discrete values. The method of representation will be different for different portions of the region under consideration. In the medium itself the solution is represented in terms of the values of the stream function $\phi$ at the nodes of a square grid. On the plate it is represented by the values of the rate of change of inclination, $\dot{\theta}$ , at a set of points separated from each other by equal arc lengths. Finally, the trigonometric series which represents the continuation of the stream function $\phi$ out to infinity is represented by its value and normal derivative at grid points along the horizontal line where it is connected to the medium solution.

2) The derivatives in the dissipation formula, equation 6, are approximated by appropriate differences of the discrete values. The integrals are calculated by summing the squares of these differences, weighting each term according to the area associated with it in the grid.

3) The constraining relations which impose the proper velocity at the outer boundary of the region, as well as those which guarantee the matching of velocities at the plate and at the boundary between the grid region and its continuation to infinity can also be written as finite difference equations. These constraining equations are used to eliminate certain of the discrete values from the dissipation expression; this elimination process insures that any velocity distribution arising from the minimization process

will satisfy the constraining relations. The symmetry of the overall problem is introduced at this stage, so that the dissipation expression contains only those discrete values needed to describe the problem with its symmetry taken into account.

4) The dissipation expression, which is a sum of products of the discrete values, is differentiated in turn with respect to each unknown discrete value, and the resulting derivatives are set equal to zero. This process yields a set of linear algebraic equations for the discrete values. By the nature of the process by which these equations were obtained, their matrix is symmetric and either positive definite or positive semi-definite (3). The symmetric nature of the matrix is convenient, though not essential, for the method used to solve the equations; the definite character of the matrix is not used directly, but it can provide a useful check on the correctness of the matrix for any particular problem.

2. $\Phi$ on the square grid

We now proceed to illustrate this procedure by showing how it is used to derive equations for the various classes of unknowns. Points of the grid region may be divided into three groups: (1) regular points whose twelve nearest neighbors are inside the grid region, (2) points that lie within two mesh lengths of a plane boundary, and (3)

---

(3) Forsythe and Wasow, op. cit., p. 184

points that are adjacent to the layer. In what follows, $\phi$ at a given point refers to the $\phi_f$ of equation 3: the contribution of $\phi_a = \underline{K}\,\underline{x}\,\underline{y}$ is handled by adding a term $\underline{K}$ to the expression for $\phi_{,12}$ .

As the first illustration, consider a point in the interior of the medium. The compass-point notation of figure 3 will be used. The value of $\phi_{,12}$ at the center of mesh square O-E-NE-N may be represented as:

$$\frac{1}{\ell^2}\left(\phi_{NE} - \phi_N + \phi_o - \phi_E + K\right)$$

where $\underline{\ell}$ is the mesh spacing. The square of this expression, multiplied by $\underline{\ell^2}$, is taken as $\iint \phi_{,12}^2\, dx\, dy$ over this square. It is more convenient to evaluate $\phi_{,11} - \phi_{,22}$ at the center of a square of side $\underline{\ell}$ which is centered on a mesh intersection; thus for the square centered on the point E:

$$\iint (\phi_{,11} - \phi_{,22})^2 dx\, dy \approx \ell^2 \left[\frac{1}{\ell^2}(\phi_{EE} - 2\phi_E + \phi_o) - \frac{1}{\ell^2}(\phi_{NE} - 2\phi_E + \phi_{SE})\right]^2$$

$$= \frac{1}{\ell^2}\left(\phi_{EE} + \phi_o - \phi_{NE} - \phi_{SE}\right)^2 .$$

To derive the equation for the point O we take the derivative of the sum of the eight energy expressions which involve O; the contributions to this derivative from mesh-centered square E and from mesh square O-E-NE-N are:

$$\frac{\partial}{\partial \phi_o}\left(\iint 2\,\phi_{,12}^2\, dx\, dy\right) = \frac{4}{\ell^2}\left(\phi_{NE} - \phi_N + \phi_o - \phi_E + K\right) ,$$

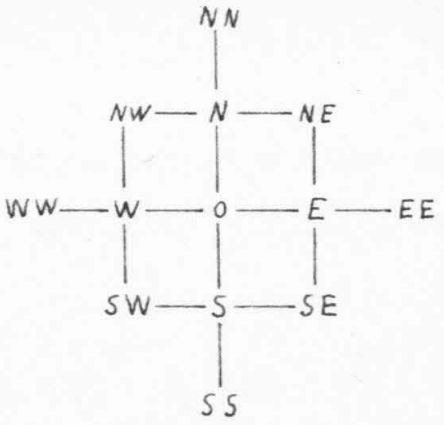


Figure 3.--Compass point notation for the grid points surrounding point 0.

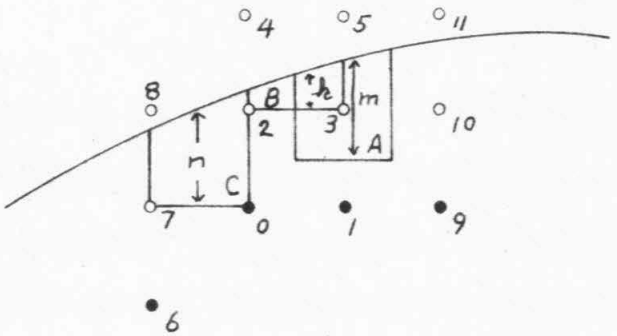


Figure 4.--Grid region adjacent to the plate.

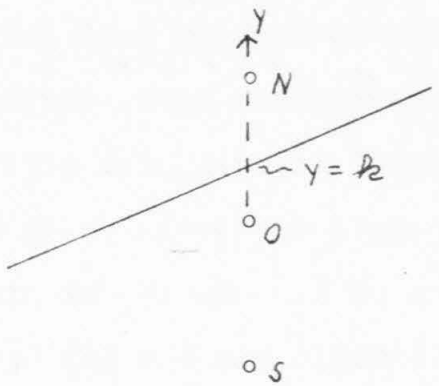


Figure 5.--Coordinate system for the elimination of grid points adjacent to the plate.

$$\frac{\partial}{\partial \phi_0}\left(\iint \tfrac{1}{2}(\phi_{,n}-\phi_{,s})^2\,dx\,dy\right) = \frac{1}{\ell^2}\left(\phi_{EE}+\phi_0-\phi_{NE}-\phi_{SE}\right) .$$

Adding the contributions from the other squares and setting the result equal to zero, the resulting equation for point 0 is:

$$20\,\phi_0 - 8\left(\phi_E+\phi_N+\phi_W+\phi_S\right)+2\left(\phi_{NE}+\phi_{NW}+\phi_{SW}+\phi_{SE}\right)$$

$$+\left(\phi_{EE}+\phi_{NN}+\phi_{WW}+\phi_{SS}\right) = 0 .$$

The left-hand side of this equation is the standard biharmonic difference operator; it is usually derived directly from the differential equation (4). Since the expression for $\phi_c$ satisfies the biharmonic equation identically, the $K$ term cancels out.

Next, consider the case where the velocities perpendicular and parallel to a given mesh line are constrained to have certain values; this is equivalent to constraining $\phi$ and $\phi_{,n}\left(=\frac{\partial\phi}{\partial n}\right)$. This mesh line is taken to be NW-N-NE in figure 3, and the given value and slope are denoted $\Phi$ and $\Phi_{,2}$ . The points NW, N, NE, and NN are considered to be "fictitious points" (5) and are eliminated from the

---

(4) F. S. Shaw, An introduction to relaxation methods: New York, Dover Publications, Inc., 1953, p. 39

(5) Ibid., p. 197

dissipation expressions using the relations:

$$\Phi_{NW} = \bar{\Phi}(NW)$$

$$\Phi_{N} = \bar{\Phi}(N)$$

$$\Phi_{NE} = \bar{\Phi}(NE)$$

$$\frac{\Phi_{NN} - \Phi_{o}}{2\ell} = \Phi_{,2}(N).$$

$\bar{\Phi}(NW)$, etc., are the given values at the point NW, etc. If mesh line NW-N-NE represents either the boundary between two regions where the velocity distribution has different representations or an external boundary on which velocities are given, there is one further change to be made in the dissipation expressions. In this case, the dissipation over half the mesh-centered square centered on point N is to be considered, so that the resulting expression is multiplied by $\ell^2/2$ instead of by $\underline{\ell^2}$. Therefore, the dissipation expressions for mesh square O-E-NE-N and for mesh-centered square N become:

$$\int\int 2\,\Phi_{,12}^{2}\,dx\,dy = \frac{2}{\ell^2}\left(\bar{\Phi}(NE) - \bar{\Phi}(N) + \Phi_{o} - \Phi_{E} + K\right)^2$$

$$\int\int \tfrac{1}{2}\left(\Phi_{,11} - \Phi_{,22}\right)^2 dx\,dy = \frac{1}{4\ell^2}\left[\bar{\Phi}(NE) + \bar{\Phi}(NW) - 2\Phi_{o} - 2\ell\,\bar{\Phi}_{,2}(N)\right]^2$$

Proceeding as outlined above for a regular point, we obtain the equation for point O:

$$21\phi_0 - 8(\phi_E + \phi_W + \phi_S) + 2(\phi_{SW} + \phi_{SE}) + (\phi_{EE} + \phi_{WW} + \phi_{SS})$$
$$+ 2[\Phi(NE) + \Phi(NW)] - 8\Phi(N) + 2\ell\,\Phi_{,x}(N) = 0.$$

As before, this equation is identical to what would be derived from the differential equation treatment. The variational method gives equations which differ from those derived from the differential equations only at points near a boundary that does not coincide with a mesh line.

In the present problem $\underline{u}_t$ is constrained to be zero and $\underline{v}_t$ remains arbitrary at the right- and left-hand walls (fig. 1, p. 23). If the right-hand wall coincides with SE-E-NE, then $\Phi$ at points SE, E, and NE must be set equal to zero in the dissipation expressions. Taking the derivative of the dissipation expression with respect to $\phi_{EE}$, we get an equation for $\phi_{EE}$:

$$\phi_{EE} + \phi_0 = 0.$$

Because this equation is so simple, it is convenient to use it to eliminate points such as EE from the system of equations before solving the system.

3. Trigonometric $\phi$

Equation 7 illustrates the way in which the values and slopes of the trigonometric series enter into the equations of mesh points near the top boundary of the mesh region. To derive equations for the values and slopes themselves we must consider the dissipation due to the

trigonometric series. Since the trigonometric series is to be represented in terms of a finite number of values and slopes, the sums must be truncated. Substituting the appropriate derivatives of the truncated series into equation 4, this dissipation may be written as:

$$\int_0^{\infty}\int_{-\frac{L_x}{4}}^{\frac{L_x}{4}}\left[\frac{1}{2}\left(\Phi_{j,11}-\Phi_{j,22}\right)^2+2\,\Phi_{j,12}^2\right]dx\,dy' =$$

$$\int_0^{\infty}\int_{-\frac{L_x}{4}}^{\frac{L_x}{4}}\left\{\frac{1}{2}\left[2\sum_{i=1}^{N}(2i-1)\frac{2\pi}{L_x}\left((2i-1)\frac{2\pi}{L_x}A_i-B_i+(2i-1)\frac{2\pi}{L_x}B_i y'\right)e^{-(2i-1)\frac{2\pi}{L_x}y'}\cos(2i-1)\frac{2\pi}{L_x}x\right.\right.$$

$$\left.+2\sum_{i=1}^{N-1}2i\frac{2\pi}{L_x}\left(2i\frac{2\pi}{L_x}C_i-D_i+2i\frac{2\pi}{L_x}D_i y'\right)e^{-2i\frac{2\pi}{L_x}y'}\sin 2i\frac{2\pi}{L_x}x\right]^2$$

$$+2\left[-\sum_{i=1}^{N}(2i-1)\frac{2\pi}{L_x}\left(B_i-(2i-1)\frac{2\pi}{L_x}A_i-(2i-1)B_i y'\right)e^{-(2i-1)\frac{2\pi}{L_x}y'}\sin(2i-1)\frac{2\pi}{L_x}x\right.$$

$$\left.\left.+\sum_{i=1}^{N-1}2i\frac{2\pi}{L_x}\left(D_i-2i\frac{2\pi}{L_x}C_i-2i\frac{2\pi}{L_x}D_i y'\right)e^{-2i\frac{2\pi}{L_x}y'}\cos 2i\frac{2\pi}{L_x}x+K\right]^2\right\}dx\,dy'.$$

This expression can be simplified as follows. We note that the cross product terms between trigonometric terms of different wave lengths will give integrals of the form:

$$\int_{-\frac{\pi}{2}}^{\frac{\pi}{2}}\sin nz\sin mz\,dz=\left[\frac{\sin(m-n)z}{2(m-n)}-\frac{\sin(m+n)z}{2(m+n)}\right]\Bigg|_{-\frac{\pi}{2}}^{\frac{\pi}{2}},$$

$$\int_{-\frac{\pi}{2}}^{\frac{\pi}{2}}\cos nz\cos mz\,dz=\left[\frac{\sin(m-n)z}{2(m-n)}+\frac{\sin(m+n)z}{2(m+n)}\right]\Bigg|_{-\frac{\pi}{2}}^{\frac{\pi}{2}},$$

and

$$\int_{-\frac{\pi}{2}}^{\frac{\pi}{2}} \cos hz \sin lz \, dz = -\left[ \frac{\cos(h-l)z}{2(h-l)} + \frac{\cos(h+l)z}{2(h+l)} \right] \Bigg|_{-\frac{\pi}{2}}^{\frac{\pi}{2}} .$$

The first two types of integral will give zero as a result, since $m$ and $n$ are either both even or both odd. The third type is zero, since here $h$ and $l$ are respectively even and odd or odd and even. In addition, the product of either the sine or the cosine term with $K$ will give zero on integration from $-L_x/4$ to $L_x/4$ .

Therefore, the different wavelengths do not interact with each other or with the uniform compression term (involving $K$). When the individual wavelengths are considered separately, a further simplification results, for the dissipation is then independent of $X$. Writing $(2i-1)\frac{2\pi}{L_x}$ or $2i\frac{2\pi}{L_x}$ as $\lambda_i$ , the dissipation becomes:

$$\frac{1}{2}\left[2\lambda_i(\lambda_i A_i - B_i + \lambda_i B_i y')e^{-\lambda_i y'}\cos\lambda_i x\right]^2 + 2\left[\lambda_i(B_i - \lambda_i A_i - \lambda_i B_i y')e^{-\lambda_i y'}\sin\lambda_i x\right]^2$$

$$= 2\lambda_i^2 e^{-2\lambda_i y'}\left[A_i\lambda_i - B_i + \lambda_i B_i y'\right]^2\left[\cos^2\lambda_i x + \sin^2\lambda_i x\right]$$

$$= 2\lambda_i^2 e^{-2\lambda_i y'}\left[A_i\lambda_i - B_i + \lambda_i B_i y'\right]^2$$

When the integration over $y'$ is carried out, the dissipation may be written as:

$$\int_0^{\infty}\int_{-\frac{L_x}{4}}^{\frac{L_x}{4}}\left[\frac{1}{2}(\phi_{,11} - \phi_{,22})^2 + 2(\phi_{,12})^2\right] dx\, dy' =$$

$$\frac{L_x}{4}\left\{ \sum_{i=1}^{N} (2i-1)\frac{2\pi}{L_x}\left[ B_i^2 - 2(2i-1)\frac{2\pi}{L_x}A_iB_i + 2\left((2i-1)\frac{2\pi}{L_x}A_i\right)^2 \right] \right.$$

$$\left. + \sum_{i=1}^{N-1} 2i\,\frac{2\pi}{L_x}\left[ D_i^2 - 4i\,\frac{2\pi}{L_x}C_iD_i + 2\left(2i\,\frac{2\pi}{L_x}C_i\right)^2 \right] \right\} \tag{8}$$

$$= \frac{L_x}{4}\left\{ \sum_{i=1}^{N} (2i-1)\frac{2\pi}{L_x}\left[ \left(B_i - (2i-1)\frac{2\pi}{L_x}A_i\right)^2 + \left((2i-1)\frac{2\pi}{L_x}A_i\right)^2 \right] \right.$$

$$\left. + \sum_{i=1}^{N-1} 2i\,\frac{2\pi}{L_x}\left[ \left(D_i - 2i\,\frac{2\pi}{L_x}C_i\right)^2 + \left(2i\,\frac{2\pi}{L_x}C_i\right)^2 \right] \right\} .$$

The last rearrangement of terms shows that the integrated dissipation can be written in terms of the combinations of constants which represent the value and slope of each trigonometric term at the line $\underline{y' = 0}$ .

This last expression defines the dissipation in terms of the coefficients of the trigonometric expansion. For reason of convenience in the solution of the equations, the velocity distribution in this region is represented in terms of values, $\Phi$ , and slopes $\Phi_{,2}$ , at the mesh points on the lower boundary of the region. To derive the equations for these values and slopes considered as unknowns, we must first express the dissipation in terms of the values and slopes. In practice it is simpler to derive expressions for $A_i$, $B_i$ , $C_i$ , and $D_i$ in terms of sums of $\Phi$ and $\Phi_{,2}$ and then use the chain rule to compute the derivatives of the

dissipation expression with respect to individual slopes and values.

The process used to find these sums is similar to that used to derive the coefficients for a finite Fourier series (6); it makes use of the fact that sine and cosine functions are orthogonal over a discrete set of points. We shall illustrate the process for a particular $A_i$, for example $A_k$. $\phi$ for a particular point on the boundary ($y' = 0$) can be written as:

$$\phi_j = \sum_{i=1}^{N} A_i \cos(2i-1)\frac{2\pi}{L_x} X_j + \sum_{i=1}^{N-1} C_i \sin 2i \frac{2\pi}{L_x} X_j ,$$

where $X_j$ is the x-coordinate of the point corresponding to $\phi_j$ and $L_x = 4N$ is the wavelength of the fold. The corresponding equation for each $\phi_j$ is multiplied by $\cos(2k-1)\frac{2\pi}{L_x} X_j$, and the resulting equations are summed over $j$:

$$\sum_{j=1}^{2N} \phi_j \cos(2k-1)\frac{2\pi}{L_x} X_j =$$

$$\sum_{i=1}^{N} A_i \left[ \sum_{j=1}^{2N} \cos(2i-1)\frac{2\pi}{L_x} X_j \cos(2k-1)\frac{2\pi}{L_x} X_j \right]$$

$$+ \sum_{i=1}^{N-1} C_i \left[ \sum_{j=1}^{2N} \sin 2i \frac{2\pi}{L_x} X_j \cos(2k-1)\frac{2\pi}{L_x} X_j \right] .$$

The second inner sum is zero for all $k$ and $i$, since

---

(6) R. W. Hamming, Numerical methods for scientists and engineers: New York, McGraw-Hill Book Co., Inc., 1962, p. 67-77

$\sin 2i\frac{2\pi}{L_x}X_i$ is zero for $i = N$ and $i = 2N$, and the terms for all the other $i$ cancel each other (if $k < N$, $X_k = (-N+k) = -(N-k) = X_{2N-k}$). The first inner sum may be written as:

$$\frac{1}{2}\sum_{i=1}^{2N} \cos(2k+2i-2)\frac{2\pi}{L_x}X_i + \cos(2i-2k)\frac{2\pi}{L_x}X_i \quad .$$

Now, it can be shown (7) that:

$$\sum_{i=1}^{2N} \cos\frac{m\pi}{N}(i-N) = 0 \quad , \quad 0 < m < 2N$$

$$= 2N \quad , \quad m = 0 \quad .$$

Therefore, the final result is:

$$\sum_{i=1}^{2N} \Phi_i \cos(2k-1)\frac{2\pi}{L_x}X_i = N A_k \quad .$$

Analogous manipulations with the expressions for the slope at a given $X_i$ lead to the following expressions for the $A_k$, $B_k$, $C_k$, and $D_k$ in terms of slopes and values at points on the boundary:

$$A_k = \frac{1}{N}\sum_{i=1}^{2N} \Phi_i \cos(2k-1)\frac{2\pi}{L_x}X_i$$

$$B_k = \frac{1}{N}\sum_{i=1}^{2N} \Phi_{i,2} \cos(2k-1)\frac{2\pi}{L_x}X_i + (2k-1)\frac{2\pi}{L_x}\frac{1}{N}\sum_{i=1}^{N} \Phi_i \cos(2k-1)\frac{2\pi}{L_x}X_i$$

---

(7) H. B. Dwight, Tables of integrals and other mathematical data: New York, The Macmillan Co., 2nd ed. rev., 1947, formula 420.4, p. 86

$$C_k = \frac{1}{N} \sum_{i=1}^{2N} \Phi_i \sin 2k \frac{2\pi}{L_x} X_i$$

$$D_k = \frac{1}{N} \sum_{i=1}^{2N} \Phi_{i,2} \sin 2k \frac{2\pi}{L_x} X_i + 2k \frac{2\pi}{L_x} \frac{1}{N} \sum_{i=1}^{2N} \Phi_i \sin 2k \frac{2\pi}{L_x} X_i .$$

Using these expressions, terms such as $\frac{\partial A_i}{\partial \Phi_j}$ can be calculated. If we denote the dissipation expression for this region by $\underline{I}_\infty$, the contributions from this region to the equations for the slopes and values on the boundary can be written:

$$\sum_{i=1}^{N} \left[ \frac{\partial I_\infty}{\partial A_i} \frac{\partial A_i}{\partial \Phi_j} + \frac{\partial I_\infty}{\partial B_i} \frac{\partial B_i}{\partial \Phi_j} \right] + \sum_{i=1}^{N-1} \left[ \frac{\partial I_\infty}{\partial C_i} \frac{\partial C_i}{\partial \Phi_j} + \frac{\partial I_\infty}{\partial D_i} \frac{\partial D_i}{\partial \Phi_j} \right] . \quad (9)$$

The complete equations for these unknowns are obtained by adding the contributions from the mesh squares just below the boundary to those from $\underline{I}_\infty$.

4. $\Phi$ near the plate

The procedure used to match the velocity in the medium near the plate with that of the plate is similar to that used at the junction of the grid portion of the medium with the continuation out to infinity, but it is complicated by the fact that the plate may intersect the grid lines at points other than mesh points. The description is broken into two parts: in the first we shall show how the constraint

is applied if we assume that values of $\phi$ and its first derivatives are known at every point on the plate; in the second we shall show how $\phi$ and its derivatives on the plate can be expressed in terms of the $\dot{\theta}$ values at a given number of equally spaced positions along the plate.

Consider a representative portion of the plate and medium as shown in figure 4 (p. 51); we shall deal with the medium below the plate. The portions of the dissipation given by $\frac{1}{2}(\phi_{,y} - \phi_{,x2})^2$ and $2\phi_{,z}^2$ evaluated for curvilinear trapezoidal areas like A, B, and C can be expressed in terms of values of $\phi$ at nearby points. It is assumed that $\phi$ near the plate varies quadratically with $x$ or $y$; a cubic or even higher order variation could be assumed, but the dissipation expressions would be more complicated. With this assumption the values of $\phi$ at the points marked with open circles can be expressed in terms of $\phi$ and its first derivatives on the plate and $\phi$ at the points marked with solid circles. The values of $\phi$ at the open-circled points are now eliminated from the dissipation expressions. This elimination insures that only velocity distributions which match at the plate will be considered in the minimumization process.

Since these open-circled points occur only in dissipation expressions for areas adjacent to the plate, they can be eliminated when these expressions are derived. Referring to figure 5 (p. 51), $\phi$ and $\phi_{,z}$ at any point on the line S-O-N are, on the assumption of quadratic variation

with $\underline{y}$ :

$$\Phi = \phi_0 + \frac{\phi_N - \phi_S}{2} y + \frac{\phi_E - 2\phi_0 + \phi_W}{2} y^2$$

$$\phi_{y/2} = \frac{\phi_N - \phi_S}{2} + (\phi_S - 2\phi_0 + \phi_N)\, y \qquad (10)$$

With these expressions $\phi_{y/2}$ at any point on the vertical bisector of square 2-3-5-4 (fig. 4) becomes:

$$\phi_{y/2}(Y) = \tfrac{1}{2}(Y-1)(\phi_1 - \phi_0) - Y(\phi_3 - \phi_2) + \tfrac{1}{2}(Y+1)(\phi_5 - \phi_4) .$$

If we denote by $\Delta\phi(\underline{y})$ the difference between $\Phi$ on the line 1-3-5 and $\Phi$ on the line 0-2-4 at any height above the base 2-3 ( $\Delta\phi(Y) \approx \frac{\partial\phi}{\partial x}\Big)_y$ and is determined from the velocity of the plate), then:

$$\Delta\phi(Y) = \frac{Y}{2}(Y-1)(\phi_1 - \phi_0) + (1-Y^2)(\phi_3 - \phi_2) + \frac{Y}{2}(Y+1)(\phi_5 - \phi_4) . \qquad (11)$$

Eliminating $\phi_4$ and $\phi_5$ from the expression for $\phi_{y/2}$ with $\underline{Y} = \pm 1/2$ by means of relation 11:

$$\phi_{y/2}\left(\frac{h}{2}\right) = \frac{1}{h}\left[\Delta\phi(h) - (\phi_3 - \phi_2)\right] . \qquad (12)$$

Following the same procedure with area C and its associated points 0, 2, 4, 6, 7, and 8, we arrive at the analogous expression:

$$\phi_{y/2}\left(\frac{\ell}{2}\right) = \frac{1}{\ell}\left[\Delta\phi(\ell) - (\phi_0 - \phi_7)\right] .$$

The dissipation expression for a $(\phi_{y/1} - \phi_{y/2})$ area like area A is derived as follows. $\phi_{y/2}$ for the point 0

in figure 5 is given by:

$$\phi_{,22} = \phi_N - 2\phi_o + \phi_s$$

The quadratic expression for the slope at $\underline{y} = \underline{h_2}$ is used to eliminate $\phi_N$ in this expression for $\phi_{,22}$, giving the curvature:

$$\phi_{,22} = \frac{1}{h_2 + \frac{1}{2}} \left[ \phi_{,2}(h_2) - \phi_o + \phi_s \right] \qquad (13)$$

If $\phi_{,11}$ cannot be written in terms of points inside the plate, it is calculated by an analogous expression.

When the slope of the plate is greater than 45°, curvilinear trapezoids with vertical rather than horizontal bases are taken; otherwise the dissipation would be averaged over areas that are too large. In the region where the slope passes through 45°, minor adjustments are necessary in the method of assigning the area weights to the dissipation expressions.

Using formulas of the types just developed we may write down dissipation expressions for all areas adjacent to the plate. These expressions will involve only points on the same side of the plate as the area itself. To eliminate the elimination points inside the plate, we solve equations 10 for $\phi_o$ in terms of $\phi$ and $\phi_{,2}$ at $\underline{y} = \underline{h_2}$ and use the resulting equation to eliminate the elimination point in every dissipation expression in which it occurs (this includes both regular and irregular expressions).

(Expressions like 12 and 13 can be derived without introducing fictitious points. Since the resulting dissipation expressions involve both $\phi_{,1}$ and $\phi_{,2}$ of the plate, it might be thought that the use of these expressions would in itself provide sufficient constraint to insure the matching of velocities without eliminating points inside the plate. When the problem is set up and solved in this fashion it is found that the resulting velocities in the medium match those of the plate to a first approximation, but that velocity gradients near the plate are abnormally high. In terms of fictitious points this partial matching corresponds to matching a linear combination of $u$ and $v$ at the plate rather than matching $u$ and $v$ separately. In certain simple situations like the compression of a homogeneous medium between plane, parallel, frictionless walls, the partial matching leads to the correct result. With a more complicated curved boundary like that of the present problem, the constraints on the matching of velocities are only approximately satisfied.)

5. Center of symmetry

The method used to impose the center of symmetry on the problem is similar to that used to impose the velocity constraints. The origin of the coordinate system in the medium is taken to coincide with the inflection point of the folded plate. Dissipation is calculated only for the region $y$ greater than zero. Certain mesh points with negative

$y$-coordinates will still occur in the dissipation expressions, but due to the center of symmetry, $\phi$ at points with negative $y$ is identically equal to $\phi$ at the symmetry-related point with positive $y$. Whenever a point with negative $y$ occurs in a dissipation expression, the appropriate point with positive $y$ is substituted for it. This procedure insures the satisfaction of the symmetry condition.

6. $\dot{\theta}$ terms

Up to now we have considered the value of $\phi$ and its first derivatives to be given quantities on the plate. This means that the above treatment is immediately applicable to a curved boundary on which the velocity is given. In our particular problem, the velocity of the plate is not known beforehand, but rather is one of the pieces of information which must be provided by the solution itself. $u$, $v$, and $\phi$ of the plate can be calculated from the $\dot{\theta}$ values for the plate by means of the following relations:

$$u = -\int_0^s \dot{\theta} \sin\theta \, ds$$

$$v = \int_0^s \dot{\theta} \cos\theta \, ds \qquad (14)$$

$$\phi = \int_S^s \left( \frac{\partial \phi}{\partial x}\frac{dx}{ds} + \frac{\partial \phi}{\partial y}\frac{dy}{ds} \right) ds = \int_S^s (u\sin\theta - v\cos\theta)\, ds$$

At the inflection point $s = 0$, and at the crest $s = S$.

If we use numerical integration formulas to replace these relations by discrete sums of $\dot{\theta}$ values, then the dissipation expressions for areas that contained points to be eliminated will now include a series of coefficients of the $\dot{\theta}$ unknowns.

The $\dot{\theta}$ values are not all independent; they must be chosen such that their integral gives the proper value of $\underline{u}$ at the crest of the fold. This value of $\underline{u}$ can be written in terms of the discrete values as:

$$u_B = -\int_0^S \dot{\epsilon} \sin\theta \, ds = -\Delta s \left\{ \frac{\dot{\theta}_0}{2} \sin\theta_0 + \sum_{i=1}^{9} \dot{\theta}_i \sin\theta_i \right\}, \quad (15)$$

where $\Delta \underline{s}$ is the arc-length spacing of the $\dot{\theta}$ values. The next-higher-order terms in this quadrature formula (8) are zero at both ends of the range of integration, since $\theta$ and $\dot{\theta}$ are zero at the crest of the fold and $\frac{d\theta}{ds}$ and $\frac{d\dot{\theta}}{ds}$ are zero at the symmetry point on the limb. To insure the satisfaction of constraint, we use the constraining relation to eliminate $\dot{\theta}_0$ from any dissipation expression in which it occurs.

The final dissipation expression which must be considered is the bending dissipation of the plate itself. This can be written in terms of the discrete $\dot{\theta}$ values as:

$$\frac{\mu_p h^3}{6} \int_0^S \left(\frac{d\dot{\theta}}{ds}\right)^2 ds = \frac{\mu_p h^3}{6\Delta s} \left[ \sum_{i=1}^{10} \left( \dot{\theta}_i - \dot{\theta}_{i-1} \right)^2 \right] \quad (16)$$

---

(8) Hamming, op. cit., p. 57

where $\underline{h}$ is the thickness of the plate. As in the expression for $\underline{u}_B$, the first difference corrections to this sum are zero at both ends of the range of integration. Before the derivatives of this expression with respect to the $\dot{\theta}$ values are taken, $\dot{\theta}_o$ must be eliminated from it in order to satisfy the constraint on $\underline{u}_B$ at the crest of the fold.

7. Summary

Since the method of deriving the difference equations is complicated by the number of special details that must be considered, the main steps in the method are outlined in this section.

1) The dissipation over the whole problem region is expressed as a sum of squares of differences of the discrete values. Contributions from the grid region to this sum of squares are of four types:

$$(\phi_E + \phi_W - \phi_N - \phi_S)^2$$

for a normal mesh-centered square (fig. 3),

$$(\phi_{NE} - \phi_{NW} + \phi_o - \phi_W)^2$$

for a normal mesh square (fig. 3),

$$\frac{1}{h^2}\left[\Delta\phi(h) - (\phi_3 - \phi_2)\right]^2$$

for a mesh-centered trapezoid adjacent to the plate (fig. 4), and

$$\left[ \phi_{10} - 2\phi_3 + \phi_2 - \frac{\phi_{,2}(m) - (\phi_3 - \phi_1)}{m + \frac{1}{2}} \right]^2$$

for a mesh trapezoid adjacent to the plate (fig. 4). Each of these terms must be weighted by its appropriate area. The dissipation for the region extending out to infinity is given by equation 8 and that for the plate by equation 16.

2) The $\phi$ values for all grid points closer than one mesh length to the plate, those for grid points with negative y-coordinates, and $\dot{\theta}_0$ are now eliminated from the dissipation expressions. This elimination is performed using equations 10, the discrete analogues of equations 14, the symmetry condition, and equation 15.

3) The equation for each unknown value is derived by differentiating the sum of squares with respect to that value and setting the result equal to zero.

In the actual numerical computation of the equations, explicit expressions for the various types of equations are never derived. The various terms in the sum of squares are computed and stored in appropriately tagged memory locations in the computer storage. All the terms are then scanned by the program and the elimination (step 2) is performed. The terms are scanned once more to perform the differentiation (step 3). Since the variety of equation types is larger than the variety of dissipation expressions, this automation of intermediate algebraic steps eases the task of programming the equation-derivation routine considerably.

The input data for computation of the velocity distribution at any stage consist of: (1) the shape of the folded layer at this stage, given as a series of eleven $\theta_i$, and (2) constants which define the grid spacing and boundary velocity at this stage. The output data are a set of $\phi$ values at the grid points and the $\dot{\theta}_i$ values at intervals on the plate; the $\phi$ values that have been eliminated and the value of $\dot{\theta}_0$ can be retrieved using the same relations by which these quantities were eliminated in the derivation of the equations.

8. Discretization of the time variable

The method discussed above yields a set of equations for the velocity distribution of a folding layer at the instant of time when the layer has a given shape. In order to study the development of a fold as a function of time, it is necessary to take into account the changing shape of the layer.

To start the study of a particular fold we assume the shape of the folded layer at a low amplitude stage. Using the equations derived above, the $\dot{\theta}_i$ on the plate can be found. On the basis of these $\dot{\theta}_i$ we can predict the average velocity of the plate over a certain interval of time. These average $\dot{\theta}_i$ are multiplied by a constant, $\Delta t$, and the resulting $\Delta \theta_i$ are added to the original $\theta_i$ to give the new shape of the layer. Since the magnitudes of the $\dot{\theta}_i$ (as distinct from their relative values) are determined only by the given rate of shortening, $\Delta t$ can be

picked in any convenient manner. Its size determines the extent to which the shape will change for the next computation. $\Delta t$ was chosen so that the increase in the dip of the symmetry point on the limb, $\Delta \theta_o$ , would be a specified number of degrees. The velocity distribution for the resulting new shape is then calculated, and the process is repeated until the fold has the desired final amplitude (9).

When the relative magnitudes of the $\dot{\theta}$ values do not change too rapidly from stage to stage, the $\dot{\theta}$ values at the beginning of the time interval are sufficiently close to their average over the time interval involved to be used to calculate the next shape. Comparison of the $\dot{\theta}$ distribution of the new shape with that of the previous shape places limits on the error involved in using the $\dot{\theta}$ values of the previous shape. With suitable decrease of the time step as the fold amplitude increased, this procedure was used for all but the last time step of the dominant-wavelength fold.

During the computation of the weak-plate fold, it became eveident that a very short time step would be needed unless a more accurate way of estimating the average velocity of the plate over each time interval were devised. It was found that, with a suitable representation of the $\dot{\theta}$

---

(9) The equation-derivation routine was designed to compute the equations for a layer with a maximum dip less than $90^{\circ}$. Extension to overturned dips would not require modification of the method of deriving the equations, but it would require changes in the computer program.

distribution, it was possible to predict fairly accurately what the plate velocity distribution of the new shape would be before it was actually computed. Using this predicted velocity distribution, it was then possible to choose a suitable time average of the $\dot{\theta}_i$ in order to compute the new shape. The representation of the velocity distribution, the method of predicting the new velocity distribution, and the accuracy of the method are discussed in Chapter VII, Section 5.

# CHAPTER VI

## SOLUTION OF THE EQUATIONS BY DIGITAL COMPUTER

### 1. Choice of method

The choice of an equation-solution method cannot be divorced from the consideration of such computational details as the form of the matrix, the type of computer available, and the precise storage requirements of the solution routine. The equations were solved on an IBM 7090 computer with 32,000 words of random-access memory and magnetic-tape auxiliary storage. Typical computation times were two minutes for a system of 175 equations and five minutes for a system of 285 equations.

A large system of linear algebraic equations such as that arising from the discretization of the problems of this study may be solved by either direct or iterative methods. A direct method is one which gives the solution as a result of a finite number of arithmetic operations; if there were no round-off error this solution would be exact. An iterative method consists of the repeated application of a simple algorithm; the exact solution is obtained only as the limit of a sequence of successive approximations.

Iterative methods are most commonly used for the solution of equations arising from the discretization of an elliptic partial differential equation; their most important

advantage is that they do not require storage of the whole matrix of equations, but only the non-zero coefficients. The Gauss-Seidel method with successive over-relaxation (1) was applied to a biharmonic difference problem during the course of this study. It was found that the rate of convergence of the iterative process was so slow that computation times would be unreasonably high. There were two alternative methods: (1) a more complicated iterative method which might provide more rapid convergence, or (2) a direct method of solution which could be adapted to machine storage requirements.

The particular direct elimination scheme used for the solution of the equations is discussed in detail below. The critical features of the method are: (1) with a suitable arrangement of the order in which the equations are solved, most of the zero elements of the original matrix remain zero throughout the elimination process and therefore need not be stored; (2) those elements of the matrix which must be stored are not all needed at any given stage of the elimination process and, therefore, magnetic tapes can economically be used for intermediate storage of results. The accumulated effects of round-off error may also present an obstacle to the use of a direct method for a large system of equations; this aspect will be discussed below, but it did not cause serious difficulty in the problems treated.

---

(1) G. E. Forsythe and W. R. Wasow, Finite-difference methods for partial differential equations: New York, John Wiley and Sons, Inc., 1960, p. 242-266

2. Method adopted

The method adopted was the "Doolittle method", a variant of Gaussian elimination which does not rearrange the equations in order to select the largest pivot for elimination (2). We shall sketch its application to the particular form of matrix arising in this study. The equations are numbered in the following order: first, the equations for $\phi$ values at the grid points, with the center-of-symmetry point first, and then proceeding from left to right and from bottom to top through the grid; second, the values of the trigonometric-continuation $\phi$ -function and then the slope values, each taken in order from left to right; and finally, the $\dot{\theta}$ values, taken consecutively from the inflection point to the crest of the fold. Any points which are eliminated in the constraining process during the derivation of the equations are simply omitted in this numbering scheme. If this scheme is followed, then all the non-zero elements of the matrix occur either in a band on both sides of the diagonal or in a vertical strip at the right side of the matrix--and a symmetric horizontal strip along the bottom of the matrix (fig. 6). Since the matrix is symmetric and remains symmetric during the elimination process, only the elements above and on the diagonal need be stored. If there are $N$ grid spacings between the right- and left-hand walls in the problem, the band will contain $2N+1$ elements

(2) Modern computing methods: New York, Philosophical Library, Inc., 2d ed., 1961, p. 7

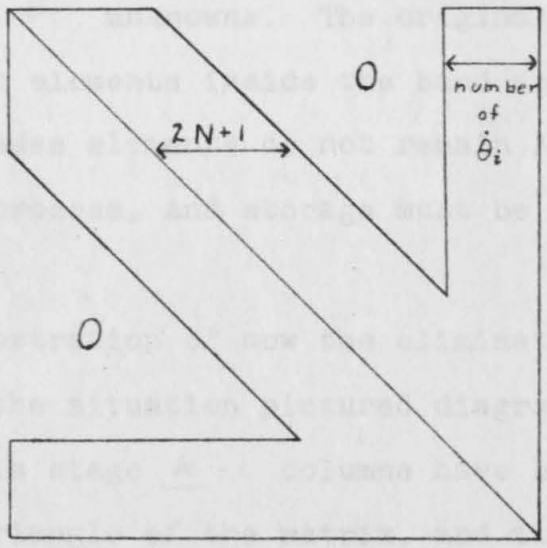


Figure 6.--Arrangement of the matrix.

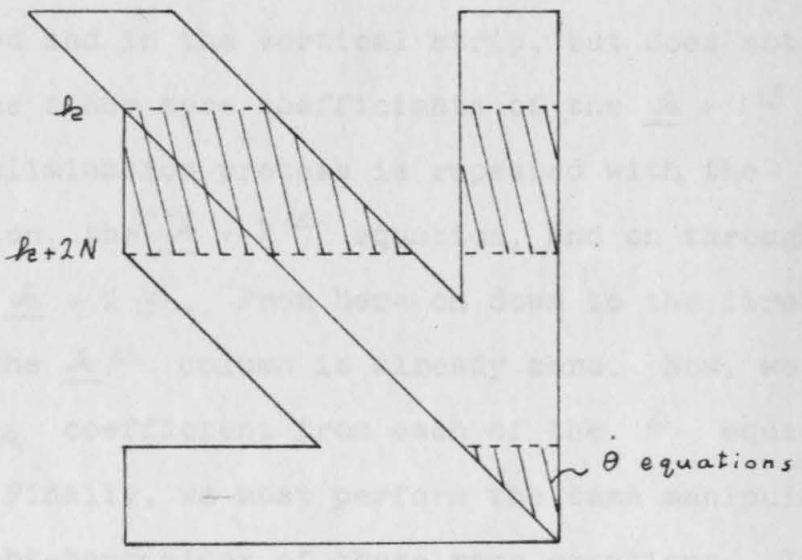


Figure 7.--Arrangement of the matrix when the $\ell_2^{th}$ column is about to be eliminated.

above and on the diagonal; the width of the strip is equal to the number of $\dot{\theta}$ unknowns. The original matrix will contain many zero elements inside the band and the strip; unfortunately, these elements do not remain zero during the elimination process, and storage must be allotted for them.

As an illustration of how the elimination process works, consider the situation pictured diagrammatically in figure 7. At this stage $k-1$ columns have been eliminated from the lower triangle of the matrix, and the $k^{th}$ column is about to be eliminated. We eliminate the $X_k$ coefficient from the $k+1^{st}$ equation by subtracting $\frac{A_{k,k+1}}{A_{k,k}}$ times the $k^{th}$ equation from the $k+1^{st}$ equation; this changes the coefficients of the $k+1^{st}$ equation both in the diagonal band and in the vertical strip, but does not affect any of the other zero coefficients of the $k+1^{st}$ equation. The elimination process is repeated with the $k+2^{nd}$ equation, the $k+3^{rd}$ equation, and on through equation number $k+2N$. From here on down to the first $\dot{\theta}$ equation, the $k^{th}$ column is already zero. Now, we eliminate the $X_k$ coefficient from each of the $\dot{\theta}$ equations in turn. Finally, we must perform the same manipulations on the right-hand sides of these same equations. It is clear from the nature of the elimination routine that only $2N+1$ equations and the coefficients linking the $\dot{\theta}$ unknowns need be in random-access memory at any given stage. Once the matrix is reduced to upper-triangular form, the

back substitution process is the standard one (3). During the back substitution the current row of the triangular matrix and those unknowns that have been found up to that stage are needed in random-access memory.

In terms of the number of arithmetic operations involved, the formation of the upper triangular matrix is the major part of the process. If it were desired, the same system of equations could be solved with several different right-hand sides with only slightly greater effort. This feature, common to all the triangular resolution direct methods, can be used to advantage in improving the accuracy of the solution. To do this we use the following technique (4). If $\underline{X}^{(1)}$ is the computed solution to the system of equations $\underline{A}\,\underline{x} = b$, and the residual $\underline{r}^{(1)}$ is defined by $\underline{r}^{(1)} = \underline{b} - \underline{A}\,\underline{x}^{(1)}$, then we have: $\underline{A}(\underline{x} - \underline{x}^{(1)}) = \underline{r}^{(1)}$. To solve this new set of equations, we need only perform the forward course on the residuals $\underline{r}^{(1)}$ and back-substitute. If the result of this second back-substitution is denoted by $\underline{X}^{(2)}$, then $\underline{x}^{(1)} + \underline{X}^{(2)}$ is a much closer approximation to the true solution. Residuals are now computed for this second approximation to the solution, and the process is repeated until the corrections are less than the desired degree of accuracy. Since the residuals are much smaller than the original right-hand sides, the process converges

---

(3) Ibid., p. 8

(4) Ibid., p. 19

rapidly. In most of the cases computed in the present study, the second corrections were already negligible. The process not only provides a simple means of improving the accuracy of a solution, but it gives a much more reliable measure of the accuracy of the final solution than would the residuals alone. For the process to be effective, the residuals must be known rather accurately; since they are small quantities computed by summing large positive and negative numbers, it is necessary to use double-precision arithmetic in calculating them.

3. Details of the computations

When the first trial problem of this study was computed, using the erroneous approximate method of constraining the matching of the velocities of the plate and the medium (Chapter V, Section 4), solution of approximately 150 equations in single precision (eight digits in floating point) failed. The failure of the process was shown by the fact that the residual-iteration process did not reduce the residuals at each step and by the fact that the last diagonal coefficient of the upper-triangular matrix was negative. (That this coefficient cannot be negative follows from the facts that the original matrix is positive definite, that the determinant of a positive definite matrix is positive, and that the determinant of a triangular matrix is equal to the product of its diagonal elements.) Use of double-precision arithmetic (16 digits in floating point) in the elimination process produced a correct solution. When the

proper method of constraining the matching of the velocities was used and several other more minor changes in the equation derivation method were introduced, it was noticed that the corrections from the residual iteration process were definitely smaller than before. It was thought that these changes in the equation-derivation method had improved the ill-conditioning of the matrix and that it might be possible to perform the elimination in single precision. Experimenting with single precision showed that this was indeed the case, and that single precision was adequate for a system of about 275 equations. The limiting size of a system of equations of this form which may be computed with single precision was not determined, but the above cited results show that it depends rather critically on the details of the way in which the equations are derived.

When the computations are done in single precision on the IBM 7090, the limiting factor which determines the computation time is not the arithmetic operation time, but the magnetic-tape manipulation time. In particular, if the triangular matrix is stored on tape one row at a time, the back-substitution process requires that the tape be backspaced two records and then read in the forward direction one record for each row which is to be retrieved from tape, a time-consuming process. If the problem size is limited to 300 equations with a row length $N$ of 28, then the whole triangular matrix may be stored in random-access memory. It is still necessary to save the original matrix on tape and

read it in order to compute the residuals, but this is a more efficient tape-reading process since the tape is read in the forward direction only. Since this size of problem gave a discretization error which was small enough for the purposes of this study, the method which made less use of magnetic tape for storage was used. (These details of the computational set-up are strongly dependent on the particular computer used. With a computer which has a smaller random-access memory than the 7090 or which has different relative rates of arithmetic operations and tape manipulation, another set-up might well be more economical.)

# CHAPTER VII

## ACCURACY OF THE DISCRETE SOLUTION

### 1. Analysis of the errors

In this chapter the degree to which the solution of the discrete problem corresponds to the solution of the continuous problem is discussed. Since the problem was made discrete both in space and in time, there are two types of discretization error to consider, the error in the velocity distribution obtained for a particular shape and the error in the new shape obtained by extrapolating this velocity distribution over a finite time interval.

Analysis of the error for a particular velocity distribution is made more difficult by the fact that there exists no analytical solution for a problem of the type considered. The type of discretization formulas used in the medium near the plate should have a discretization error proportional to the mesh length, but the formulas are so complicated that it is not possible to carry out an explicit analysis of this discretization error. At very low amplitude, the solution should reduce to the sinusoidal dependence of $\dot{\theta}$ and $\underline{v}$ on $\underline{x}$ found in the treatment of Biot (1). Due

---

(1) M. A., Biot, Theory of folding of stratified viscoelastic media and its implications in tectonics and orogenesis: Geol. Soc. America Bull., v. 72, 1961, p. 1595-1620

to complications in the equation-derivation program, it was not possible to use an initial shape with a maximum dip of less than $10^{\circ}$. Also, the formulation of the problem in terms of a given shortening-rate breaks down at very low amplitude where an infinitesimal rate of shortening produces a finite rate of folding. Therefore, it was not possible to use the infinitesimal-amplitude solution as a direct check, although it could be expected that the $10^{\circ}$ dip solution would be close to the infinitesimal solution. Aside from this general agreement, it was necessary to rely on the internal consistency and smoothness of the computed results as a check on their accuracy.

Errors in the velocity of the plate are most important, since they are propagated on to the next time step. A much less precise knowledge of the velocity distribution in the medium would suffice for geologic purposes, since the geologic techniques for measuring the strains in the medium are necessarily rather inaccurate. At the dominant wavelength, when the bending resistance of the plate is relatively large, the $\dot{\theta}$ 's will be a smooth function of $\underline{s}$, since any short-range variation would imply large dissipations in the plate. However, there is a mathematical limiting case where this damping effect is not present, and examination of the smoothness of the $\dot{\theta}_i$ for this case provides a strong test of the accuracy of the solution as far as effects due to the medium are concerned. This is the case of a plate which has zero bending resistance but which

is still inextensible. Physically this condition is approached when the thickness of the plate, $h$, becomes very small while the viscosity of the plate $\mu_p$ becomes large, since the dissipation due to compression is proportional to $\mu_p h$ and that due to bending is proportional to $\mu_p h^3$. This case will be referred to as the zero-viscosity plate, since it corresponds to setting the viscosity of the plate equal to zero in the thin-plate problem as formulated mathematically. Though the problem of the zero-viscosity plate is well-defined mathematically, it is extremely sensitive to any variation in the resistance of the medium. Now, the general effect of the discretization error in the medium near the plate will be to introduce irregularities in the degree of resistance that the medium exerts on the plate as it advances. Since the zero-viscosity plate has no bending resistance to damp out short range variations in the rate of change of inclination, these irregularities will show up as local irregularities in the $\dot{\theta}_i$.

This sensitivity of the zero-viscosity plate to errors in the discrete solution for the medium implies that the degree of smoothness of the $\dot{\theta}_i$ for this case is a good measure of the accuracy of the solution; the next question is how to evaluate this smoothness. One simple test is to tabulate the differences of the $\dot{\theta}_i$; this test is valuable for locating irregularities, but it does not provide any convenient method of judging how important these irregularities are in determining the new shape of the plate.

2. Harmonic analysis

A more useful test is to perform a harmonic analysis of the $\dot{\theta}_i$ ; an extensive discussion of the use of harmonic analysis in smoothing equally spaced data is found in Lanczos (2). Because of the symmetry properties of the $\dot{\theta}_i$ , they may be expanded in a series of odd cosine harmonic terms:

$$\dot{\theta}(s) = \sum_{i=1}^{10} \dot{A}_i \cos (2i-1)\frac{\pi s}{20}$$

If all ten terms of the sum are retained, the harmonic analysis of the $\dot{\theta}$ 's is exactly equivalent to the original $\dot{\theta}$ 's themselves, but if the $\dot{\theta}$ distribution is a smooth one, the higher harmonics will be small in relation to the lower ones. Truncating the sum after a number of terms which is less than the total number of data points gives a least squares fit of the retained harmonic series to the data. This is proved for the continuous case by Hamming (3); the proof for the discrete case is similar.

Not only does the harmonic analysis provide a test for the smoothness of the $\dot{\theta}$ distribution, but it also provides a means of smoothing the data and a convenient way to describe the successive shape changes. If we smooth the $\dot{\theta}$ 's from any given stage by truncating the harmonic

---

(2) C. Lanczos, Applied analysis: Englewood Cliffs, N. J., Prentice-Hall, Inc., 1956, p. 207-245

(3) R. W. Hamming, Numerical methods for scientists and engineers: New York, McGraw-Hill Book Co., Inc., 1962, p. 237

expansion at a limited number of terms, there are two types of error which we may make: First, we may truncate too many terms and so miss a significant shape change; this is not serious if the noise level of the data is not excessive, since the amplitudes of the lower harmonics are definitely larger than those of the higher harmonics. If such a mistake is made, it will probably affect only one or two terms, and these will be small enough so that their effect on the new shape is negligible. Second, we may not truncate enough terms and thereby include some noise in the new shape. Inclusion of some noise is unavoidable unless the $\dot{\theta}$ distribution is free from noise, since this noise will also affect the lowest harmonics. The smoothing process is practical because not all of the ten $\dot{\theta}_i$ are needed to describe the plate velocity. It would probably be more efficient to use the harmonic analysis to describe the plate velocity in setting up the original equations. However, this possibility was not realized until late in the present study.

3. Smoothness of the $\dot{\theta}_i$

To see how the smoothness test and the smoothing process work out in practice, consider the initial stage ($10^{\circ}$ dip of the limb) for: (1) the dominant wavelength, ( $L = L_d$ ), (2) a plate viscosity which is 1/100 of that for the dominant wavelength ( $L = \sqrt[3]{100}\, L_d \approx 4.6 L_d$), and (3) the zero plate-viscosity case ( $L \gg L_d$ ). The $\dot{\theta}_i$ for these three cases are tabulated in table 1, and the harmonic coefficients are tabulated in table 2.

TABLE 1.-- $\dot{\theta}$ at equally spaced values of $s$ for 10° limb-dip

| | $\mu_p = \mu_{dom.}$ | $\mu_p = \frac{\mu_{dom.}}{100}$ | $\mu_p = 0$ |
|---|---|---|---|
| $s$ | $\dot{\theta}$ | $\dot{\theta}$ | $\dot{\theta}$ |
| 0 | 11.3470 | 11.2329 | 11.5269 |
| 1 | 11.2087 | 11.1051 | 10.8728 |
| 2 | 10.7978 | 10.7346 | 10.7522 |
| 3 | 10.1231 | 10.1067 | 10.1176 |
| 4 | 9.1995 | 9.2275 | 9.2576 |
| 5 | 8.0482 | 8.1115 | 8.1545 |
| 6 | 6.6962 | 6.8113 | 6.8720 |
| 7 | 5.1760 | 5.3003 | 5.2020 |
| 8 | 3.5255 | 3.6249 | 3.6299 |
| 9 | 1.7856 | 1.8396 | 1.8920 |
| 10 | 0 | 0 | 0 |

---

A difference table of $\dot{\theta}_i$ for the dominant-wavelength case shows that the fifth differences show irregulatities in sign and magnitude. Examination of the harmonic ratios shows that the first two harmonics are certainly significant and contain most of the information about the shape of the velocity distribution and that the later harmonics from four to ten are probably not significant. Consideration of the third harmonic ratios of successive time stages for this case shows that the third harmonic is not yet significant, since it does not begin to show a regular trend from

stage to stage until the fifth stage, in which the maximum dip is 56°. Examination of the first stage only does not permit this sort of judgment, however, and we might have left this harmonic in if we were smoothing these results. (In fact, no smoothing was done in the lower amplitude stages of the dominant-wavelength case, so that the problem did not arise.)

TABLE 2.--Harmonic coefficients of $\dot{\Theta}$ values for 10° limb-dip

| $k$ | $\mu_p = \mu_{dom.}$ $\dot{A}_k$ | $\mu_p = \frac{\mu_{dom.}}{100}$ $\dot{A}_k$ | $\mu_p = 0$ $\dot{A}_k$ |
|---|---|---|---|
| 1 | 11.3643 | 11.3636 | 11.3635 |
| 2 | -0.0173 | -0.1332 | -0.1485 |
| 3 | -0.0003 | 0.0066 | -0.0160 |
| 4 | -0.0000 | -0.0029 | 0.0038 |
| 5 | 0.0001 | -0.0064 | 0.0434 |
| 6 | 0.0000 | 0.0020 | 0.0004 |
| 7 | 0.0001 | 0.0031 | 0.0689 |
| 8 | 0.0001 | -0.0010 | 0.0703 |
| 9 | 0.0000 | -0.0012 | 0.0486 |
| 10 | 0.0000 | 0.0023 | 0.0925 |

Though cursory examination of the $\dot{\theta}_i$ from the case $\mu = \mu_d/100$ does not show it, these $\dot{\theta}$'s are not nearly as smooth as those for the dominant wavelength: the third

differences show irregularities. Consideration of the later time stages shows that the third harmonic is actually significant, though the fourth is not. In proceeding to the next time stage, a velocity distribution using the first three harmonics was used; this distribution has regular fifth differences.

The zero plate-viscosity case is considerably noisier; the second differences show irregularities in sign and magnitude, and even examination of the $\dot{\theta}$'s themselves shows that $\dot{\theta}_0$ is suspiciously high. This higher noise level is confirmed by consideration of the harmonic ratios, but comparison of the first two harmonic ratios with those of the $\mu = \mu_d/100$ case shows that the velocity distributions are similar except for this difference in noise level. This is what we should expect, since the bending dissipation is about half the medium dissipation for the dominant-wavelength case, about 0.5% of the medium dissipation for the $\mu = \mu_d/100$ case, and strictly zero for the zero plate-viscosity case, while the medium dissipations remain essentially the same in all three cases. Therefore, the $\mu = \mu_d/100$ case is physically much closer to the zero plate-viscosity case than to the dominant-wavelength case, and the velocity distributions reflect this similarity.

The difference tables for the $\mu = \mu_d/100$ case and the zero plate-viscosity case show that the irregularities in the $\dot{\theta}$ distributions occur where the plate crosses a horizontal mesh line. In this situation, the curvilinear

trapezoids over which the medium dissipations are averaged change from very short trapezoids to very tall ones below the plate and change in the opposite sense above the plate. It is reasonable to surmise that the size and probably the sign of the discretization error changes at this point. Although we can thus localize a probable trouble spot in the discretization process, the only way to eliminate the difficulty within the framework of the discretization scheme used would be to reduce the mesh spacing, $\ell$. Since the number of equations increases as $1/\ell^2$ and the solution time increases approximately as the cube of the number of equations, a significant decrease in the mesh spacing would entail a very large increase in computation time.

The infinitesimal analysis (4) predicts the presence of only the first harmonic in the $\dot{\theta}$ distribution for folds of very small amplitude. More accurate analyses for the free-plate case and for the case of a plate with zero bending resistance constrained by a distribution of discrete dashpots shows that the second harmonic should indeed by present for small but not infinitesimal amplitude. A more convincing demonstration of the significance of the second harmonic for finite amplitudes is given by figure 16, where it is evident that the second harmonic grows as the amplitude of the fold increases. The magnitude of the second harmonic is also related to the shape of the layer (Chapter VIII, Section 4).

The noise present in the results of the dominant-

wavelength case will not disturb the smoothness of the shape used for the computation of the next stage, but the case of a wavelength much longer than the dominant wavelength can only be treated if some sort of smoothing technique is used at each stage. In order to exhibit the widest possible variation in shape as a function of the ratio of initial wavelength to the dominant wavelength, it was decided to compute the $\mu = \mu_d/100$ case and smooth the results at each stage. Going to the limiting case of the zero-viscosity plate gives a more noisy $\dot{\theta}$ distribution and does not significantly modify the harmonics (1 and 2) which are above the noise level. The smoothing was done by examination of the harmonic analysis of the $\dot{\theta}$ distribution at each stage according to the criteria outlined above; in general the rule was followed that it was better to leave in a harmonic coefficient if there was some doubt as to its significance.

4. Strain-rates in the medium

So far we have focused attention on the plate viscosity distribution, since it is more likely to cause errors that accumulate from one time step to the next. In examining the medium velocity distribution, we are concerned only that it be accurate enough to justify conclusions which we may deduce from it. The most convenient representation of the medium velocity distribution for geologic purposes is the orientation of the principal strain-rate axes; since

this orientation angle depends on the ratio of second differences of $\phi$ at a given point, it is rather sensitive to errors and irregularities in the $\phi$ distribution. If we take the differences of the orientation angles at successive points along a horizontal or a vertical mesh line, the differences are very regular except where there is a transition from orientations which are computed with some elimination and some regular points to orientations which are computed entirely with regular points. These irregularities are small--in almost all cases they cannot be detected by visual examination of a plot of the principal strain-rate axes--and they certainly will not affect the conclusions based on a consideration of the strain-rate distribution.

5. Choice of the time step; cumulative errors in the shape

Up to the 81° stage of the dominant-wavelength fold and the 33° stage of the weak-plate fold, simple extrapolation of the velocity of the plate was used to find the new shape. That is, the velocity given by the calculation of one stage was taken to be the average velocity in the time interval up to the next stage. When the $\dot{\theta}_i$ values calculated for the new shape were normalized to have the same $\dot{\theta}_0$ as that of the previous stage, the maximum difference between any of the $\dot{\theta}_i$ of the two sets was always less than about 10%.

It was found that the ratios of the harmonic coefficients of the $\dot{\theta}$ distributions, $\dot{A}_i/\dot{A}_1$, had an approximately exponential dependence on the dip of the limb, and

that they were relatively insensitive to the finer details of the shape. These features made possible a method of combined prediction and extrapolation which was used to calculate the shapes of the final stage of the dominant-wavelength fold and the further stages of the weak-plate fold.

The method used was the following one: (1) The ratios $\dot{A}_i/\dot{A}_1$ were plotted against the dip of the limb on semi-logarithmic coordinate paper, and the expected ratio for the next stage was estimated. (2) On the basis of these predicted $\dot{A}_i/\dot{A}_1$ and those from the previous stage, the average $\dot{A}_i$ over the next time interval were calculated. (3) The new velocity distribution for the shape determined using this set of average $\dot{A}_i$ was then computed, and the ratios $\dot{A}_i/\dot{A}_1$ obtained from this velocity distribution were compared with those predicted in step 1. A revised shape for the stage just computed was determined using the plate velocities from this stage and the previous stage. If the predicted and calculated harmonic ratios were sufficiently close, this revised shape was used to determine the next stage as in steps 1 and 2. If they were not sufficiently close, the velocity distribution for this stage was recalculated using the revised shape before proceeding to the next stage.

The lower harmonics were required to match to within 10%; a larger tolerance was accepted for the higher harmonics, since their magnitude was much smaller than that of the

lower harmonics.

This process worked well up to the 69° stage of the weak-plate fold, but after that point it was no longer possible to predict the velocity distribution with sufficient accuracy. The reasons for this difficulty are associated with the shape of the fold at these high-dip stages and are discussed in Chapter VIII, Section 6.

# CHAPTER VIII

## RESULTS

### 1. Introduction

The principal results of the numerical computations are the shape and velocity of the layer at each stage and the velocity distribution in the medium at each stage.

The $\theta_i$ and $\dot{\theta}_i$ and the corresponding harmonic coefficients $\underline{A}_i$ and $\underline{\dot{A}}_i$ are tabulated in Appendix B for the three folds computed: the free plate ( $\underline{L} << \underline{L}_d$ ), the dominant-wavelength fold ( $\underline{L} = \underline{L}_d$ ), and the weak-plate fold ( $\underline{L} = 4.6\,\underline{L}_d$ ). The initial shape for the free plate was a sine wave, $\underline{y} = \underline{y}_0 \sin \frac{2\pi x}{L}$, with a maximum dip of $1^\circ$; that for the other two folds ( $\underline{L} = \underline{L}_d$ , $\underline{L} = 4.6\,\underline{L}_d$ ) was a sine wave with a maximum dip of $10^\circ$. Successive shapes of these three folds are plotted in figures 8, 9, and 10. In figures 11, 12, and 13 selected stages of the three folds are plotted together for visual comparison; in these figures the symmetry of the problem is used to extend the fold over a longer range of arc length.

For discussion of the growth of the various folds, it is convenient to plot the ratios of the Fourier coefficients of $\theta$ and $\dot{\theta}$ logarithmically as a function of the dip of the limb. $\underline{A}_2/\underline{A}_1$ and $\underline{A}_3/\underline{A}_1$ are plotted in figures 14 and 15, while $\underline{\dot{A}}_2/\underline{\dot{A}}_1$ and $\underline{\dot{A}}_3/\underline{\dot{A}}_1$ appear in figures

16 and 17. The significance of these curves is discussed in Section 3.

Principal strain-rates and finite strains for selected fold stages are plotted in figures 21 to 27. The calculation of these quantities is described in Appendix A; the interpretation of the diagrams is discussed in Section 7.

Table 4 summarizes the principal results for the cases $\underline{L} \ll \underline{L}_d$, $\underline{L} = \underline{L}_d$, and $\underline{L} = 4.6\,\underline{L}_d$ respectively.

## 2. Stages of development of a finite-amplitude fold

Although the folding process is a continuous one, for ease of discussion it may be separated into three portions, each with its characteristic style. These styles may be called the low-dip style, the high-dip style, and the isoclinal style.

In the following discussion, the fold is thought of as an anticline, and the portion of the medium above the anticlinal hinge is referred to as being outside the crest, that below the hinge as inside the crest. In speaking of planar features such as the planes of maximum flattening rate (perpendicular to the maximum compressive stress), we shall designate planes which dip toward the anticlinal axial plane as fanning, those which dip away from the axial plane as anti-fanning.

The low-dip stages represent a direct continuation of infinitesimal-amplitude folding. The competent layer is still pushing the medium aside, and velocities due to folding

are greater than those due to the compression of the medium. This style is shown by figures 21 and 22 for the dominant wavelength and 25 for the weak plate. Throughout these stages the planes of maximum flattening rate form an anti-fan below the crest.

In the high-dip stages the medium begins to play a more active role: (1) At the crest of the fold the vertical velocity is less than it would be if there were no layer and the medium were undergoing the same uniform compression rate. (2) The vertical velocities along the x-axis inside the crest of the fold begin to be negative, and the material inside the crest starts to be extruded from the fold. (3) When this occurs, the planes of maximum flattening rate change from anti-fanning to fanning. This style is pictured in figures 23 and 24 for the dominant wavelength and in figure 26 for the weak plate.

As the limbs continue to steepen and approach each other, the portion of the medium inside the crest becomes more and more confined, and the extrusion of this material is the dominant aspect of the folding process. The onset of this isoclinal style is less well defined than the transition between the low- and high-dip styles, but it clearly represents another style of deformation. Figure 27 illustrates this style. A more precise definition and a discussion of the special features of this style are found in Section 6.

Although transition from one style to the next is

gradual, we can determine the approximate dip of the limb at which the transitions occur. For the dominant wavelength, the limit between the low- and high-dip stages is probably close to 66°. At a dip of 66°, the planes of maximum flattening rate form an anti-fan, and the crest of the fold has a vertical velocity less than it would have had if the fold had not been present. However, the vertical velocity along the x-axis inside the crest of the fold does not become negative until the 70° stage is reached. The 89° stage of the dominant-wavelength fold does not show the characteristics of the isoclinal style (Section 6).

For the weak plate, the transition from the low-dip to the high-dip style occurs between limb-dips of 53° and 63°; all three criteria indicate that the 63° case belongs in the high-dip stages. Signs of the transition to the isoclinal style begin to occur when the dip of the limb is 69°; the 79° and 89° examples are clearly isoclinal stages (Section 6).

3. Shape analysis

Differences in shape between the three folds can be detected by visual examination (figs. 8-13) only after the dip of the limbs is greater than about 45°; as the amplitudes become larger, the differences are sufficiently pronounced so that it would probably be possible to detect them even in natural folds--where the shapes would naturally not be as ideal as in the computed examples. It will be shown that a Fourier analysis exhibits differences in the trends of the

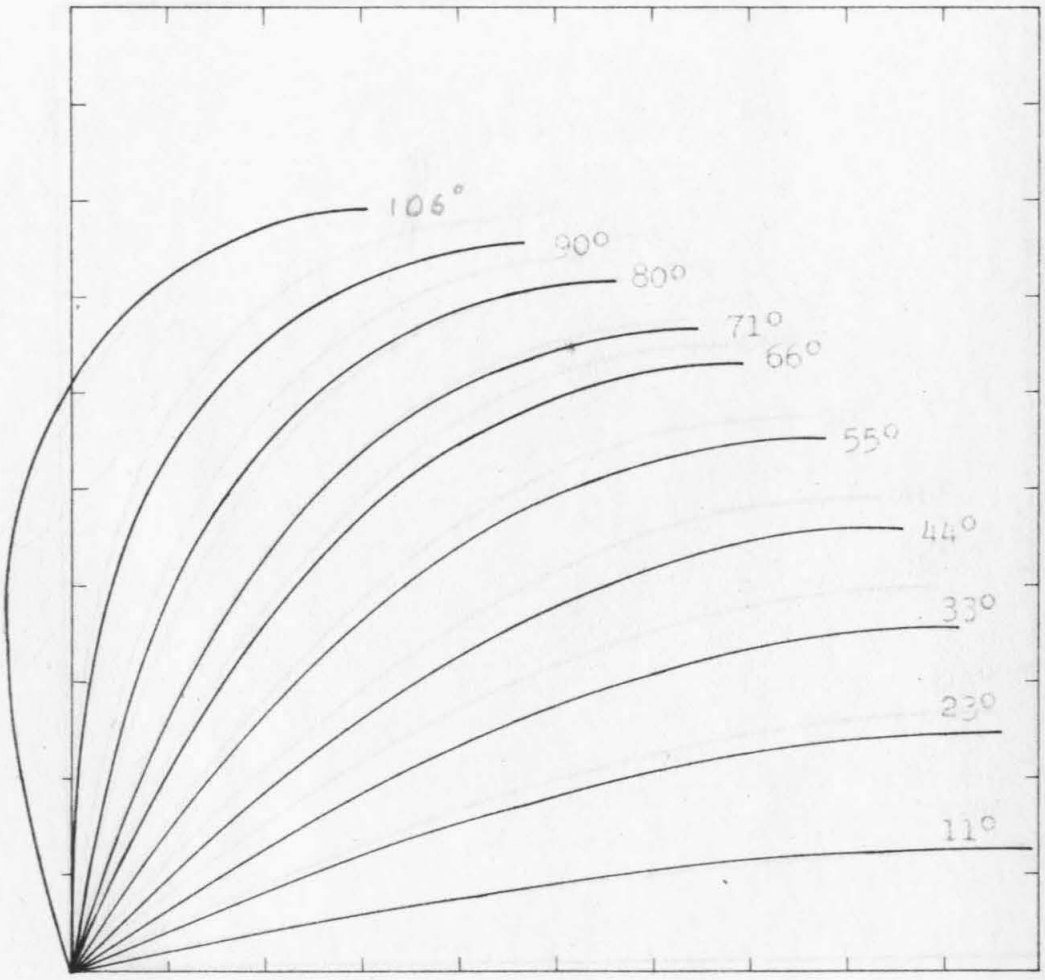


Figure 8.--Successive shapes of the free-plate fold ($L \ll L_d$). The dip of the limb of each stage is indicated.

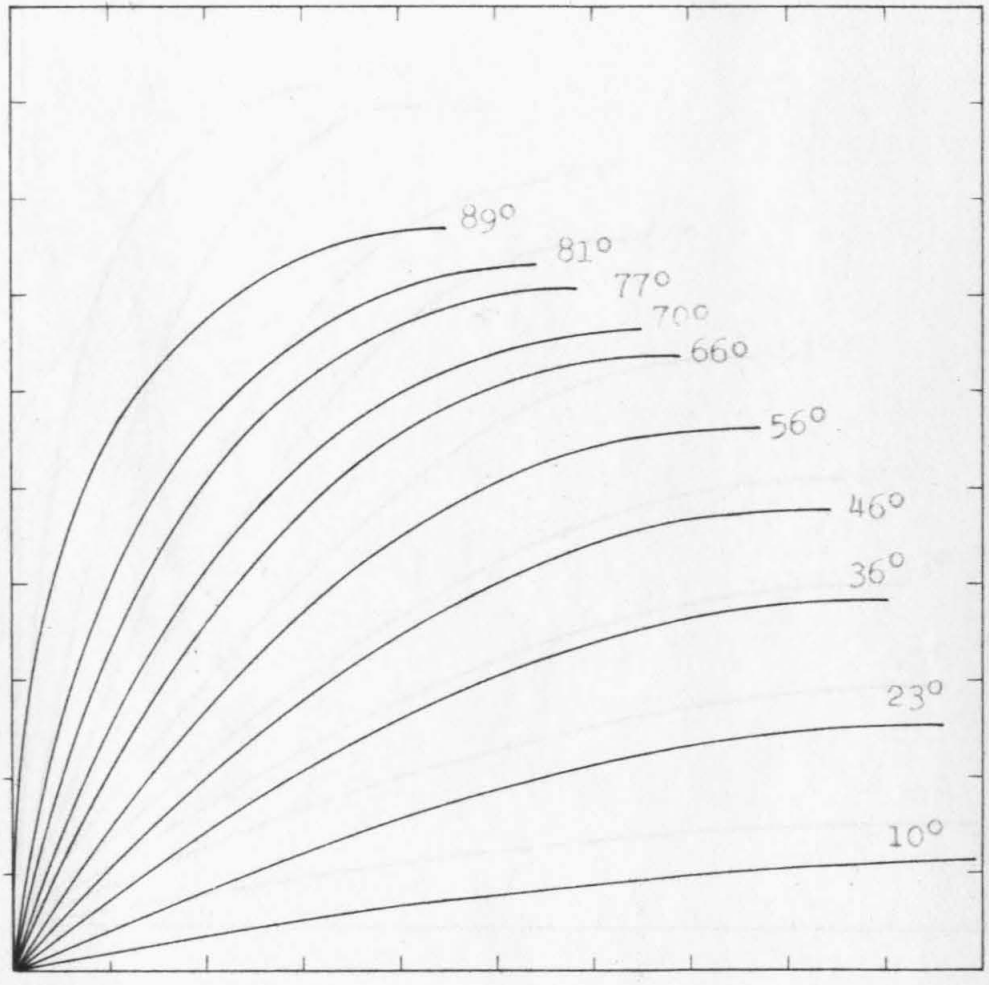


Figure 9.--Successive shapes of the dominant-wavelength fold ( $L = L_d$ ). The dip of the limb of each stage is indicated.

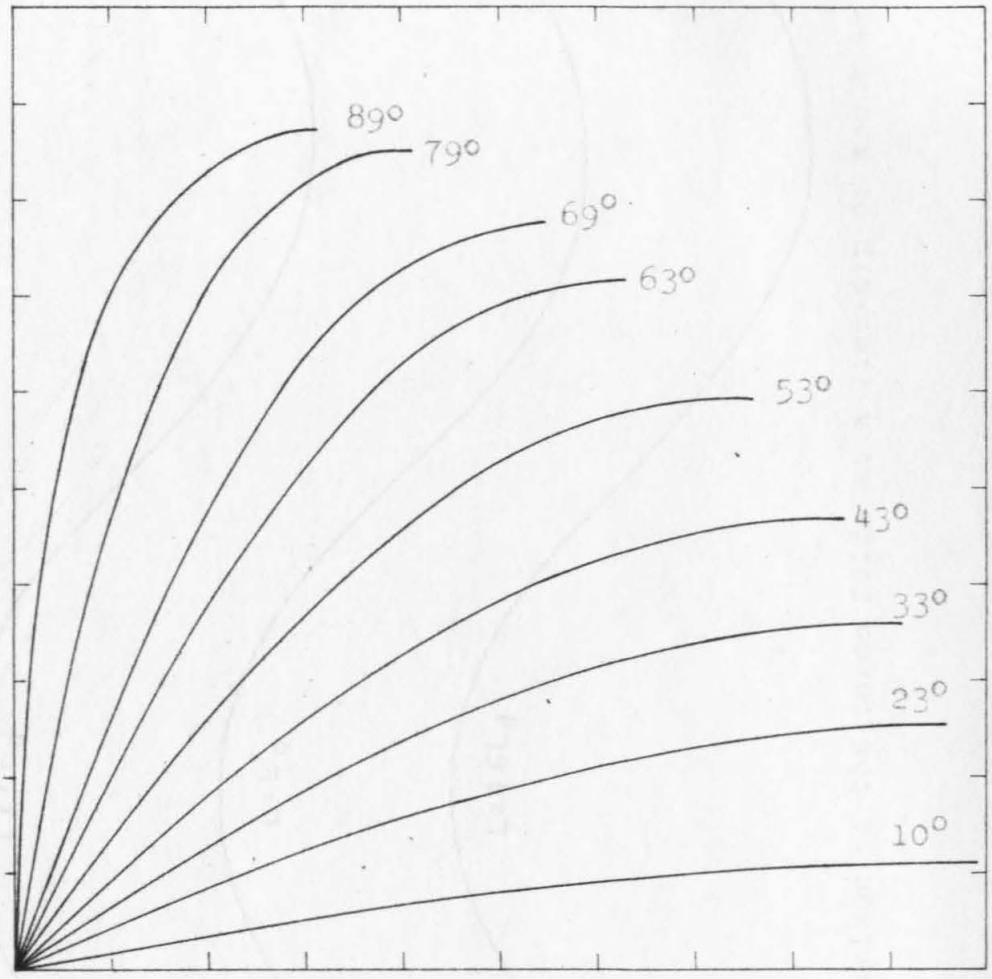


Figure 10.--Successive shapes of the weak-plate fold ($L = 4.6\, L_d$). The dip of the limb of each stage is indicated.

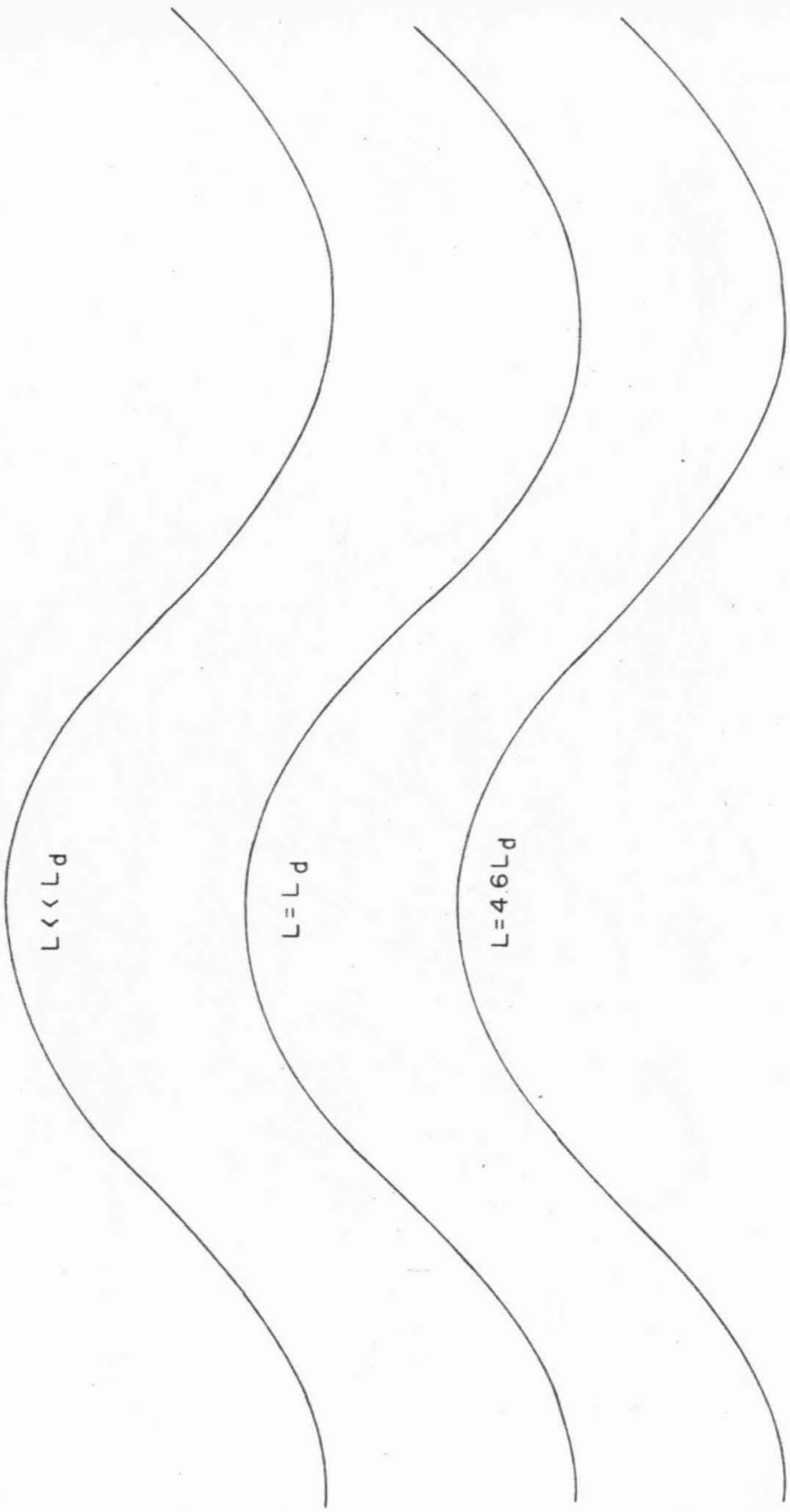


Figure 11.--Comparison of the three folds at a limb-dip of about 45°.

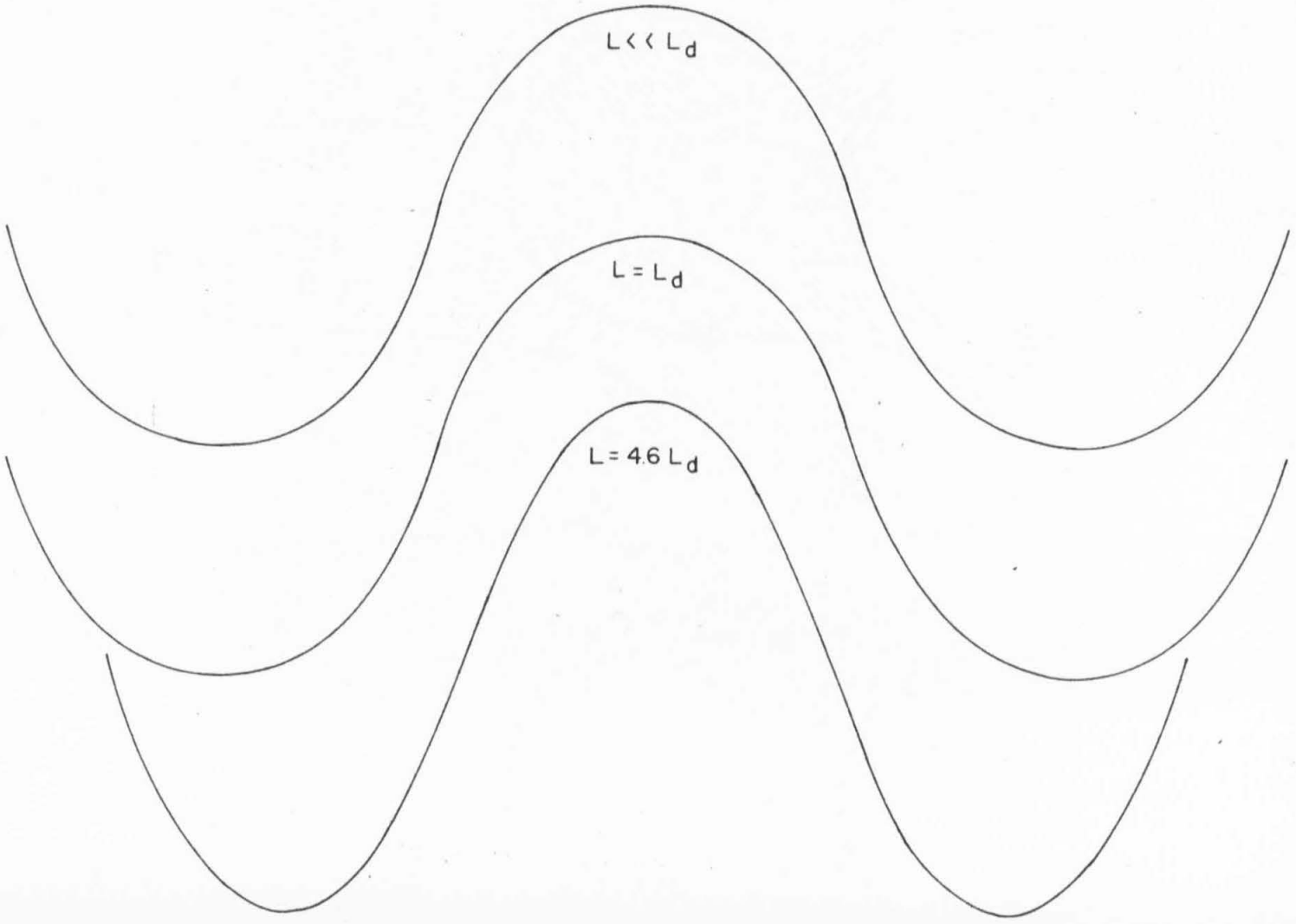


Figure 12.--Comparison of the three folds at a limb-dip of about 70°.

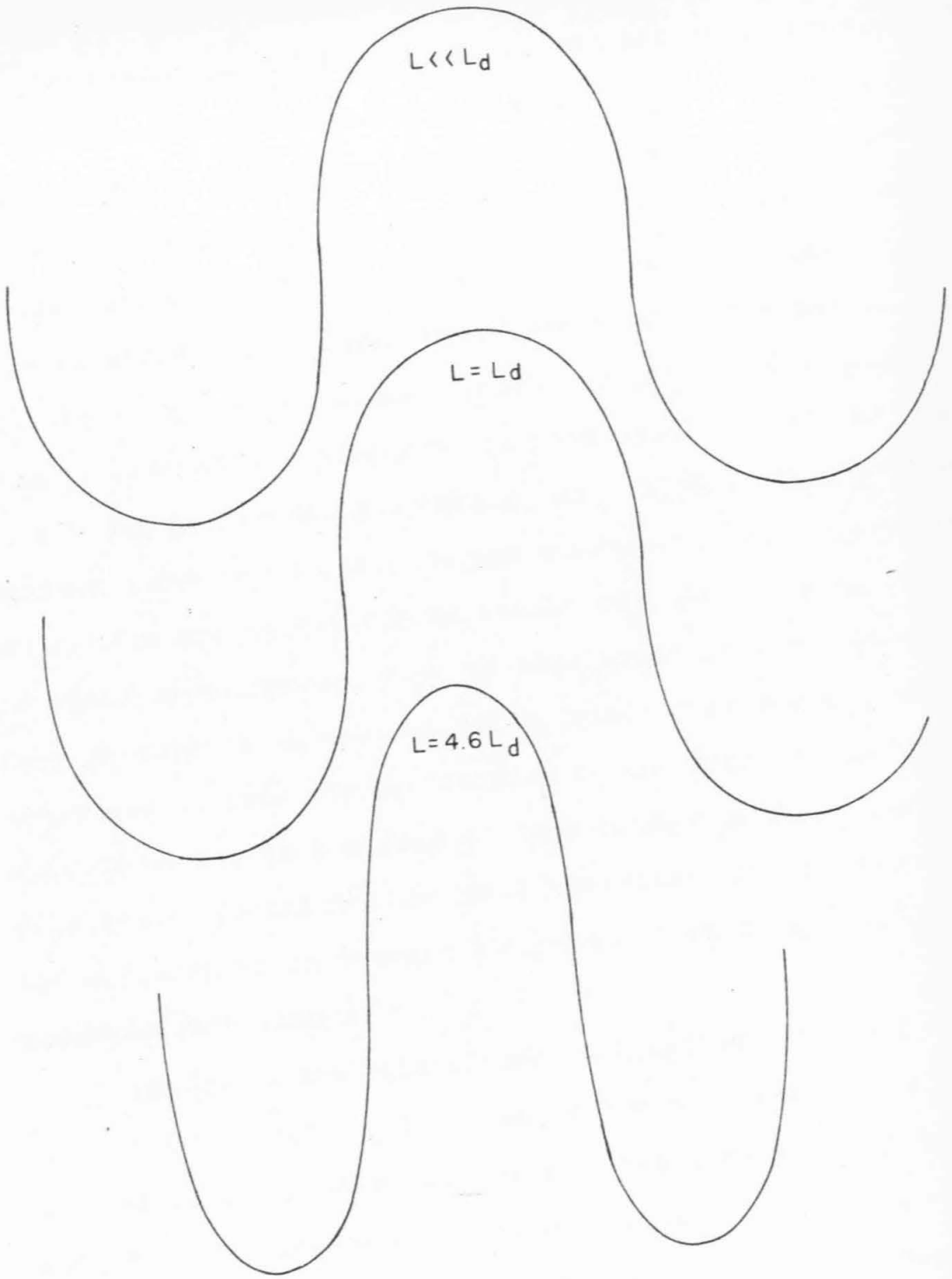


Figure 13.--Comparison of the three folds at a limb-dip of 89°.

shape development at lower amplitudes also.

Examination of the folded shapes and consideration of the balance between bending dissipation in the layer and dissipation in the medium suggest that the important characteristic of the shape which distinguishes the three cases is the "sharpness" of the crest. There are a number of ways to express this "sharpness" property, for example: (1) the relative length over which the limb of the fold remains essentially straight, (2) the amplitude of the fold at a given horizontal shortening, and (3) the ratio of the maximum curvature to the average curvature. Although these parameters are useful for an intuitive understanding of what is meant by sharpness, none of them would be very satisfactory in describing natural folds, since they are all rather sensitive to local irregularities in the shape of the fold. What is needed is a method of describing the shape that is relatively insensitive to local variations but sensitive to the differences in overall sharpness shown by the different computed fold shapes.

Harmonic analysis of the inclination $\theta$ as a function of arc length $s$ is probably the most useful way of describing fold shape, at least in the low- and high-dip stages. This method is discussed in Chapter 5, Section 2. Its usefulness is dependent on the possibility of describing the shape in terms of a small number of harmonic coefficients. If this is possible, then a natural fold can be described in terms of the first few harmonic coefficients, and the omission

of the higher harmonic terms provides an automatic method of smoothing the observed inclination data. The more intuitive measures of sharpness mentioned above can be expressed in terms of the harmonic coefficients if desired.

In order to discuss the growth of a fold with time, we must choose a parameter to measure the stage which the folding has reached. Two such parameters are (1) the maximum dip of the limb, and (2) the percentage of shortening that has occurred. It will be shown later (Section 5) that the way in which the plate deforms at a given stage is relatively independent of the details of the shape at that stage. To the extent that this independence holds, it makes little difference which stage parameter is used. The dip of the limb proves to be satisfactory, and since it is easily determined, it is used here as the "stage" variable to which the development of fold shape is referred. For a naturally observed fold, the dip of the limb may be taken as the value calculated from the terms of the harmonic analysis that are judged to be significant; this will smooth out any irregularities in inclination in the neighborhood of the center of the limb.

In figures 14 and 15 the ratios of the harmonic coefficients $A_2/A_1$ and $A_3/A_1$ are plotted logarithmically as a function of the dip of the limb. If we except the first three stages of the $L = L_d$ curve (discussed in Section 5 below) and the last three stages of the $L = 4.6\,L_d$ curve (discussed in Section 6 below), the following

conclusions can be drawn.

1) The importance of the higher harmonics in the shape representation increases approximately exponentially with increasing dip of the limb for all three folds.

2) The ratios of the harmonic coefficients should describe a smooth curve. Therefore, the deviation of the ratios from a smooth curve gives a measure of the errors committed in the discretization process.

3) The separation of the curves for the three $\underline{L}/\underline{L_d}$ values at any given stage is large. From this standpoint, the shape of finite-amplitude folds is sensitive to the variations in physical parameters among the three cases, and the harmonic representation of the shape is therefore an appropriate method to describe these shape variations.

4) The shape of folds that have not reached the isoclinal stage of deformation can be described in terms of a small number of harmonic coefficients. The description of the shape of the free plate is contained in the first two harmonic coefficients: the ratio $\underline{A_3}/\underline{A_1}$ is always less than $4 \times 10^{-5}$ over the shortening range studied; the maximum value is reached for a limb-dip of 90°. The third harmonic becomes significant in the dominant-wavelength fold only after the dip of the limb reaches 66°; the fourth is still negligible when the limb dips 89°. The description of the shape of the weak plate is complicated by two features: (1) since the weak plate has a much "sharper" shape, higher harmonics are necessary for its description; and (2) the

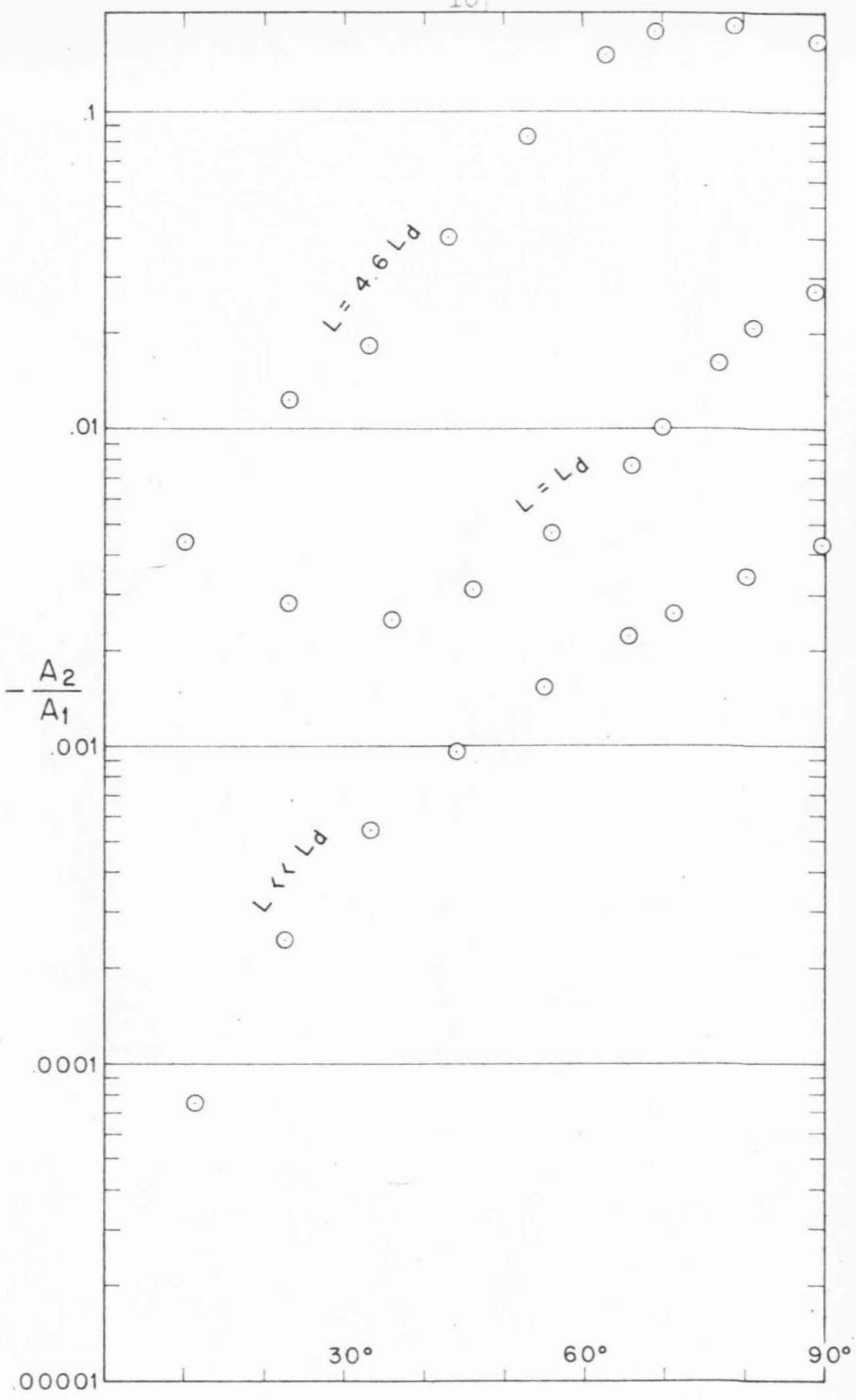


Figure 14.-- $A_2/A_1$ plotted logarithmically against limb-dip.

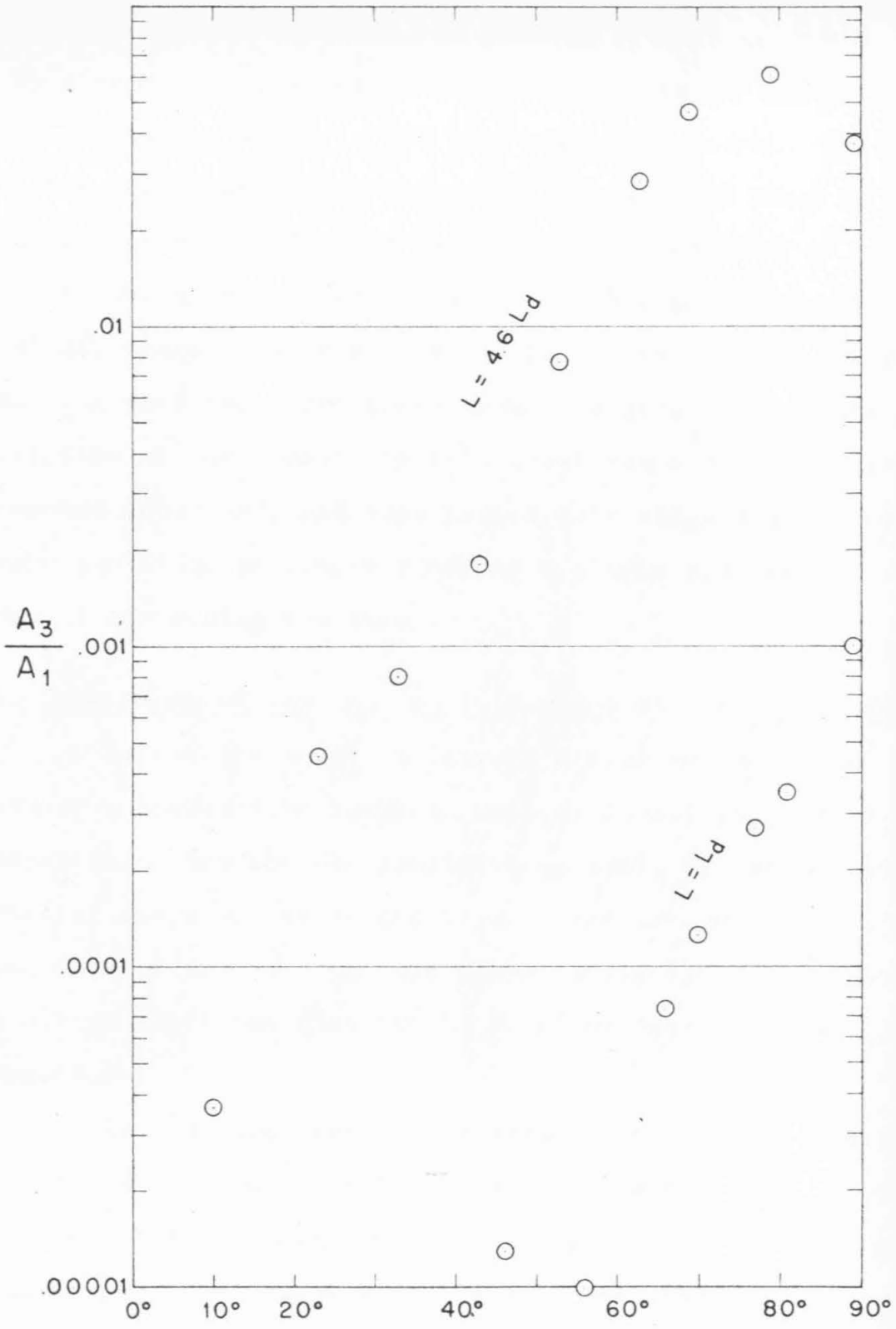


Figure 15.-- $A_3/A_1$ plotted logarithmically against limb-dip. Values for $L \ll L_d$ and $L = L_d$ with dips less than 46° are below the significance level of the computation.

magnitude of the higher harmonic coefficients in the velocity distribution is less well known because of the higher discretization error in the weak-plate solutions. The ratios of the second and third harmonics to the first show a regular growth in figures 14 and 15, but the sign of the fourth harmonic changes between the 53° dip stage and the 63° dip stage. The most reasonable interpretation of the data is that the first three harmonics give an adequate description of the weak-plate fold until the dip of the limb reaches about 65°, and that beyond this stage the harmonic representation no longer provides a simple and convenient way of describing the shape.

4. Dependence of the $\dot{A}_i$ on fold shape at low amplitude

Before the shape variations discussed in Section 3 can be compared with those in natural folds, it must be shown that they are not sensitive to small variations in the initial shape of the folded layer. The nature of the dependence of the $\dot{A}_i$ on fold shape is different at moderate and high amplitude (Section 5) from the dependence at low amplitude.

In order to test the dependence of harmonic coefficients $\dot{A}_i$ (describing the bending in terms of $\dot{\theta}_i$) on the harmonic coefficients $A_i$ (describing the $\theta_i$ and hence the shape), the velocity fields were calculated for the dominant-wavelength folds of two different shapes, both having 10° limb-dips. The first shape, which was taken as the starting shape for the full dominant-wavelength fold,

was a pure sine curve, $\underline{Y} = \underline{Y}_0 \sin \frac{2\pi}{\underline{L}} \underline{X}$ ; described in terms of $\theta$ and $\underline{s}$, this shape is closely approximated by the first two harmonic coefficients, with $\underline{A}_2/\underline{A}_1 = -0.00446$. The second shape was also composed of these two harmonics, but in the ratio $\underline{A}_2/\underline{A}_1 = -1/9$. This ratio is the largest possible which does not cause a change in sign of the curvature between the limb and the crest of the fold.

The solutions of the two problems gave $\underline{A}_2/\underline{A}_1 = -0.00152$ for the first fold and $\underline{A}_2/\underline{A}_1 = -0.03481$ for the second. If we form the ratio $\underline{A}_2/\underline{A}_1 \,/\, \underline{A}_2/\underline{A}_1$ , its value is 0.34 for the first fold and 0.31 for the second. The near equality of these two values suggests that the rate of growth of a particular $\underline{A}_i$ is proportional to its relative amplitude in the initial shape. This proportionality is not that of the conventional infinitesimal-amplitude treatment of $\underline{Y}$ as a function of $\underline{X}$ (1). The conventional treatment predicts that a sine wave, $\underline{Y}(\underline{X})$ with a $10^\circ$ dip of the limb will fold into another sine wave with the same arc length and higher amplitude. It can be shown that if this were to happen $\dot{\underline{A}}_2/\dot{\underline{A}}_1$ would be -0.037, as opposed to the value -0.00152 calculated in this study. Thus the infinitesimal treatment in its conventional form gives a very erroneous prediction for the shape development of even this low-amplitude fold.

---

(1) M. A. Biot, Theory of folding of stratified viscoelastic media and its implications in tectonics and orogenesis: Geol. Soc. America Bull., v. 72, 1961, p. 1595-1620

It is proposed that the range of validity of the infinitesimal treatment might be extended to folds of small but finite amplitude, provided that the harmonics of $y$ as a function of $x$, hitherto considered in the infinitesimal theory, are replaced by harmonics of $\theta$ as a function of $s$. On the basis of the infinitesimal treatment (2) the ratio of the growth rates of any two harmonics is proportional to the ratio of the amplitudes of the two harmonics in the initial shape. If it is assumed that the constant of proportionality would be the same if the infinitesimal treatment were formulated in terms of $\theta(s)$ rather than $y(x)$, the proportionality constant $\dot{A}_2/\dot{A}_1 \,/\, A_2/A_1$ is 0.310. This value is close to the values 0.34 and 0.31 derived from the numerical calculations of the two 10° dominant-wavelength folds. Applying the same assumption to the first two harmonics of the 10° weak-plate fold, $\dot{A}_y/\dot{A}_1 \,/\, A_2/A_1 = 2.65$, while the value calculated for the 10° stage of the weak-plate fold is 2.63.

These results are suggestive, but not conclusive. There is no basis within the framework of the conventional infinitesimal treatment for preferring a shape representation of $\theta$ as a function of $s$ to a representation of $y$ as a function of $x$, since the two are identical in the limit as the amplitude goes to zero. However, the numerical results do suggest that an analytical theory of the shapes of low but finite amplitude folds might be based on the bending

---

(2) Biot, op. cit.

of a slightly curved plate where the shape perturbations are harmonically analyzed in terms of $\theta$ as a function of $s$.

5. Dependence of the $\dot{A}_i$ on fold shape at higher amplitudes

The proportionality discussed in Section 4 does not persist as the fold grows: for the dominant-wavelength fold with a limb-dip of 23° the ratio is $\dot{A}_2/\dot{A}_1 \,/\, A_2/A_1 = 0.69$, while for 36° it is 2.15.

The nature of the dependence of the $\dot{A}_i$ on fold shape beyond the amplitude where proportionality holds can be studied by comparing two plate velocity distributions computed from fold shapes which have the same limb-dip, but slightly different $A_i$. Such pairs of examples were computed for the 81° stage of the dominant-wavelength fold and the 63° stage of the weak-plate fold. The second shape in each case was calculated by using the velocity distribution obtained from the first shape to refine the estimate of average velocity of the plate used to compute successive shapes (Chapter VIII, Section 5). The harmonic ratios of the two shapes and their corresponding $\dot{\theta}_i$ values are tabulated in table 3 (3).

Examination of the table shows that: (1) the changes in the $\dot{A}_i$ are certainly not proportional to the changes in

---

(3) After the two dominant-wavelength cases were computed, the method of eliminating points near a steeply dipping portion of the plate was made more accurate. The second, a posteriori, shape of the 81° stage was then recomputed, and it is the results of this computation that are plotted in figures 8, 11 to 17, 20, and 24, and tabulated in Appendix B. The more accurate method was used for all stages of the weak-plate fold.

TABLE 3.--Variation in $\dot{A}_i/\dot{A}_1$ when $A_i/A_1$ are changed and limb-dip is held constant.

| | | I | | II | |
|---|---|---|---|---|---|
| | $i$ | $A_i/A_1$ | $\dot{A}_i/\dot{A}_1$ | $A_i/A_1$ | $\dot{A}_i/\dot{A}_1$ |
| $L = L_d$ 81° Limb-dip | 2 | -0.01941 | -0.1317 | -0.02314 | -0.1342 |
| | 3 | 0.00055 | 0.0004 | 0.00033 | 0.0009 |
| | 4 | -0.00011 | -0.0024 | -0.00015 | -0.0023 |
| $L = 4.6\ L_d$ 63° Limb-dip | 2 | -0.15946 | -0.4356 | -0.14400 | -0.4568 |
| | 3 | 0.04727 | 0.1637 | 0.02769 | 0.1854 |
| | 4 | 0.00065 | -0.0646 | -0.00662 | -0.0396 |

the $A_i$, and in some cases they even have the opposite sign; and (2) except for $\dot{A}_3/\dot{A}_1$ in the dominant-wavelength example, the changes in the velocities are relatively much smaller than the changes in the shape. ($\dot{A}_3/\dot{A}_1$ and $A_3/A_1$ are so small that their variation is probably not significant within the framework of the numerical computation.) Comparison of the changes in the $\dot{A}_i$ shown in this table with the changes due to the normal growth of the shapes illustrated in figures 16 and 17 demonstrates that the rate of growth of the various harmonics is determined mainly by the ratio $L/L_d$ and the stage of folding as measured by the dip of the limb, rather than by the amplitudes of the individual Fourier components.

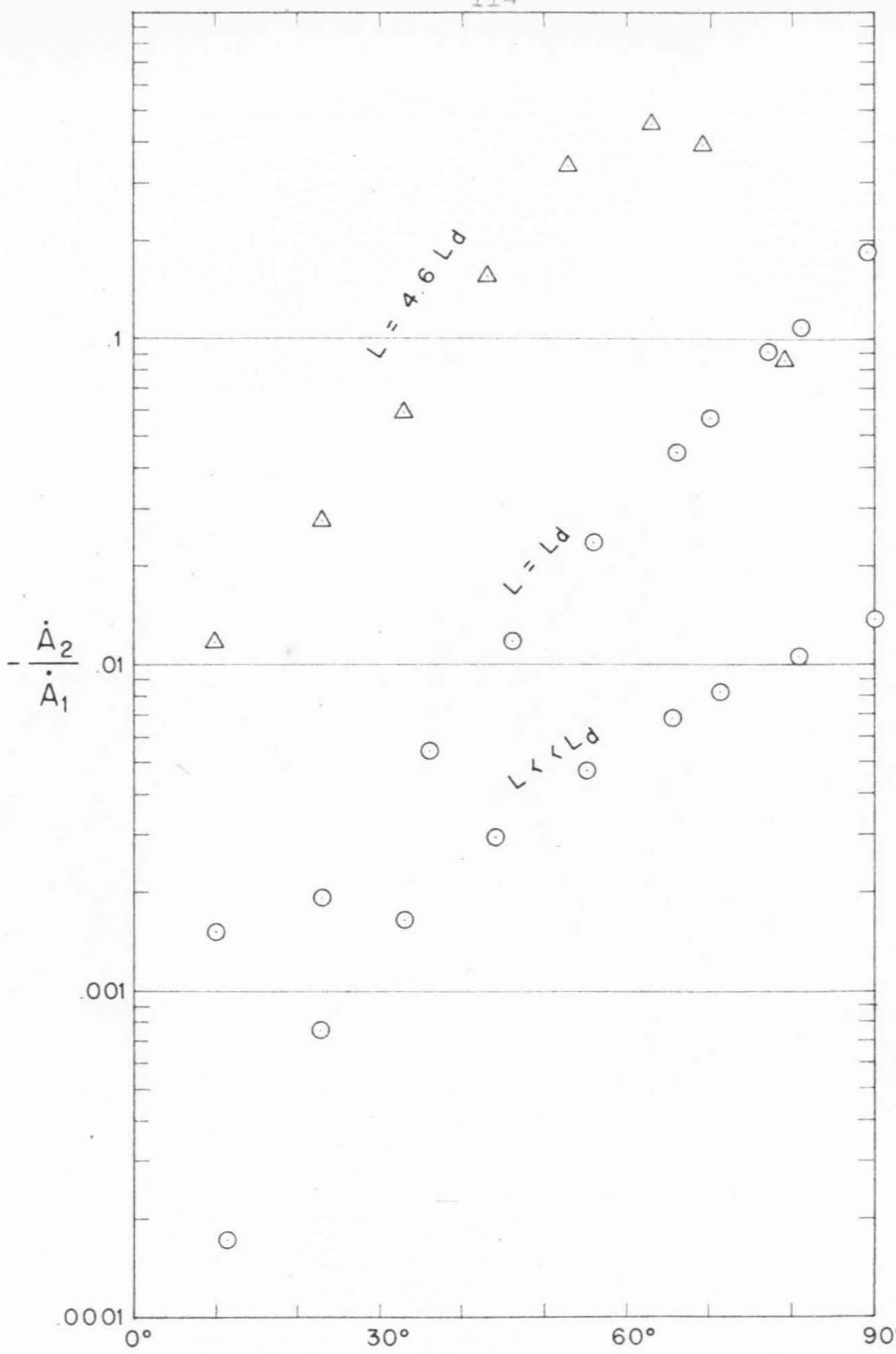


Figure 16.--$\dot{A}_2/\dot{A}_1$ plotted logarithmically against limb-dip.

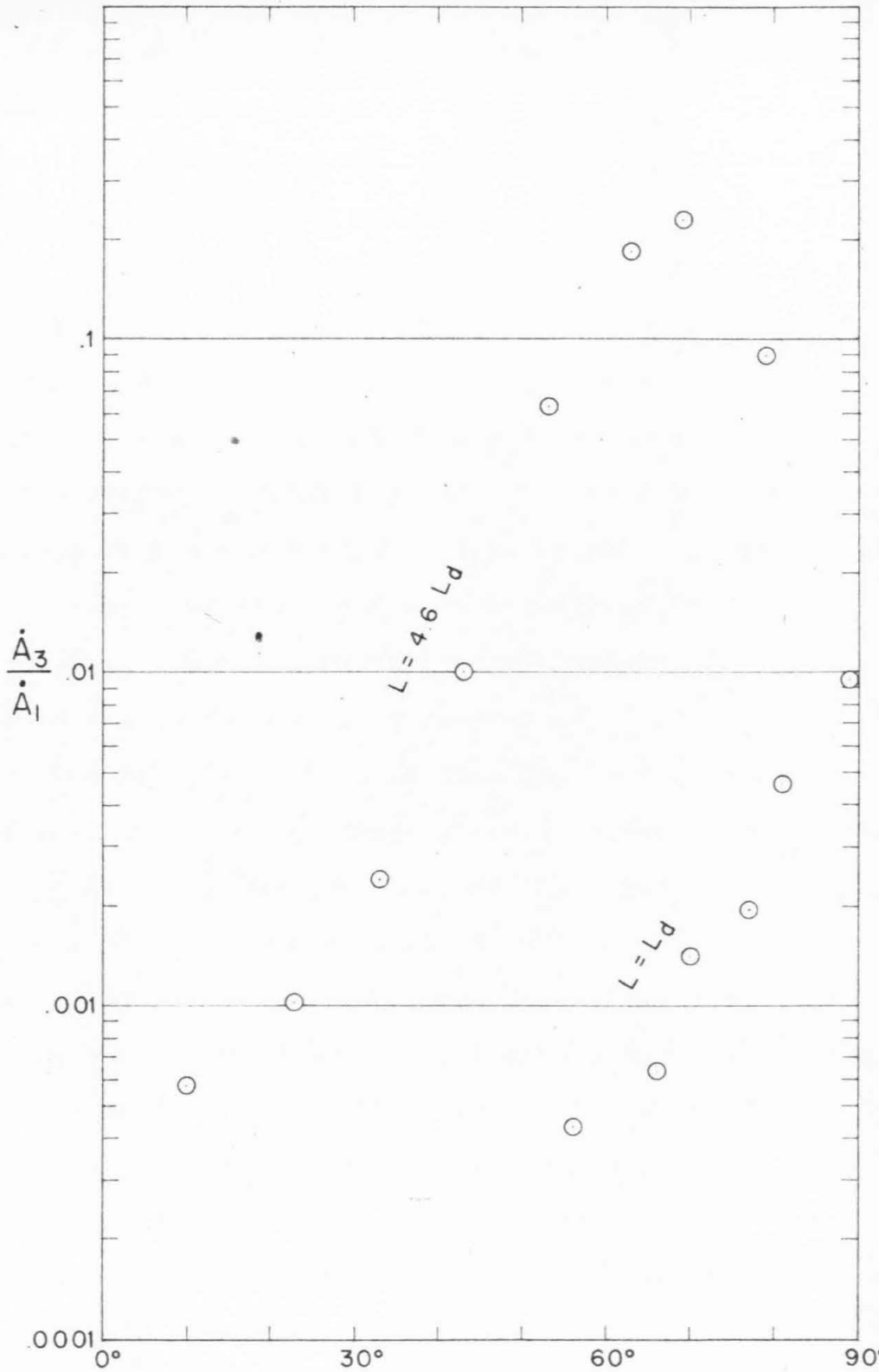


Figure 17.-- $\dot{A}_3/\dot{A}_1$ plotted logarithmically against limb-dip. Values for $L = L_d$ below 56° and for $L \ll L_d$ are below the significance limit of the computation.

The transition from the very-low-dip stages ( $\dot{A}_2/\dot{A}_1$ is proportional to $A_2/A_1$ ) to the later stages ( $\dot{A}_2/\dot{A}_1$ depends only on limb-dip and $L/L_1$ ) occurs at a limb-dip of about 15°, since the 23° stage of the dominant-wavelength fold no longer shows the proportionality discussed in Section 4. A dip of the limb of 15° is taken as the upper limit of the wavelength-selection process of the infinitesimal-amplitude theory (4), even though the conventional infinitesimal-amplitude theory breaks down before the dip of the limb reaches 10° (Section 4). The fact that the rate of change of the shape of a fold is relatively independent of the details of its shape when the dip of the limb is greater than 15° is an important conclusion. Its geologic significance is discussed in Chapter IX, Section 1.

The results of this section and Section 4 can be used to discuss the low-dip stages of the dominant-wavelength fold. $\dot{A}_2/\dot{A}_1$ for the 10° stage of this fold is too high to fall on a smooth curve determined by the $\dot{A}_2/\dot{A}_1$ of the other stages (fig. 16). At a 10° limb-dip the value of $\dot{A}_2/\dot{A}_1$ is proportional to $A_2/A_1$ , so that the pure sine curve $y(x)$ chosen for the initial shape is too sharp for $\dot{A}_2/\dot{A}_1$ to rise smoothly with the approximately exponential dependence on limb-dip determined by $L/L_1$ . The effect of this abnormal sharpness persists until the 36° stage, when the normal growth of $A_2/A_1$ begins to mask its presence (fig. 14).

---

(4) Biot, op. cit.

The compensation mechanism by which the sharpness of the initial shape is masked at higher dips by the normal development of the fold shape will be effective only if the absolute magnitudes of the higher harmonics in the initial shape are small in comparison to the values they would have at high limb-dips in the normal growth of a fold with the given $L/L_d$. Apart from this restriction the shape at relatively high limb-dips (greater than 45°) is relatively independent of the starting shape. This independence allows the arbitrary assumption of a particular initial shape at the 10° stage, provided that the initial shape is a smooth one.

6. Isoclinal style

The isoclinal style of deformation shows certain special features. When the limbs of the fold become steep and straight, their shape remains constant, and they merely move closer as the folding proceeds. The strain-rate field in the medium becomes one of simple extrusion between walls of fixed length. In contrast to this simple behavior in the limb region, near the crest the $\dot{\theta}$ of the plate must change rapidly. $\dot{\theta}$ will be small in the limb region; as the crest is approached it must rise to a maximum and then decrease to zero at the crest itself. The rate of change of the curvature must be close to zero on the limb, positive and large where the layer is "unrolling", and negative and large near the crest itself. This region of rapid change

must be concentrated closer and closer to the crest as the folding proceeds. The portion of the medium just inside the crestal region must exert large stresses on the plate, and it is probable that the orientation and magnitude of the strain-rates change rapidly with distance.

Although these features affect the validity of the computations of the present study in the isoclinal stages, a definition of the isoclinal style can be proposed. This definition is based on the $\dot{\theta}$ distribution, although it might be possible to define the stage on the basis of the strain distribution in the medium or the shape of the fold. In figures 18a through 18d $\dot{\theta}$ is plotted as a function of $s$ for selected stages of the weak-plate fold. It can be seen that as the dip of the limb increases from 43° to 69° the maximum value of $\dot{\theta}$ moves nearer to the crest. For the 69° stage, $\dot{\theta}$ in the limb region is still relatively high, but it is essentially constant. When $\dot{\theta}$ is essentially constant over two thirds of the distance from limb to crest and rises to a sharp maximum before falling to zero, the style of folding may be called isoclinal. Three hypothetical $\dot{\theta}$ distributions in the isoclinal stages are pictured in figure 18h.

A consequence of the special features of the isoclinal style is that mathematical simplifications that were valid in the earlier stages of folding may break down during the isoclinal stage. When the curvature at the crest of the fold becomes large, the layer can no longer be considered

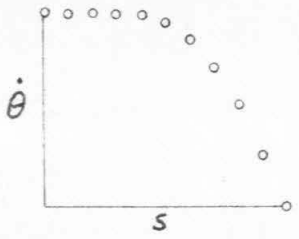


a) L = 4.6$L_d$, 43° limb-dip.

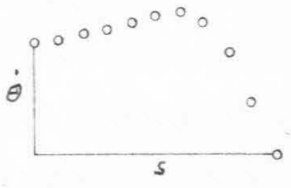


b) L = 4.6$L_d$, 53° limb-dip.

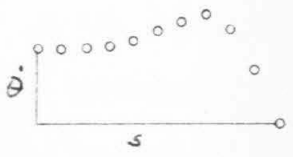


c) L = 4.6$L_d$, 63° limb-dip.

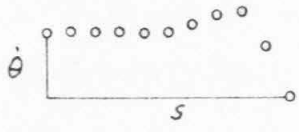


d) L = 4.6$L_d$, 69° limb-dip.

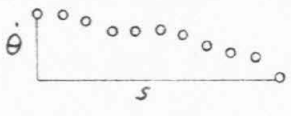


e) L = 4.6$L_d$, 79° limb-dip.

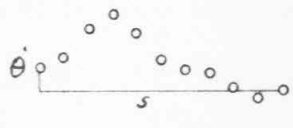


f) L = 4.6$L_d$, 89° limb-dip.

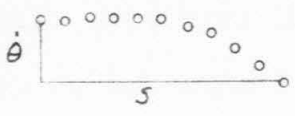


g) L = $L_d$, 89° limb-dip.

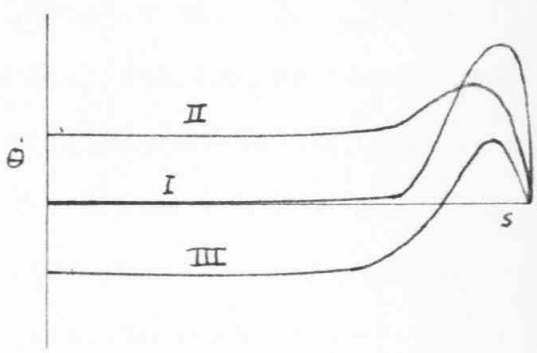


h) Hypothetical curves demonstrating the isoclinal style.

Figure 18.-- $\dot{\theta}$ plotted as a function of s for selected stages of the L = 4.6$L_d$ and L = $L_d$ folds. $\dot{\theta}$ scale is arbitrary.

as a thin plate. It is probable that the stress distribution across the plate is no longer linear. Strong tension in the limb and probable strong compression in the horizontal part of the crest make the validity of the assumption of inextensibility of the plate somewhat dubious, especially for the weak-plate fold where $\mu_p/\mu_m$ is relatively low.

The rapid change of the pattern of deformation in and near the crestal region also affects the validity of the discrete treatment of the problem. It may no longer be sufficient to describe the shape and the velocity of the plate by only ten $\Theta$ values and ten $\dot{\Theta}$ values. The description of the shape and the velocity in terms of two or three harmonic coefficients is no longer possible. The lower harmonics in the $\dot{\theta}$ distribution decrease in amplitude, and the higher harmonics increase, because the changes in inclination are all concentrated in a narrow range of arc length near the fold crest (figs. 16 and 17). This adversely affects the smoothing process (Chapter VII, Section 3), since the discretization errors affect the higher harmonics more strongly. The most serious consequence is the breakdown of the extrapolation process by which the new shape is determined (Chapter VII, Section 5). For this extrapolation to be effective, it is necessary that the various harmonics in the $\dot{\theta}$ distribution change regularly as the dip of the limb increases. In the isoclinal stage this is no longer true, at least with the time step used, and extrapolation of the harmonic coefficients becomes very difficult.

This difficulty in extrapolation is illustrated in figures 16 and 17 where $\dot{A}_2/\dot{A}_1$ and $\dot{A}_3/\dot{A}_1$ are seen to drop sharply for the 79° stage. $\dot{A}_2/\dot{A}_1$ and $\dot{A}_3/\dot{A}_1$ for the 89° stage cannot be plotted in figures 16 and 17, since they change sign ( $\dot{A}_2/\dot{A}_1 = 0.0474$, $\dot{A}_3/\dot{A}_1 = -0.3300$). Figures 18e and 18f show the $\dot{\theta}$ distribution for the 79° and 89° stages of the weak plate. It is concluded that the shapes of these two stages do not have quantitative significance, even though a visual examination of the fold shapes does not indicate that they are in error (fig. 10).

Difficulties also arise in the treatment of the medium. The radius of curvature is no longer large relative to the mesh length, and it is probable that the strain-rate changes rapidly from one mesh point to the next. For example, in the 89° stage of the weak-plate fold, the radius of curvature at the crest is 2.7 mesh lengths. (Note that the plate thickness corresponding to a viscosity ratio $\mu_p/\mu_m$ of 16 is about one mesh length.)

The strain-rate field in the medium for the 79° and 89° stages does not reflect the irregularities shown by the $\dot{\theta}$ distributions (figs. 18e and 18f). This may be due to the fact that the velocities of points on the plate are found by integrating $\dot{\theta}$ ; the plate velocities for these stages are therefore more regular than the $\dot{\theta}_i$ . If a much shorter time step had been used in the isoclinal stages, the resulting shape of the 89° stage would show more compression and considerably higher amplitude. Except for this effect, the

strain-rate and strain fields for the 89° stage (fig. 27) are probably still valid. Increased amplitude would probably not change the strain-rate field appreciably, but it would increase the cumulative strains.

With a smaller mesh spacing and a considerably smaller time step, the present method could be used to calculate the development of the folding in the isoclinal stage. However, since the physical assumptions break down at the same time as the numerical treatment, it would be more logical to conduct a quantitative study using a different formulation of the problem. Such a formulation would have to account for the finite thickness and possible elongation of the plate.

The isoclinal style defined above does not coincide with the conventional geologic definition of isoclinal folding. The 89° stage of the dominant-wavelength fold has an isoclinal shape, since the limbs are parallel, but the $\dot{\theta}$ distribution of this stage (fig. 18g) does not show the characteristics of the isoclinal style.

When the $\dot{\theta}$ distributions of the weak-plate fold and the dominant-wavelength fold are compared, it seems probable that the limb-dip of the $L = L_d$ fold will become considerably greater than 90° before the limb begins to return to the vertical. An overturning of at least 10° is to be expected from the growth of the $\dot{A}_i$ (figs. 16 and 17), although further extrapolation is of doubtful value, since the $\dot{\theta}$ distribution may start to change more rapidly

after the limb becomes overturned. Such a fold with both limbs overturned is called a fan fold (5).

If the horizontal shortening continues, any fold must eventually deform in the isoclinal style, provided that the layer remains coherent. As the vertical portions of a fan fold approach each other, the material inside the fold will be compressed strongly at the same time that it becomes more difficult for it to be extruded from the core of the fold. As the pressure in the core continues to rise, the stresses due to the extrusion process will become large in comparison to the bending resistance of the plate, and the limb will approach the vertical again.

Figure 18h shows three hypothetical curves indicating the isoclinal stage. Curve I shows the isoclinal style when the limbs are parallel. Curve II, which is modeled after figure 18d, shows an earlier isoclinal stage when the limbs are not yet vertical. Curve III shows the way in which the dominant-wavelength fold will probably approach the final isoclinal stages. $\dot{\theta}$ in the limb region must be negative for the limb to return to the vertical position.

This discussion of the isoclinal style is necessarily somewhat hypothetical. Nevertheless, two conclusions are clearly indicated by the results of the computations: (1) In the 69° stage of the weak-plate fold the limbs approach each other while remaining essentially straight; all of the

---

(5) M. P. Billings, Structural geology: New York, Prentice-Hall, Inc., 2d ed., 1954, p. 42

bending is concentrated in the crestal region (fig. 18d). (2) The dominant-wavelength fold will become a fan fold.

7. Deformation of the medium

As examples of the $\phi$ field in the medium, figures 19 and 20 show $\phi_t$ at the grid points for two stages of the dominant-wavelength fold. To get the total $\phi$ at each point, $\phi_c = -xy$ must be added to the plotted values. Figure 19 shows the 23° stage, where the medium velocities associated with the folding are much larger than those associated with the uniform compression (low-dip style); figure 20 shows the 81° stage, where the reverse is true (high-dip style).

A contour map of the $\phi$ values could be used to represent the velocity field. The velocity at any point is parallel to the contour of equal $\phi$ at that point, and the magnitude of the velocity is proportional to the value of the gradient of the field. However, for geologic interpretation of the velocity field in the medium, it is more convenient to plot the strain-rates and the accumulated finite strain at points in the medium.

In figures 21 to 27 the orientations and magnitudes of the principal extension rates and the major and minor axes of strain ellipses are plotted for various time stages of the dominant-wavelength and weak-plate folds. Strain-rates are plotted below the layer and finite strains above the layer. The original orientation of the major axes of

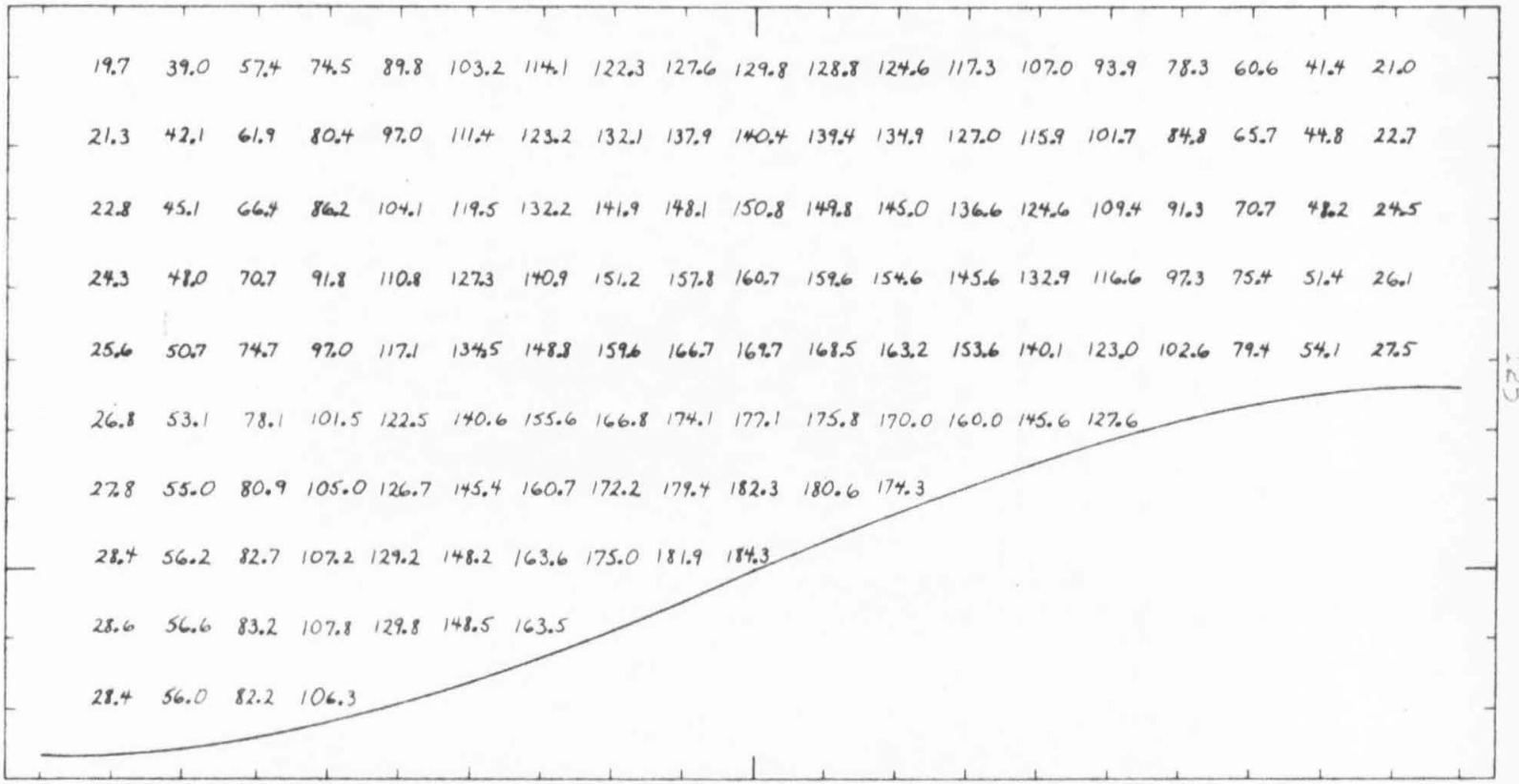


Figure 19.-- $\phi_f$ at grid points for the 23° stage of the $L = L_d$ fold. Total $\phi$ is obtained by adding $\phi_e = -xy$ to these values of $\phi_f$.

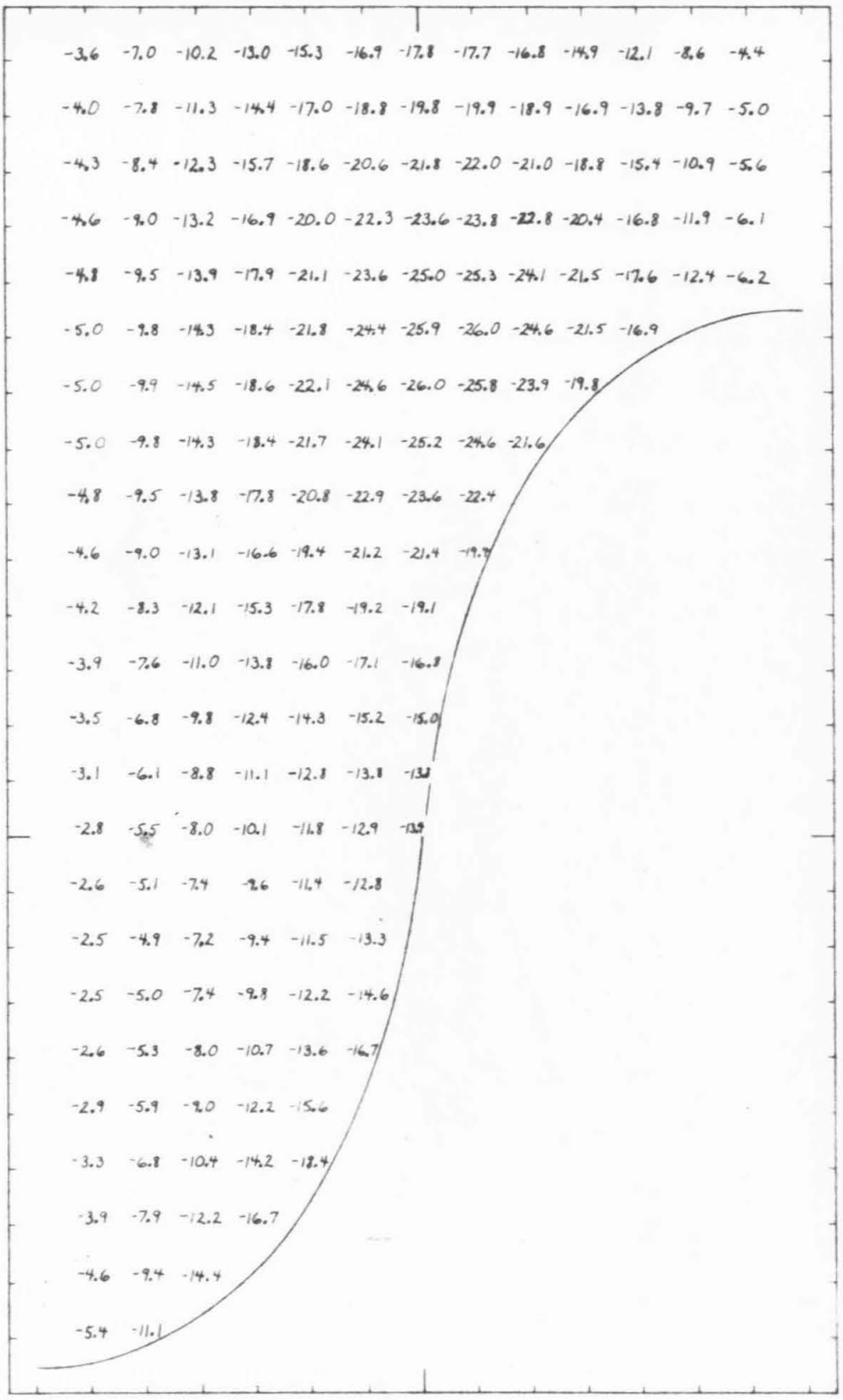


Figure 20.--$\Phi_f$ at grid points for the 81° stage of the $L = L_c$ fold. Total $\Phi$ is obtained by adding $\Phi_c = -xy$ to these values of $\Phi_f$.

UL

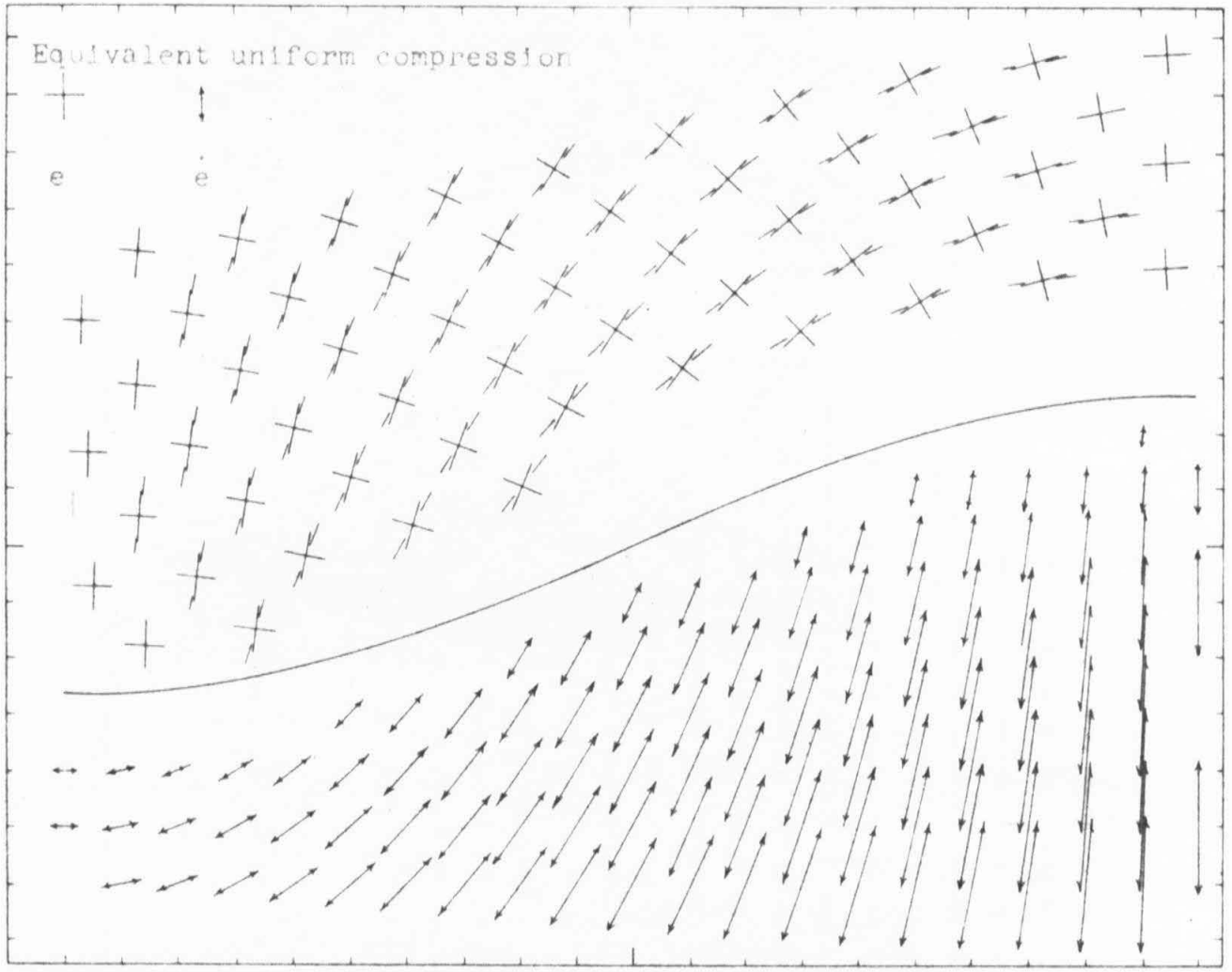


Figure 21.--Strain-rates and finite strains: $L = L_d$, 23° limb-dip. Dashed lines indicate original orientation of the major axis of the strain ellipse.

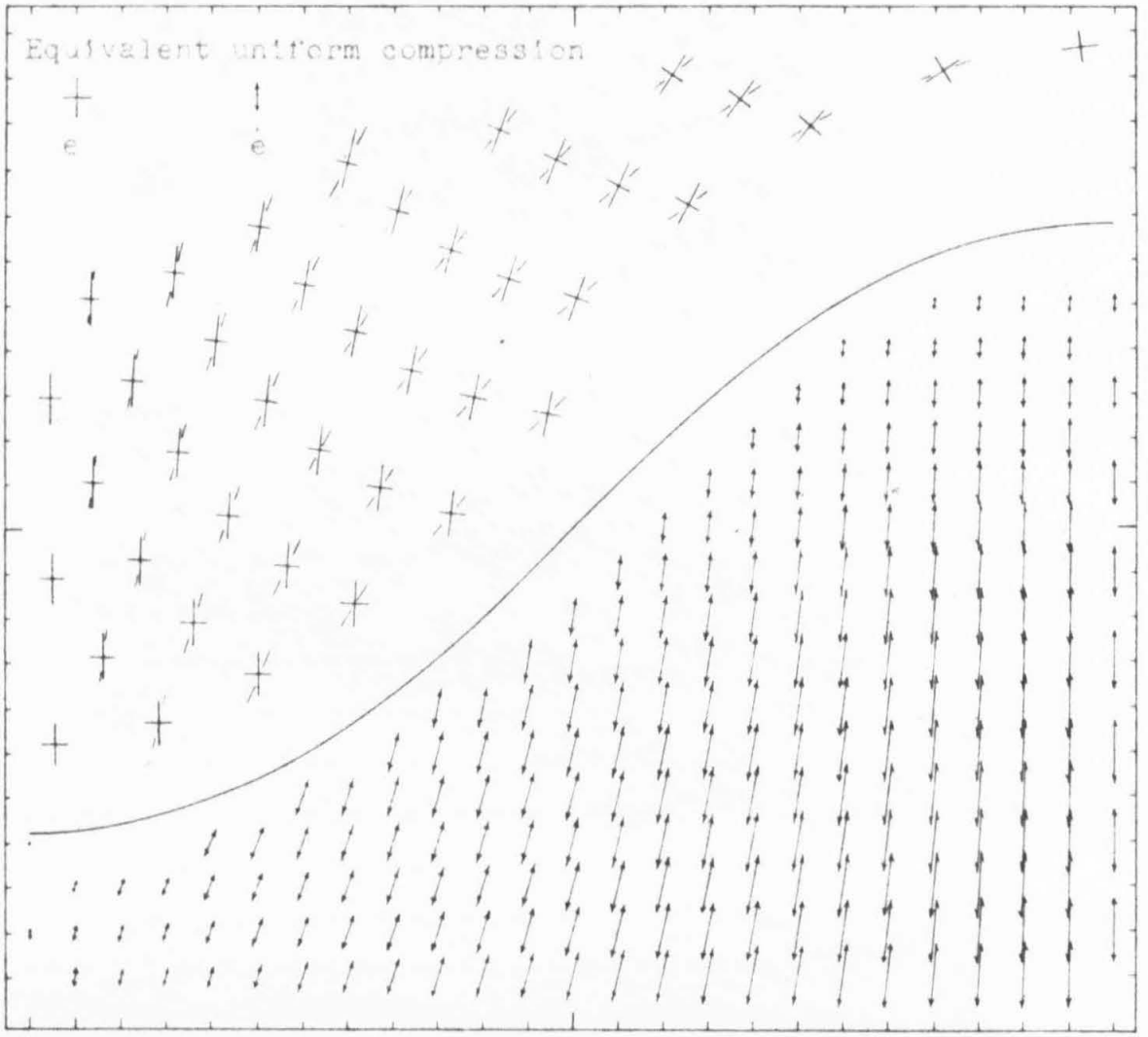


Figure 22.--Strain-rates and finite strains: $L = L_d$, 46° limb-dip. Dashed lines indicate original orientation of the major axis of the strain ellipse.

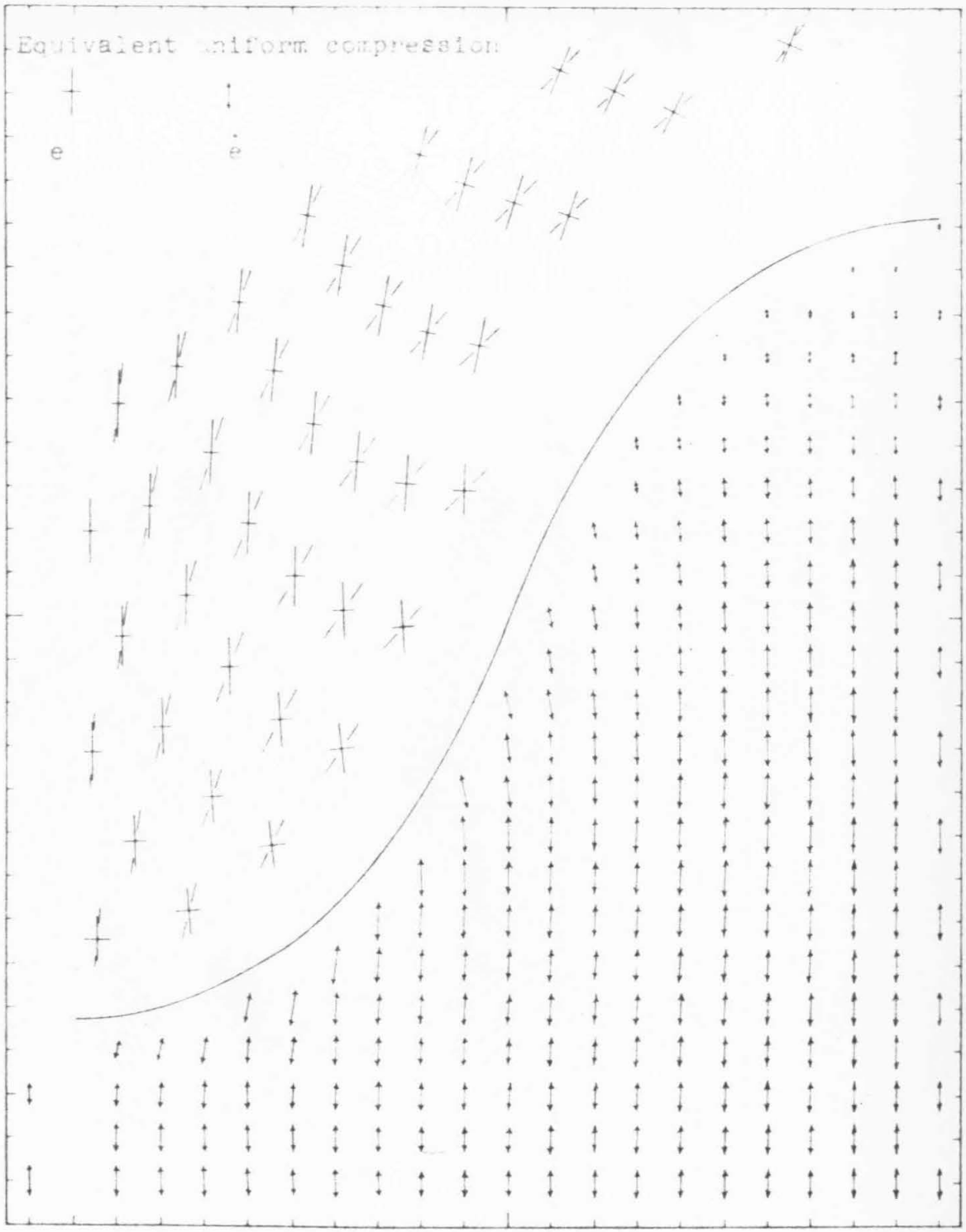


Figure 23.--Strain-rates and finite strains: L = Ld 60° limb-dip. Dashed lines indicate original orientation of the major axis of the strain ellipse.

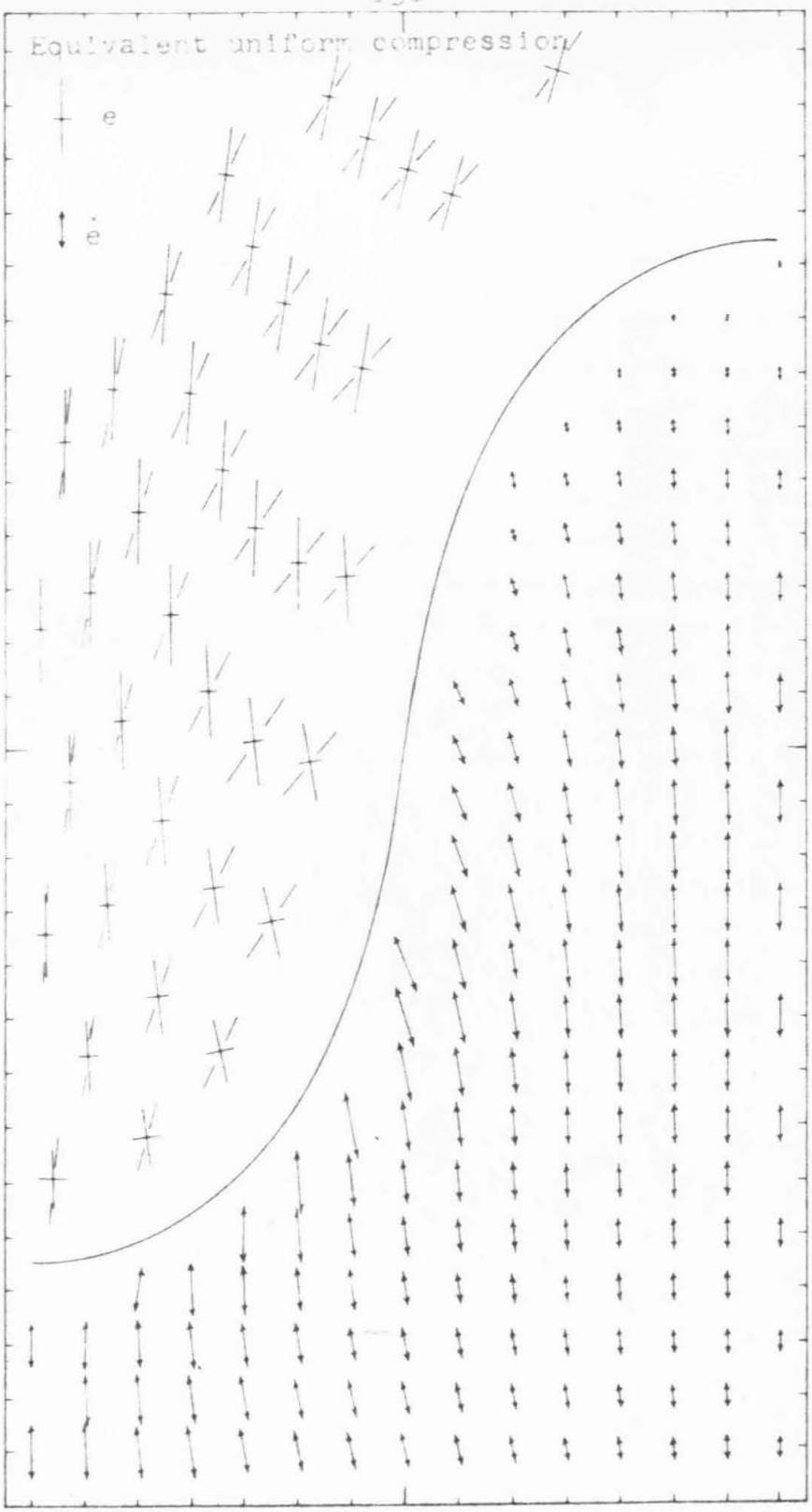


Figure 24 --Strain-rates and finite strains: L = Ld 81° limb-dip. Dashed lines indicate original orientation of the major axis of the strain ellipse.

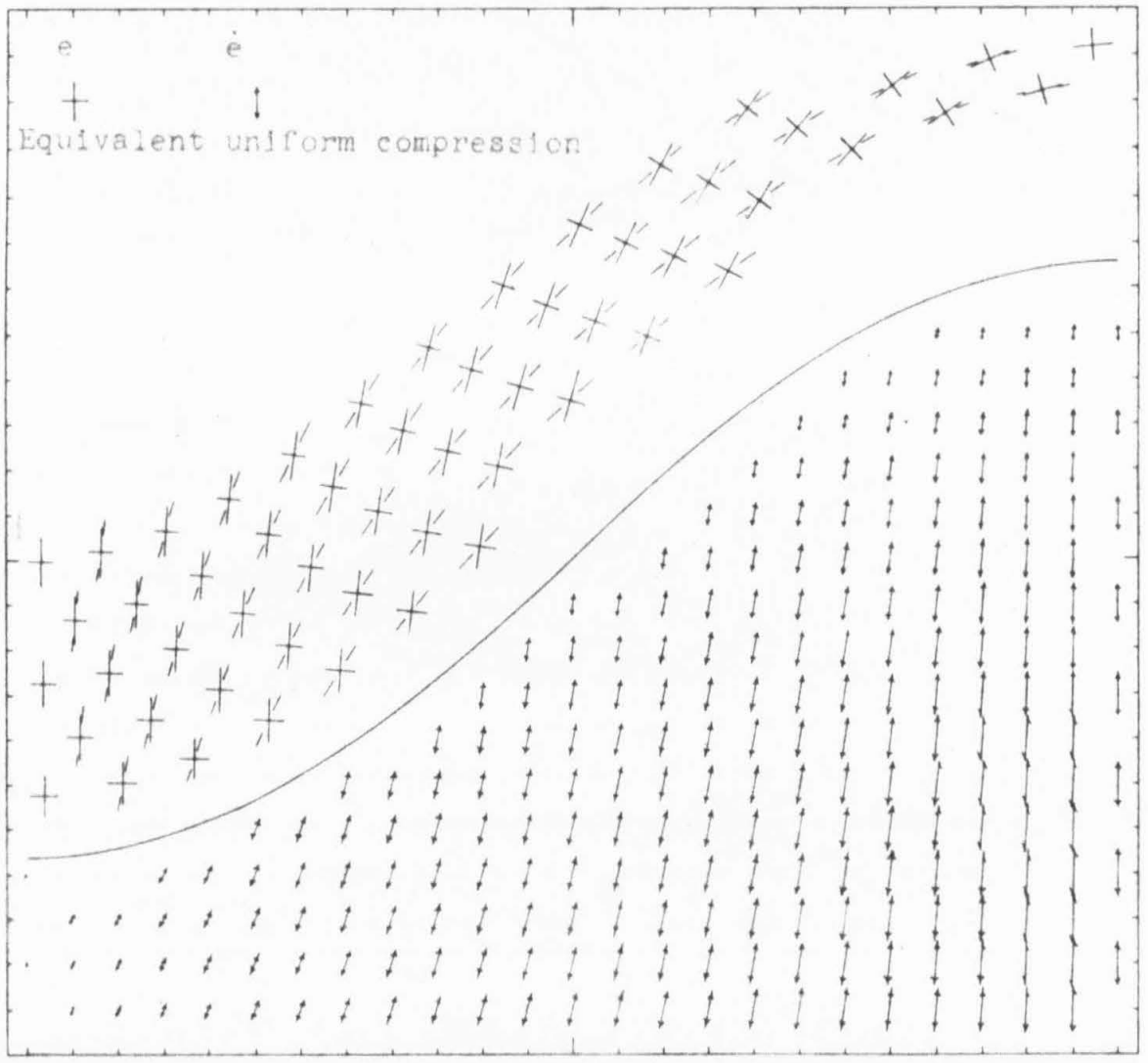


Figure 25.--Strain-rates and finite strains: $L = 4.6L_0$, 43° limb-dip. Dashed lines indicate original orientation of the major axis of the strain ellipse.

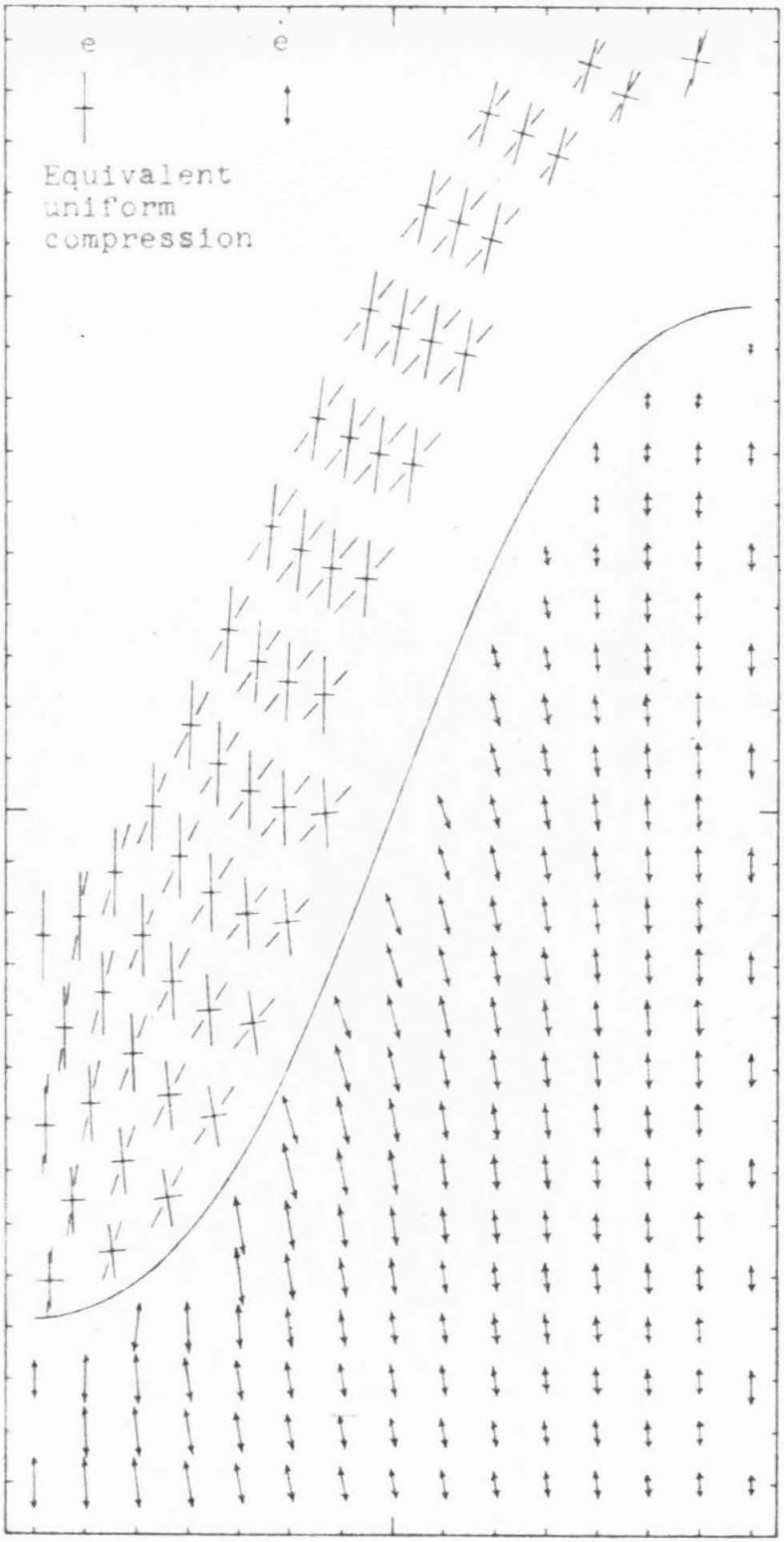


Figure 26.--Strain-rates and finite strains: $L=4.6L_d$, 69° limo-dip. Dashed lines indicate original orientation of the major axis of the strain ellipse.


Figure 27.--Strain-rates and finite strains: $L = 4.6L_d$, $89^\circ$ limb-dip. Dashed lines indicate original orientation of the major axis of the strain ellipse.

the strain ellipses are shown by dashed lines. The finite strain can be considered to be the sum of a pure strain and a rigid rotation.

The methods used to calculate the strain-rates and the finite strains are described in Appendix A. It should be mentioned that the method used to calculate finite strain is somewhat inaccurate; therefore, the finite strains plotted in figures 21 to 27 should be regarded as approximate only. In particular, the principal axis orientation for the smaller strains is not well determined.

Certain aspects of the strain-rate fields have been discussed in connection with the stages of folding (Section 2). In the present section prominent features of the strain-rate and total strain fields are pointed out, and certain peculiarities are explained. Interpretation of the strains and the strain-rates in terms of geologic strain indicators is made in the next chapter.

The most prominent feature of the strain and strain-rate fields is the relatively uniform orientation of the planes of maximum flattening and maximum flattening rate. By the time the dip of the limb reaches $45^{\circ}$ the planes of flattening and flattening rate are oriented approximately parallel to the axial plane of the fold, and they preserve this orientation into the isoclinal stage. The behavior of the cumulative strain closely parallels that of the strain-rate. The symmetry of the problem requires that the planes of maximum flattening be parallel to the axial plane at the

right- and left-hand walls, and the assumption of inextensibility of the plate requires that they make an angle of 45° with the plate as they approach it. The fact that they are sub-parallel to the axial plane over most of the interior of the fold is an important result of this study; its geologic interpretation will be discussed in the next chapter.

There are several significant deviations from this axial-plane orientation. In the early portion of the low-dip stage, the material in the medium above the crest of the fold is extending in a horizontal direction; by the time the dip of the limb reaches 45° the extension in this region is vertical, though it remains small due to the shielding effect of the inextensible plate. In the low-dip stage $\frac{\partial v}{\partial x}$ is positive inside the crest of the fold (6), and the resulting shear strain-rate causes the planes of maximum extension rate to form an anti-fan with respect to the axial plane.

When the high-dip stage is reached, the extrusion of the medium out of the inside of the crest past the limbs causes $\frac{\partial v}{\partial x}$ to become negative and the planes of maximum extension rate to form a fan rather than an anti-fan. Even in the high-dip stage, the folding of the layer produces a positive $\frac{\partial v}{\partial x}$ just inside the crest of the fold, and the planes of maximum flattening rate continue to dip away from the axial plane here. This effect is probably exaggerated

---

(6) The anticlinal portion of the fold is taken to be in the upper right-hand quadrant of the coordinate system in this section.

by the high curvature of the plate in the 89° stage of the weak-plate fold (fig. 27). The strain-rates in this region are very small, however. The same effect is present above the crest of the fold.

This transition from fanning to anti-fanning is reflected in the cumulative strains. It is somewhat surprising that the transition takes place at the same dip of the limb for both the strain rates and the cumulative strains. For the cumulative strains, the transition is caused by the rotation. Comparison of the initial and final orientations of the major axes of the strain ellipses in figures 22 and 23 shows that the rate of rotation is large at the transition from low-dip style to high-dip style. Rotation rates can be calculated from the $\phi$ field at any stage: between the 46° and 56° stages of the dominant-wavelength fold the rotation rate would produce a positive rotation of several degrees.

The cumulative strains are computed on the basis of the new positions of the points of an originally square grid, so that the strains of a particular small region can be traced from stage to stage by picking plotted strain axes in corresponding positions with respect to the layer. If we follow a particular strain axis from stage to stage, we see that the rotations increase rapidly in the early stages of the folding and continue to increase, but at a slower rate, in the later stages. Comparison of the strain axes with reference axes showing the finite strains that would result

from a uniform compression with the same shortening shows that: (1) the crestal region near the plate is shielded from deformation and shows less flattening in the high-dip stages than would be due to uniform compression; (2) in the limb region the flattening is larger than would be produced by uniform compression.

8. Energy dissipation

Additional information about the physical nature of the folding process can be obtained from a consideration of the relative values of the dissipations in the different sub-regions of the region considered.

The bending dissipation in the plate is calculated directly from the sum of the squares of the differences of the $\dot{\theta}_i$ . The dissipation in the grid portion of the medium is calculated from the strain rates at each grid point. Although it is not strictly correct to use the strain-rate calculated from a 9-point array which includes points on both sides of the plate, the dissipations calculated from these arrays were included in the total medium dissipation. The error introduced in this way will not be large enough to affect any of the conclusions drawn from a consideration of the total dissipation. Since the problem region extends to infinity in the direction of the y-axis, the total dissipation in the medium would be infinite if the dissipation due to uniform compression were included. To avoid this problem, and to focus attention on the dissipation due to the folding process itself, the dissipation due to the uniform compression

of a strip of the same width as the problem region is subtracted from the dissipation calculated for the medium. This removal of the uniform compression makes the dissipations calculated directly comparable to those of the infinitesimal treatment, since in the infinitesimal range the uniform compression is negligible in comparison to the folding.

In figures 28a and 28b the ratio of the dissipation in the medium to the bending dissipation in the plate is plotted as a function of the dip of the limb for the dominant-wavelength and the weak-plate folds. The ratios given by the infinitesimal treatment (7) are 2 for $\underline{L} = \underline{L}_d$ and 200 for $\underline{L} = 4.6\,\underline{L}_d$ .

In the low-dip stage of folding this ratio decreases steadily as the velocity of points on the plate approaches more and more closely the velocity which would be associated with the uniform compression of the medium if the layer were not present. At a dip of the limb approximately corresponding to the start of the high-dip stage, the ratio passes through a minimum and starts to rise rather steeply. This steep rise is caused by the extrusion of material in the medium from the inside of the crest of the fold. Presumably, the ratio would continue to rise during the isoclinal stage and would become very large as the limbs approach each other more and more closely. The scatter of the last two points in figure 28b is caused by breakdown of

---

(7) Biot, op. cit.

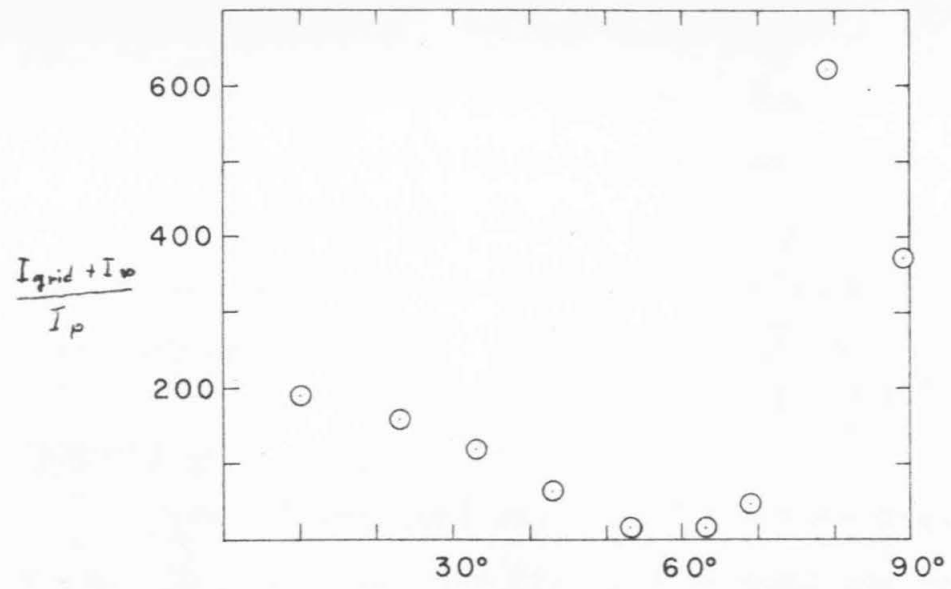


b) $L = 4.6L_d$.

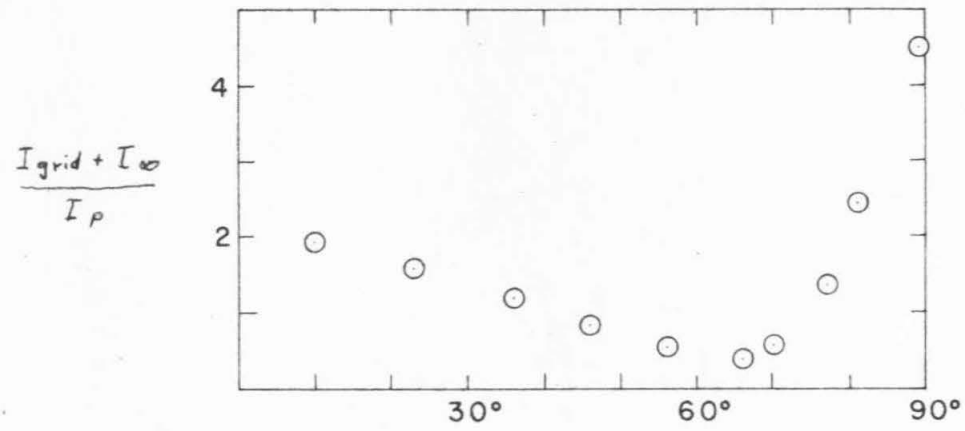


a) $L = L_d$.

Figure 28.--Ratio of dissipation rate in the medium, exclusive of uniform compression, to bending dissipation rate in the plate plotted as a function of limb-dip for the dominant-wavelength and weak-plate folds.

the calculation in the isoclinal range (Section 6). The position of the minima of the curves of figures 28a and 28b is an indication of the validity of the separation of the folding into high-dip and low-dip styles, since these minima occur at limb-dips corresponding to the transition between the two styles.

## 9. Summary of results

In table 4 selected results of the numerical computations are tabulated for the free-plate, dominant-wavelength, and weak-plate folds.

TABLE 4.--Summary of the results of the computations

| | free plate | dominant wavelength | weak plate |
|---|---|---|---|
| $L/L_d$ | $\ll 1$ | 1 | $\sqrt[3]{100} \approx 4.6$ |
| $\mu_p/\mu_m$ for thickness $h = L/40$ | $\infty$ | 1650 | 16.5 |
| Limb-dip of transitions between styles: | | | |
| low-dip to high-dip | -- | 66° | 60° |
| high-dip to isoclinal | -- | >90° | 69° |
| Probable maximum limb-dip | 120° | 100° | 90° |
| Ratio of maximum curvature to average curvature at limb-dips of: | | | |
| 23° | 1.571 | 1.587 | 1.625 |
| 45° | 1.575 | 1.589 | 1.798 |
| 55° | 1.579 | 1.598 | 2.198 |
| 70° | 1.586 | 1.634 | 3.285 |
| Ratio of medium-dissipation to plate-dissipation: | | | |
| infinitesimal treatment | 0 | 2 | 200 |
| minimum | 0 | 0.40 | 10 |
| Limb-dip at minimum ratio | -- | 66° | 59° |

# CHAPTER IX

# DISCUSSION

## 1. Significance of the shape variations

The variation in the shapes of finite-amplitude folds corresponding to variation in the ratio of the fold wavelength to the dominant wavelength is clearly recognizable by visual examination of the computed fold shapes (figs. 8-13). We now investigate whether or not this variation can be recognized in natural folds. In order to discuss this we must examine three questions: (1) The initial starting shape for each fold has been chosen to be very regular. Since natural folds will not necessarily start from such regular shapes, are initial irregularities likely to mask the regular shape variation found in this study? (2) To what extent is the shape variation found in this study sensitive to the details of the mathematical assumptions made in formulating the problem? (3) Can this systematic shape variation be separated from shape irregularities which are found to some extent in all natural folds?

1) Initial shape.--On the basis of the infinitesimal treatment and of the finite-amplitude analysis of the present study, the following picture of the growth of a train of natural folds may be presented. The growth process starts from an essentially plane layer, with a random distribution

of small deviations from a perfectly plane shape. The wavelength of each individual fold in the train is determined by the wavelength-selection process described by Biot (1). If the initial irregularities are small enough, the folds will have a relatively uniform wavelength, the dominant wavelength. If the initial irregularities are large enough so that a regular wavelength has not developed by the time the maximum dips of the folded layer are about fifteen degrees, there will be a range of wavelengths in the fold train, since the wavelength-selection process is not operative beyond this stage (Chapter VIII, Section 5). In the later portion of this stage, the "primary" shape of the individual folds is also determined. This primary shape will be determined to a certain extent by the initial irregularities present in the infinitesimal stage. Sufficiently small irregularities at the start of the infinitesimal stage will tend to produce a regular shape in the primary stage as well as a regular wavelength. From this fifteen-degree-dip stage on, the rate of change of the shape is determined by the amplitude of the fold and by the ratio of the fold wavelength to the dominant wavelength. No evidence was found in this study that the magnitude of any harmonic coefficient in the shape could decrease at any stage short of the isoclinal stage. Initial irregularities will therefore persist beyond the fifteen-degree-dip stage, but they

---

(1) M. A. Biot, Theory of folding of stratified viscoelastic media and its implications in tectonics and orogenesis: Geol. Soc. America Bull., v. 72, 1961, p. 1595-1620

will not be magnified. The final shape will not be completely independent of the primary stage but will be determined mainly by growth beyond the primary stage.

Two qualitative predictions can be made on the basis of this picture of the course of growth of a fold. First, in a fold train which includes folds with a range of wavelengths, the longer wavelength folds should have sharper shapes than the shorter wavelength folds. Second, if a train of folds with a regular wavelength and relatively constant shape is found, the shape of these folds should be sharp if the viscosity ratio, $\mu_p/\mu_m$ , has decreased significantly during the folding process and less sharp if the viscosity ratio has remained constant or increased.

2) Detailed assumptions of the calculation.--With regard to the shapes produced, the two most critical assumptions are probably the assumptions of linear viscosity and inextensibility of the plate. As the stresses in the bending layer become high, it is possible that new mechanisms of deformation come into play. The effect of these new mechanisms would be to decrease the apparent viscosity of the plate. Also, high stress could lower the apparent viscosity even if no new mechanisms operate, if the stress-strain-rate relation is non-linear. Therefore, natural folds which develop at the dominant wavelength may have shapes which are sharper than those calculated for the dominant-wavelength fold.

It seems likely that this effect is present in nature,

since the shapes of the dominant-wavelength fold appear to be too broad, especially at high amplitudes. The results of the present study predict that the dip of the limb of the dominant-wavelength fold will increase beyond 90°; fan folds of this sort are found in nature, but they are the exception rather than the rule. Since the infinitesimal treatment predicts that the dominant wavelength should be the most common one in natural folds, the finite-amplitude shape associated with the dominant wavelength should be the most common shape. Clear evidence that most natural folds deviate from the shapes calculated in this study for $\underline{L} = \underline{L}_d$ would strongly suggest that the natural layers had followed a non-linear rheological law.

This possibility of recognizing the presence of non-linear rheological properties is an important result. In order to exploit this possibility, further work is indicated: (1) A theoretical study of the finite amplitude shape of a layer with non-linear rheological properties should be made. Investigation of a non-linear free plate would be mathematically feasible, and the effects of the medium could be estimated on the basis of the results of the present study. (2) A critical study of the shapes of single-layer natural folds should be made to determine more precisely what is the most common natural shape.

Although the consequences of the assumption of an inextensible plate are more difficult to assess, we can get an idea of their seriousness by examining the limiting

case of equal plate and medium viscosities. In this limiting case an initial sinusoidal fold will retain its sinusoidal shape under uniform compression. If the layer were not assumed to be inextensible, its shape would tend toward this sinusoidal limit as the viscosity ratio is decreased. In table 5 are tabulated the ratios of the first few harmonic coefficients for the 56° stage of the dominant-wavelength fold, the 53° stage of the weak-plate fold, and a sine wave which coincides with the weak-plate fold at the limb and the crest.

TABLE 5.--Comparison of $A_i/A_1$ for $L = L_d$ and $L = 4.6\,L_d$ folds with $A_i/A_1$ for a sine curve

| | $L = L_d$ 56° limb-dip | $L = 4.6\,L_d$ 53° limb-dip | sine curve |
|---|---|---|---|
| $i$ | $A_i/A_1$ | $A_i/A_1$ | $A_i/A_1$ |
| 2 | -0.0047 | -0.0827 | -0.1256 |
| 3 | 0.0000 | 0.0078 | 0.0296 |
| 4 | 0.0000 | 0.0008 | -0.0084 |

This table shows that the change in shape between the dominant wavelength and the weak plate is consistent with a trend toward the sine shape of the equal-viscosity case. It thus appears that the assumption of inextensibility does not seriously affect the shape analysis, although it may affect the strain fields in the medium, as discussed

in Section 2.

3) Irregularities in the shapes of natural folds.--A systematic analysis of the shapes of natural folds has not yet been carried out. However, on the basis of the writer's experience with natural folds, he believes that it would be possible to detect natural shape variations of the magnitude found in the present study. Fourier analysis of dip as a function of arc length can be used to define the average shape of a train of regular, natural folds, and consideration of the size of the neglected harmonic coefficients can provide a measure of the meaningfulness of this average shape. If sufficiently regular natural folds are selected, comparison of the average shapes with the shapes computed in this study will give valuable information about the deformational history of the natural folds and the rheological laws under which they have deformed.

## 2. Strain field and strain-rate field in the medium

The strain and strain-rate fields plotted in figures 21 to 27 can be compared with observable geologic features. The directions and amounts of cumulative flattening can be measured by means of deformed fossils and oolites, and it may be possible to interpret the finite rotations in terms of rolled garnets. Strain rates are not directly observable, but the dynamic analysis of calcite twin lamellae (2) provides

---

(2) F. J. Turner, Nature and dynamic interpretation of deformation lamellae in calcite of three marbles: Am. Jour. Sci., v. 251, 1953, p. 276-298

a measure of the last increment of strain; the orientation of this strain increment will be given by the orientation of the strain-rate during the last stage of the deformation.

With the possible exception of rolled garnets, the strain indicators discussed in the previous paragraph can be interpreted in a relatively straightforward manner, but since they require microscopic observation they are not commonly measured. Cleavage, on the other hand, is a macroscopic property, and its orientation is commonly recorded in field studies of deformed rocks. For this reason, we shall discuss the way in which cleavage in folded rocks can be related to the calculated strain-rate and cumulative strain fields, even though its interpretation is not as well understood as that of the strain indicators mentioned in the previous paragraph. Cleavage is defined as the property possessed by certain rocks of splitting more easily along planes with a certain orientation (3). The following discussion will refer to cleavage that is determined by the alignment of micaceous minerals or by a preferred plane of flattening of other mineral grains.

There are two classic geologic explanations of cleavage: (1) cleavage is parallel to planes of maximum shear stress or planes across which maximum shearing movements have taken place, and (2) cleavage is parallel to the planes of maximum flattening or perpendicular to the maximum

---

(3) E. S. Hills, Outlines of Structural Geology: London, Methuen and Co., Ltd., 3d ed. rev., 1953, p. 104

compressive stress. Goguel (4) gives an extensive, though somewhat polemical, discussion of the problem. In the following discussion the second mode of formation is assumed. This explanation seems preferable on the basis of geologic observations, and it is compatible with the results of the present computations.

Even if we restrict consideration to the second mode of origin, there are two possibilities for the physical conditions that determine cleavage orientation: (1) it is perpendicular to the maximum compressive stress at any given instant; (2) it is parallel to the plane of flattening of the strain ellipsoid at any time. Preferred flattening of grains is best explained by the second possibility, but the alignment of micaceous minerals might be determined by either mechanism. Unfortunately, the results of the present study do not provide a clear method of distinction between these possibilities, since the orientations of the finite strains do not differ markedly from those of the strain-rates.

When found in association with folded rocks, cleavage is usually sub-parallel to the axial planes of the folds, and it often shows a characteristic fan pattern, with the cleavage dipping slightly toward the axial planes in the crests of anticlines and away from the axial planes in the troughs of synclines. The axial-plane orientation is shown by both the planes of maximum extension rate and the planes

---

(4) J. Goguel, Traité de tectonique: Paris, Masson et Cie, Editeurs, 1952, p. 40-44

of maximum cumulative flattening in all stages of both the weak-plate fold and the dominant-wavelength fold after the 23° stage. The fan-like orientation is shown after the folds reach the high-dip stages. An anti-fanning of the cleavage planes outside the crests of anticlines is commonly observed (5); this feature is also shown by the calculated strain fields.

Cleavage planes which show an anti-fanning relationship inside the crests of folds are not common in nature, although they have been observed (6). This may be due to the fact that well-developed cleavage is associated with strong deformation, so that most folds showing cleavage are in the high-dip stages. However, the presence of this feature in the results of the present study may represent a failure of one or more of the underlying assumptions of the mathematical treatment. Most published discussions of cleavage do not distinguish between single- and multiple-layer folds, so that a study of single-layer folds that show cleavage would be necessary to determine whether this anti-fanning is present in nature.

The anti-fanning of the planes of maximum extension rate in the high-dip style of folding occurs only immediately below the crest of the fold where the strain-rates are small. Although it may have been overlooked in nature, it is equally

---

(5) L. U. de Sitter, Structural Geology: London, McGraw-Hill Book Co., Inc., 1956, p. 96

(6) Hills, op. cit., p. 111

probable that it may be a result of the assumption of inextensibility of the plate.

Since the planes of maximum flattening and flattening rate remain approximately parallel to the axial plane throughout the course of the folding, it may be possible to observe the rotations of principal axes of strain ellipsoids in natural folds. Minerals such as garnet which grow during the course of deformation often incorporate trains of inclusions which are parallel to the schistosity. If the portion of rock surrounding the garnet rotates with respect to the external stress system while the garnet is growing, the inclusions will be parallel to the direction of the schistosity at the time they are incorporated. The resulting curved trains of inclusions will then measure the finite rotation with respect to the relatively constant stress field.

The close correspondence between the principal features of axial-plane cleavage and the computed strain-rate and strain fields is considered to be a verification of the principal assumptions made in the mathematical treatment. A more detailed examination of cleavage and other strain indicators in natural folds is needed before it can be ascertained whether the finer details of the strain fields are really present in nature or whether they result from some of the idealizations of the present study. Isotropy of the medium was assumed in all the computations, but it is clear that rocks with a well developed cleavage cannot be strictly

isotropic. A consideration of anisotropy might modify some of the conclusions, but such a consideration is beyond the scope of the present treatment.

3. Conclusion

The study of the finite-amplitude folding of a single layer leads to the following conclusions.

1) The shape of the folded layer varies systematically with the ratio of the fold wavelength to the dominant wavelength.

2) A fold whose wavelength is equal to or shorter than the dominant wavelength will develop into a fan fold if the folding progresses far enough.

3) The final shape of the folded layer is relatively insensitive to the details of the initial shape of the layer; in this respect the shape variation is analogous to the wavelength-selection mechanism of the infinitesimal-amplitude treatment.

4) The results in the very-low-dip stages show that the infinitesimal-amplitude treatment breaks down as far as fold shape is concerned before the maximum dip of the fold is $10^{\circ}$. A possible extension of the treatment up to limb-dips of about $15^{\circ}$ has been found, but beyond the $15^{\circ}$ stage the wavelength-selection process is no longer operative. Analysis of the limit of the infinitesimal stage makes it clear that the main prerequisite for the development of a regular wavelength is that the initial shape irregularities

be sufficiently small or sufficiently regular. If this condition is satisfied, the resulting fold train will have a regular shape as well as a regular wavelength.

5) Single layer folds progress through three styles of deformation as the folding proceeds. Each style is characterized by its own pattern of deformation in the medium.

Retention of the fundamental physical assumptions of the infinitesimal treatment, coupled with relaxation of its geometrical restrictions, has made possible a number of predictions which can be tested against naturally occurring folds. Comparison of two of these predictions with natural folds shows that the theory provides a reasonable approximation to the natural folding process: (1) The shapes of the calculated folds are relatively close to those found in nature. (2) The calculated strain-rate and finite strain fields in the medium show the characteristic orientation and fanning of axial-plane cleavage.

More detailed study of natural folds is needed to test the other predictions: (1) The predicted shape variation can be tested only by a detailed study of the shapes of naturally occurring single-layer folds. Such a study might yield important results regarding the rheological properties of the layer. (2) The details of the strain-rate and finite strain fields can be tested by detailed examination of natural folds.

# APPENDIX A

## CALCULATION OF THE STRAIN-RATES AND CUMULATIVE FINITE STRAINS

### 1. Strain-rates

With the notation of figure 3 (p. 51) the strain-rates are given by the following expressions:

$$\dot{e}_{12} = \frac{1}{2}\left(\frac{\partial u}{\partial x} + \frac{\partial v}{\partial y}\right) = \frac{1}{2}(\phi_{,11} - \phi_{,22}) = \frac{\phi_E + \phi_W - \phi_N - \phi_S}{2},$$

$$\dot{e}_{11} = -\dot{e}_{22} = \frac{\partial u}{\partial x} = \phi_{,12} = \frac{\phi_{NE} - \phi_{NW} + \phi_{SE} - \phi_{SW}}{4}.$$

The principal strain-rates and the orientation of the principal axes are calculated by the standard formulas. (1)

### 2. Finite strains

The first step in the computation of the finite strains is to compute the new coordinates of an originally square grid after it has been deformed. If $\underline{X}(\underline{t})$ and $\underline{Y}(\underline{t})$ represent the coordinates of a particular point imbedded in the medium during an interval of time $o < t < \Delta t$ when the spatial distribution of the velocity remains essentially constant, then the final positions of the point are given by:

---

(1) J. C. Jaeger, Elasticity, fracture and flow: London, Menthuen and Co., Ltd., 1956, p. 40-41

$$X(\Delta t) = X(0) + \int_0^{\Delta t} u(X(t), Y(t))\, dt ,$$

$$Y(\Delta t) = Y(0) + \int_0^{\Delta t} v(X(t), Y(t))\, dt .$$

The numerical computation of these integrals, when $\underline{u}$ and $\underline{v}$ are known only at a set of grid points, would be very complicated; the new grid positions calculated would still not be accurate, since $\underline{u}$ and $\underline{v}$ vary with time as well as with $\underline{X}$ and $\underline{Y}$ . Since a high degree of accuracy is not really necessary for the purposes of interpretation to which the finite strains will be put, and since errors in the finite strain calculations do not affect the rest of the numerical results of the study, the following much simpler formulas were used to calculate the new coordinates of a point:

$$X(\Delta t) = X(0) + u(X(0), Y(0))\, \Delta T ,$$

$$Y(\Delta t) = Y(0) + v(X(0), Y(0))\, \Delta T .$$

$\Delta \underline{t}$ represents the time interval between one time step and the next; $\Delta \underline{T}$ is chosen so that the new $\underline{x}$-coordinates of the points on the right-hand wall of the problem region agree with the new $\underline{x}$-coordinate of the crest of the fold. $\Delta t$ and $\Delta T$ are not equal since the actual trajectories of points are curved. After the first time step, $\underline{X}$ and $\underline{Y}$ are not integers; the appropriate $\underline{u}$ and $\underline{v}$ are found by interpolation, using the nine $\phi$ values nearest the point under consideration.

Using this method, the positions of an originally

square grid of points can be found at each time stage. The final and original positions of a group of points can then be used to calculate the finite strain in the neighborhood of the points. The strain is treated as homogeneous over the quadrilateral enclosed by four points. The new coordinates of the points are given in terms of their original coordinates by the expressions:

$$x' = ax + by + e,$$

$$y' = cx + dy + f.$$

A group of four points will provide eight equations to determine the six coefficients $a$, $b$, $c$, $d$, $e$, and $f$; the values of the coefficients were determined by a least squares fit. Knowing the transformation coefficients it is a simple matter to compute the orientations of the principal-strain axes in the original and final coordinate systems and the relative extensions of the principal axes. Formulas for these computations are derived by Jaeger. (2)

Since the medium was assumed to be incompressible, a measure of the error involved in the computation of the distorted grid and in the assumption of local homogeneous strain can be obtained by consideration of the volume change associated with the computed strain values. The ratio of

---

(2) Ibid., p. 23-28

the area of the deformed ellipse to the original circle in the undeformed state ranged from 0.8 to 1.2. The maximum deviations from no volume-change were associated with large strains (whose ratio of major to minor axis is 9 to 1). It is thought that the main source of error lies in the computation of the deformed grid.

# APPENDIX B

## TABULATION OF THE NUMERICAL RESULTS

| | $L \ll L_d$ | | 11.4° Limb-dip | |
|---|---|---|---|---|
| $i$ | $\theta_i$ | $A_i$ | $\dot{\theta}_i$ | $\dot{A}_i$ |
| 1 | 0.19961 | 0.19962 | 0.18924 | 0.18927 |
| 2 | 0.19715 | -0.00001 | 0.18691 | -0.00003 |
| 3 | 0.18984 | -0.00000 | 0.17999 | -0.00000 |
| 4 | 0.17786 | -0.00000 | 0.16863 | 0.00000 |
| 5 | 0.16150 | 0.00000 | 0.15313 | -0.00000 |
| 6 | 0.14116 | 0.00000 | 0.13386 | -0.00000 |
| 7 | 0.11735 | -0.00000 | 0.11128 | 0.00000 |
| 8 | 0.09064 | -0.00000 | 0.08596 | -0.00000 |
| 9 | 0.06170 | 0.00000 | 0.05851 | -0.00000 |
| 10 | 0.03123 | 0.00000 | 0.02962 | 0.00000 |
| 11 | 0. | | 0. | |

| | $L \ll L_d$ | | 22.6° Limb-dip | |
|---|---|---|---|---|
| $i$ | $\theta_i$ | $A_i$ | $\dot{\theta}_i$ | $\dot{A}_i$ |
| 1 | 0.39406 | 0.39416 | 0.38440 | 0.38468 |
| 2 | 0.38922 | -0.00010 | 0.37969 | -0.00029 |
| 3 | 0.37481 | -0.00000 | 0.36569 | 0.00000 |
| 4 | 0.35118 | 0.00000 | 0.34271 | 0.00000 |
| 5 | 0.31891 | 0.00000 | 0.31130 | 0.00000 |
| 6 | 0.27878 | 0.00000 | 0.27221 | 0.00000 |
| 7 | 0.23177 | 0.00000 | 0.22638 | -0.00000 |
| 8 | 0.17904 | -0.00000 | 0.17493 | -0.00000 |
| 9 | 0.12188 | -0.00000 | 0.11911 | -0.00000 |
| 10 | 0.06170 | -0.00000 | 0.06031 | 0.00000 |
| 11 | 0. | | 0. | |

| | $L \ll L_d$ | | 33.3° Limb-dip | |
|---|---|---|---|---|
| $i$ | $\theta_i$ | $A_i$ | $\dot{\theta}_i$ | $\dot{A}_i$ |
| 1 | 0.76962 | 0.77037 | 0.70968 | 0.71175 |
| 2 | 0.76022 | -0.00074 | 0.70114 | -0.00208 |
| 3 | 0.73222 | 0.00000 | 0.67569 | 0.00001 |
| 4 | 0.68628 | 0.00000 | 0.63385 | -0.00000 |
| 5 | 0.62347 | 0.00000 | 0.57646 | 0.00000 |
| 6 | 0.54525 | -0.00000 | 0.50475 | -0.00000 |
| 7 | 0.45352 | 0.00000 | 0.42034 | -0.00000 |
| 8 | 0.35047 | -0.00000 | 0.32519 | 0.00000 |
| 9 | 0.23866 | -0.00000 | 0.22163 | 0.00000 |
| 10 | 0.12085 | -0.00000 | 0.11229 | -0.00000 |
| 11 | 0. | | 0. | |

| | $L \ll L_d$ | | 44.1° Limb-dip | |
|---|---|---|---|---|
| $i$ | $\theta_i$ | $A_i$ | $\dot{\theta}_i$ | $\dot{A}_i$ |
| 1 | 0.58036 | 0.58067 | 0.55313 | 0.55404 |
| 2 | 0.57324 | -0.00031 | 0.54641 | -0.00091 |
| 3 | 0.55207 | 0.00000 | 0.52639 | 0.00000 |
| 4 | 0.51733 | 0.00000 | 0.49351 | 0.00000 |
| 5 | 0.46987 | 0.00000 | 0.44850 | -0.00000 |
| 6 | 0.41082 | 0.00000 | 0.39240 | -0.00000 |
| 7 | 0.34161 | 0.00000 | 0.32652 | -0.00000 |
| 8 | 0.26393 | -0.00000 | 0.25242 | -0.00000 |
| 9 | 0.17969 | -0.00000 | 0.17194 | 0.00000 |
| 10 | 0.09098 | -0.00000 | 0.08708 | 0.00000 |
| 11 | 0. | | 0. | |

| | $L \ll L_d$ | | 55.3° Limb-dip | |
|---|---|---|---|---|
| $i$ | $\theta_i$ | $A_i$ | $\dot{\theta}_i$ | $\dot{A}_i$ |
| 1 | 0.96501 | 0.96649 | 0.85110 | 0.85509 |
| 2 | 0.95327 | -0.00149 | 0.84100 | -0.00402 |
| 3 | 0.91831 | 0.00001 | 0.81088 | 0.00002 |
| 4 | 0.86091 | -0.00000 | 0.76125 | -0.00000 |
| 5 | 0.78236 | 0.00000 | 0.69300 | 0.00000 |
| 6 | 0.68446 | 0.00000 | 0.60747 | 0.00000 |
| 7 | 0.56950 | 0.00000 | 0.50643 | 0.00000 |
| 8 | 0.44025 | -0.00000 | 0.39219 | -0.00000 |
| 9 | 0.29987 | -0.00000 | 0.26751 | 0.00000 |
| 10 | 0.15187 | -0.00000 | 0.13561 | -0.00000 |
| 11 | 0. | | 0. | |

| | $L \ll L_d$ | | 65.7° Limb-dip | |
|---|---|---|---|---|
| $i$ | $\theta_i$ | $A_i$ | $\dot{\theta}_i$ | $\dot{A}_i$ |
| 1 | 1.14661 | 1.14914 | 0.96063 | 0.96715 |
| 2 | 1.13274 | -0.00253 | 0.94942 | -0.00658 |
| 3 | 1.09140 | 0.00001 | 0.91595 | 0.00005 |
| 4 | 1.02348 | -0.00000 | 0.86067 | -0.00000 |
| 5 | 0.93044 | -0.00000 | 0.78442 | -0.00000 |
| 6 | 0.81434 | -0.00000 | 0.68850 | 0.00000 |
| 7 | 0.67786 | -0.00000 | 0.57474 | 0.00000 |
| 8 | 0.52421 | -0.00000 | 0.44562 | -0.00000 |
| 9 | 0.35717 | 0.00000 | 0.30424 | -0.00000 |
| 10 | 0.18092 | 0.00000 | 0.15432 | -0.00000 |
| 11 | 0. | | 0. | |

| | $L \ll L_d$ | | 71.4° Limb-dip | |
|---|---|---|---|---|
| $i$ | $\theta_i$ | $A_i$ | $\dot{\theta}_i$ | $\dot{A}_i$ |
| 1 | 1.24532 | 1.24858 | 1.01028 | 1.01851 |
| 2 | 1.23030 | -0.00328 | 0.99863 | -0.00831 |
| 3 | 1.18555 | 0.00002 | 0.96378 | 0.00008 |
| 4 | 1.11197 | 0.00000 | 0.90615 | -0.00000 |
| 5 | 1.01112 | -0.00000 | 0.82648 | -0.00000 |
| 6 | 0.88519 | -0.00000 | 0.72601 | -0.00000 |
| 7 | 0.73702 | 0.00000 | 0.60657 | -0.00000 |
| 8 | 0.57010 | 0.00000 | 0.47066 | -0.00000 |
| 9 | 0.38851 | -0.00000 | 0.32154 | -0.00000 |
| 10 | 0.19682 | -0.00000 | 0.16316 | -0.00000 |
| 11 | 0. | | 0. | |

| | $L \ll L_d$ | | 80.3° Limb-dip | |
|---|---|---|---|---|
| $i$ | $\theta_i$ | $A_i$ | $\dot{\theta}_i$ | $\dot{A}_i$ |
| 1 | 1.40197 | 1.40671 | 1.07371 | 1.08512 |
| 2 | 1.38516 | -0.00477 | 1.06157 | -0.01154 |
| 3 | 1.33506 | 0.00004 | 1.02522 | 0.00014 |
| 4 | 1.25261 | -0.00000 | 0.96494 | -0.00000 |
| 5 | 1.13949 | -0.00000 | 0.88130 | -0.00000 |
| 6 | 0.99804 | -0.00000 | 0.77536 | -0.00000 |
| 7 | 0.83137 | 0.00000 | 0.64879 | -0.00000 |
| 8 | 0.64336 | 0.00000 | 0.50414 | -0.00000 |
| 9 | 0.43859 | 0.00000 | 0.34480 | -0.00000 |
| 10 | 0.22225 | 0.00000 | 0.17509 | -0.00000 |
| 11 | 0. | | 0. | |

| | $L \ll L_d$ | | 89.8° Limb-dip | |
|---|---|---|---|---|
| $i$ | $\theta_i$ | $A_i$ | $\theta_i$ | $A_i$ |
| 1 | 1.56680 | 1.57354 | 1.11901 | 1.13439 |
| 2 | 1.54815 | -0.00680 | 1.10668 | -0.01562 |
| 3 | 1.49253 | 0.00006 | 1.06969 | 0.00025 |
| 4 | 1.40092 | -0.00000 | 1.00813 | -0.00000 |
| 5 | 1.27506 | 0.00000 | 0.92232 | 0.00000 |
| 6 | 1.11743 | -0.00000 | 0.81300 | 0.00000 |
| 7 | 0.93137 | -0.00000 | 0.68163 | 0.00000 |
| 8 | 0.72114 | -0.00000 | 0.53060 | 0.00000 |
| 9 | 0.49182 | 0.00000 | 0.36343 | -0.00000 |
| 10 | 0.24929 | 0.00000 | 0.18472 | -0.00000 |
| 11 | 0. | | 0. | |

| | $L = L_d$ | | 10° Limb-dip | |
|---|---|---|---|---|
| $i$ | $\theta_i$ | $A_i$ | $\dot{\theta}_i$ | $\dot{A}_i$ |
| 1 | 0.17453 | 0.17531 | 11.34703 | 11.36426 |
| 2 | 0.17246 | -0.00078 | 11.20865 | -0.01727 |
| 3 | 0.16627 | 0.00001 | 10.79784 | -0.00025 |
| 4 | 0.15607 | -0.00000 | 10.12310 | -0.00000 |
| 5 | 0.14206 | 0.00000 | 9.19951 | 0.00011 |
| 6 | 0.12451 | -0.00000 | 8.04819 | -0.00000 |
| 7 | 0.10379 | -0.00000 | 6.69615 | 0.00006 |
| 8 | 0.08037 | -0.00000 | 5.17602 | 0.00005 |
| 9 | 0.05481 | -0.00000 | 3.52549 | 0.00004 |
| 10 | 0.02778 | -0.00000 | 1.78556 | 0.00005 |
| 11 | 0. | | 0. | |

| | $L = L_d$ | | 23° Limb-dip | |
|---|---|---|---|---|
| $i$ | $\theta_i$ | $A_i$ | $\dot{\theta}_i$ | $\dot{A}_i$ |
| 1 | 0.40143 | 0.40255 | 4.85754 | 4.86667 |
| 2 | 0.39658 | -0.00113 | 4.79836 | -0.00945 |
| 3 | 0.38218 | 0.00000 | 4.62283 | 0.00009 |
| 4 | 0.35849 | -0.00000 | 4.33467 | 0.00006 |
| 5 | 0.32601 | 0.00000 | 3.94006 | 0.00003 |
| 6 | 0.28544 | -0.00000 | 3.44793 | 0.00004 |
| 7 | 0.23768 | 0.00000 | 2.86958 | 0.00002 |
| 8 | 0.18386 | 0.00000 | 2.21883 | 0.00003 |
| 9 | 0.12531 | 0.00000 | 1.51160 | 0.00002 |
| 10 | 0.06349 | 0.00000 | 0.76560 | 0.00001 |
| 11 | 0. | | 0. | |

| | $L = L_d$ | | 36° Limb-dip | |
|---|---|---|---|---|
| $i$ | $\theta_i$ | $A_i$ | $\dot{\theta}_i$ | $\dot{A}_i$ |
| 1 | 0.62832 | 0.62987 | 2.99841 | 3.01443 |
| 2 | 0.62071 | -0.00157 | 2.96298 | -0.01617 |
| 3 | 0.59811 | 0.00001 | 2.85737 | 0.00008 |
| 4 | 0.56096 | 0.00000 | 2.68320 | 0.00008 |
| 5 | 0.51005 | 0.00000 | 2.44362 | -0.00001 |
| 6 | 0.44649 | 0.00000 | 2.14296 | 0.00001 |
| 7 | 0.37172 | 0.00000 | 1.78727 | -0.00004 |
| 8 | 0.28750 | 0.00000 | 1.38456 | 0.00002 |
| 9 | 0.19591 | 0.00000 | 0.94467 | -0.00001 |
| 10 | 0.09925 | 0.00000 | 0.47881 | 0.00002 |
| 11 | 0. | | 0. | |

| | $L = L_d$ | | 46° Limb-dip | |
|---|---|---|---|---|
| $i$ | $\theta_i$ | $A_i$ | $\dot{\theta}_i$ | $\dot{A}_i$ |
| 1 | 0.80285 | 0.80533 | 2.24816 | 2.27496 |
| 2 | 0.79318 | -0.00251 | 2.22308 | -0.02683 |
| 3 | 0.76443 | 0.00001 | 2.14774 | -0.00001 |
| 4 | 0.71715 | 0.00001 | 2.02283 | 0.00004 |
| 5 | 0.65229 | 0.00000 | 1.84879 | -0.00001 |
| 6 | 0.57123 | 0.00000 | 1.62761 | 0.00007 |
| 7 | 0.47575 | 0.00000 | 1.36271 | -0.00002 |
| 8 | 0.36810 | 0.00000 | 1.05935 | 0.00002 |
| 9 | 0.25090 | 0.00000 | 0.72474 | -0.00003 |
| 10 | 0.12712 | 0.00000 | 0.36790 | -0.00002 |
| 11 | 0. | | 0. | |

| | $L = L_d$ | | 56° Limb-dip | |
|---|---|---|---|---|
| $i$ | $\theta_i$ | $A_i$ | $\dot{\theta}_i$ | $\dot{A}_i$ |
| 1 | 0.97738 | 0.98194 | 1.73600 | 1.77759 |
| 2 | 0.96577 | -0.00459 | 1.71864 | -0.04231 |
| 3 | 0.93117 | 0.00001 | 1.66571 | 0.00077 |
| 4 | 0.87419 | 0.00001 | 1.57656 | 0.00005 |
| 5 | 0.79582 | 0.00000 | 1.45043 | 0.00000 |
| 6 | 0.69759 | 0.00001 | 1.28631 | -0.00002 |
| 7 | 0.58155 | -0.00000 | 1.08518 | -0.00002 |
| 8 | 0.45034 | 0.00001 | 0.84929 | -0.00003 |
| 9 | 0.30717 | -0.00000 | 0.58429 | -0.00005 |
| 10 | 0.15568 | 0.00000 | 0.29778 | 0.00002 |
| 11 | 0. | | 0. | |

| | $L = L_d$ | | 66° Limb-dip | |
|---|---|---|---|---|
| $i$ | $\theta_i$ | $A_i$ | $\dot{\theta}_i$ | $\dot{A}_i$ |
| 1 | 1.15192 | 1.16066 | 1.34618 | 1.40856 |
| 2 | 1.13856 | -0.00885 | 1.33612 | -0.06265 |
| 3 | 1.09864 | 0.00009 | 1.30290 | 0.00090 |
| 4 | 1.03269 | 0.00002 | 1.24494 | -0.00023 |
| 5 | 0.94164 | 0.00000 | 1.15802 | -0.00015 |
| 6 | 0.82691 | 0.00001 | 1.03937 | 0.00006 |
| 7 | 0.69065 | -0.00000 | 0.88731 | -0.00005 |
| 8 | 0.53572 | 0.00000 | 0.70216 | -0.00006 |
| 9 | 0.36591 | -0.00001 | 0.48702 | -0.00007 |
| 10 | 0.18562 | 0.00000 | 0.24941 | -0.00011 |
| 11 | 0. | | 0. | |

| | $L = L_d$ | | 70° Limb-dip | |
|---|---|---|---|---|
| $i$ | $\theta_i$ | $A_i$ | $\dot{\theta}_i$ | $\dot{A}_i$ |
| 1 | 1.22173 | 1.23415 | 1.21019 | 1.28122 |
| 2 | 1.20788 | -0.01262 | 1.20265 | -0.07217 |
| 3 | 1.16633 | 0.00024 | 1.17623 | 0.00180 |
| 4 | 1.09752 | -0.00003 | 1.12910 | -0.00007 |
| 5 | 1.00213 | 0.00001 | 1.05691 | -0.00016 |
| 6 | 0.88141 | 0.00000 | 0.95568 | -0.00003 |
| 7 | 0.73739 | -0.00000 | 0.82163 | -0.00013 |
| 8 | 0.57291 | -0.00000 | 0.65438 | -0.00006 |
| 9 | 0.39186 | -0.00001 | 0.45616 | -0.00006 |
| 10 | 0.19899 | -0.00000 | 0.23432 | -0.00013 |
| 11 | 0. | | 0. | |

| | $L = L_d$ | | 77° Limb-dip | |
|---|---|---|---|---|
| $i$ | $\theta_i$ | $A_i$ | $\dot{\theta}_i$ | $\dot{A}_i$ |
| 1 | 1.34390 | 1.36442 | 0.98111 | 1.07910 |
| 2 | 1.32936 | -0.02100 | 0.97989 | -0.09789 |
| 3 | 1.28533 | 0.00064 | 0.97024 | 0.00210 |
| 4 | 1.21206 | -0.00010 | 0.94536 | -0.00084 |
| 5 | 1.10973 | 0.00002 | 0.90093 | -0.00065 |
| 6 | 0.97914 | -0.00001 | 0.82989 | -0.00029 |
| 7 | 0.82185 | -0.00001 | 0.72705 | -0.00023 |
| 8 | 0.64059 | -0.00001 | 0.58823 | -0.00011 |
| 9 | 0.43935 | -0.00002 | 0.41533 | -0.00012 |
| 10 | 0.22354 | -0.00002 | 0.21494 | 0.00004 |
| 11 | 0. | | 0. | |

$L = L_d$ 81° Limb-dip

| $i$ | $\theta_i$ | $A_i$ | $\dot{\theta}_i$ | $\dot{A}_i$ |
|---|---|---|---|---|
| 1 | 1.41371 | 1.44706 | 0.86271 | 0.96229 |
| 2 | 1.39963 | -0.03349 | 0.86103 | -0.10378 |
| 3 | 1.35679 | 0.00048 | 0.85429 | 0.00450 |
| 4 | 1.28403 | -0.00022 | 0.83837 | -0.00033 |
| 5 | 1.18054 | -0.00012 | 0.80616 | 0.00002 |
| 6 | 1.04633 | -0.00000 | 0.75049 | 0.00006 |
| 7 | 0.88227 | 0.00000 | 0.66391 | -0.00007 |
| 8 | 0.69044 | -0.00000 | 0.54248 | 0.00009 |
| 9 | 0.47488 | -0.00000 | 0.38628 | -0.00003 |
| 10 | 0.24199 | 0.00000 | 0.20095 | -0.00004 |
| 11 | 0. | | 0. | |

$L = L_d$ 89° Limb-dip

| $i$ | $\theta_i$ | $A_i$ | $\dot{\theta}_i$ | $\dot{A}_i$ |
|---|---|---|---|---|
| 1 | 1.55334 | 1.62144 | 0.64462 | 0.77886 |
| 2 | 1.54159 | -0.06698 | 0.64817 | -0.14172 |
| 3 | 1.50390 | 0.00056 | 0.65750 | 0.00742 |
| 4 | 1.43520 | -0.00112 | 0.66655 | 0.00000 |
| 5 | 1.33181 | -0.00056 | 0.66639 | 0.00001 |
| 6 | 1.19231 | -0.00000 | 0.64582 | -0.00004 |
| 7 | 1.01603 | -0.00000 | 0.59252 | 0.00000 |
| 8 | 0.80299 | -0.00000 | 0.49886 | 0.00002 |
| 9 | 0.55654 | -0.00000 | 0.36270 | 0.00008 |
| 10 | 0.28490 | 0.00000 | 0.19150 | -0.00002 |
| 11 | 0. | | 0. | |

$L = 4.6L_d$ $10^\circ$ Limb-dip

| $i$ | $\theta_i$ | $A_i$ | $\dot{\theta}_i$ | $\dot{A}_i$ |
|---|---|---|---|---|
| 1 | 0.17453 | 0.17531 | 11.23295 | 11.36359 |
| 2 | 0.17246 | -0.00078 | 11.10509 | -0.13322 |
| 3 | 0.16627 | 0.00001 | 10.73461 | 0.00657 |
| 4 | 0.15607 | -0.00000 | 10.10671 | -0.00286 |
| 5 | 0.14206 | 0.00000 | 9.22753 | -0.00640 |
| 6 | 0.12451 | -0.00000 | 8.11149 | 0.00203 |
| 7 | 0.10379 | -0.00000 | 6.81130 | 0.00313 |
| 8 | 0.08037 | -0.00000 | 5.30033 | -0.00102 |
| 9 | 0.05481 | -0.00000 | 3.62493 | -0.00114 |
| 10 | 0.02778 | -0.00000 | 1.83964 | 0.00228 |
| 11 | 0. | | 0. | |

$L = 4.6L_d$ $23^\circ$ Limb-dip

| $i$ | $\theta_i$ | $A_i$ | $\dot{\theta}_i$ | $\dot{A}_i$ |
|---|---|---|---|---|
| 1 | 0.40143 | 0.40476 | 4.71625 | 4.83642 |
| 2 | 0.39678 | -0.00347 | 4.66168 | -0.13220 |
| 3 | 0.38291 | 0.00014 | 4.52088 | 0.00495 |
| 4 | 0.36000 | -0.00000 | 4.28043 | 0.00356 |
| 5 | 0.32839 | 0.00000 | 3.94985 | -0.00040 |
| 6 | 0.28856 | -0.00000 | 3.51120 | 0.00221 |
| 7 | 0.24121 | -0.00000 | 2.96996 | -0.00126 |
| 8 | 0.18728 | -0.00000 | 2.33230 | 0.00066 |
| 9 | 0.12803 | -0.00000 | 1.60577 | 0.00067 |
| 10 | 0.06499 | -0.00000 | 0.81281 | 0.00164 |
| 11 | 0. | | 0. | |

| | $L = 4.6L_d$ | | 33° Limb-dip | |
|---|---|---|---|---|
| $i$ | $\theta_i$ | $A_i$ | $\dot{\theta}_i$ | $\dot{A}_i$ |
| 1 | 0.57596 | 0.58387 | 3.09105 | 3.26967 |
| 2 | 0.56952 | -0.00837 | 3.06296 | -0.19478 |
| 3 | 0.55030 | 0.00032 | 2.98944 | 0.00783 |
| 4 | 0.51857 | 0.00013 | 2.87622 | 0.00639 |
| 5 | 0.47459 | 0.00000 | 2.69354 | -0.00237 |
| 6 | 0.41864 | -0.00000 | 2.44557 | 0.00283 |
| 7 | 0.35128 | -0.00000 | 2.11440 | 0.00082 |
| 8 | 0.27359 | 0.00000 | 1.68551 | 0.00214 |
| 9 | 0.18741 | 0.00000 | 1.17292 | -0.00102 |
| 10 | 0.09525 | 0.00000 | 0.59344 | -0.00045 |
| 11 | 0. | | 0. | |

| | $L = 4.6L_d$ | | 43° Limb-dip | |
|---|---|---|---|---|
| $i$ | $\theta_i$ | $A_i$ | $\dot{\theta}_i$ | $\dot{A}_i$ |
| 1 | 0.75049 | 0.77646 | 2.02114 | 2.34757 |
| 2 | 0.74307 | -0.02829 | 2.01240 | -0.36168 |
| 3 | 0.72120 | 0.00127 | 2.01625 | 0.02348 |
| 4 | 0.68546 | 0.00106 | 2.01442 | 0.00775 |
| 5 | 0.63532 | -0.00000 | 1.98641 | -0.00438 |
| 6 | 0.56890 | 0.00000 | 1.89703 | 0.00565 |
| 7 | 0.48430 | -0.00000 | 1.73239 | -0.00065 |
| 8 | 0.38151 | -0.00000 | 1.44603 | 0.00222 |
| 9 | 0.26324 | -0.00000 | 1.04010 | -0.00119 |
| 10 | 0.13426 | 0.00000 | 0.52817 | 0.00237 |
| 11 | 0. | | 0. | |

| | $L = 4.6L_d$ | | $53^\circ$ Limb-dip | |
|---|---|---|---|---|
| $i$ | $\theta_i$ | $A_i$ | $\dot{\theta}_i$ | $\dot{A}_i$ |
| 1 | 0.92502 | 1.00565 | 1.17317 | 1.63294 |
| 2 | 0.91922 | -0.08993 | 1.19319 | -0.55105 |
| 3 | 0.90242 | 0.00733 | 1.23700 | 0.10353 |
| 4 | 0.87485 | 0.00197 | 1.30343 | -0.00322 |
| 5 | 0.83344 | -0.00000 | 1.38602 | -0.01123 |
| 6 | 0.77090 | -0.00000 | 1.45921 | 0.00708 |
| 7 | 0.67851 | 0.00000 | 1.48027 | -0.00494 |
| 8 | 0.55087 | -0.00000 | 1.37254 | 0.00160 |
| 9 | 0.38926 | -0.00000 | 1.06228 | -0.00169 |
| 10 | 0.20158 | 0.00000 | 0.55728 | 0.00014 |
| 11 | 0. | | 0. | |

$L = 4.6L_d$ — 63° Limb-dip (first approximation)

| $i$ | $\theta_i$ | $A_i$ | $\dot{\theta}_i$ | $\dot{A}_i$ |
|---|---|---|---|---|
| 1 | 1.09956 | 1.23760 | 0.74554 | 1.11786 |
| 2 | 1.08825 | -0.19735 | 0.76903 | -0.48692 |
| 3 | 1.06055 | 0.05850 | 0.81135 | 0.18295 |
| 4 | 1.02967 | 0.00081 | 0.86311 | -0.07226 |
| 5 | 1.00347 | -0.00000 | 0.89949 | 0.00161 |
| 6 | 0.97387 | 0.00000 | 0.95571 | 0.00793 |
| 7 | 0.91590 | 0.00000 | 1.04294 | -0.00640 |
| 8 | 0.79826 | -0.00000 | 1.10609 | 0.00509 |
| 9 | 0.59994 | -0.00000 | 0.99683 | -0.00374 |
| 10 | 0.32384 | 0.00000 | 0.57253 | -0.00059 |
| 11 | 0. | | 0. | |

$L = 4.6L_d$ — 63° Limb-dip (second approximation)

| $i$ | $\theta_i$ | $A_i$ | $\dot{\theta}_i$ | $\dot{A}_i$ |
|---|---|---|---|---|
| 1 | 1.09956 | 1.25366 | 0.76680 | 1.10333 |
| 2 | 1.09816 | -0.18052 | 0.76749 | -0.50404 |
| 3 | 1.09107 | 0.03471 | 0.76951 | 0.20452 |
| 4 | 1.07243 | -0.00829 | 0.80154 | -0.04369 |
| 5 | 1.03787 | -0.00000 | 0.86475 | 0.00464 |
| 6 | 0.98371 | 0.00000 | 0.96594 | 0.00630 |
| 7 | 0.90068 | -0.00000 | 1.07255 | -0.00383 |
| 8 | 0.77070 | -0.00000 | 1.14216 | -0.00016 |
| 9 | 0.57487 | -0.00000 | 0.99225 | 0.00231 |
| 10 | 0.31001 | 0.00000 | 0.58148 | -0.00257 |
| 11 | 0. | | 0. | |

$L = 4.6L_d$ $69^\circ$ Limb-dip

| $i$ | $\theta_i$ | $A_i$ | $\dot{\theta}_i$ | $\dot{A}_i$ |
|---|---|---|---|---|
| 1 | 1.20428 | 1.38959 | 0.66772 | 0.89528 |
| 2 | 1.19897 | -0.23914 | 0.67803 | -0.34966 |
| 3 | 1.18484 | 0.06226 | 0.68816 | 0.20499 |
| 4 | 1.16581 | -0.01152 | 0.68287 | -0.09721 |
| 5 | 1.14189 | 0.00402 | 0.67097 | 0.01846 |
| 6 | 1.10303 | -0.00094 | 0.68301 | -0.00006 |
| 7 | 1.03145 | 0.00000 | 0.75871 | -0.00784 |
| 8 | 0.90486 | 0.00000 | 0.84912 | 0.00936 |
| 9 | 0.69541 | -0.00000 | 0.87297 | -0.00907 |
| 10 | 0.38514 | 0.00000 | 0.53038 | 0.00347 |
| 11 | 0. | | 0. | |

$L = 4.6L_d$ $79^\circ$ Limb-dip

| $i$ | $\theta_i$ | $A_i$ | $\dot{\theta}_i$ | $\dot{A}_i$ |
|---|---|---|---|---|
| 1 | 1.37882 | 1.61642 | 0.69287 | 0.65923 |
| 2 | 1.37843 | -0.30504 | 0.66172 | -0.05645 |
| 3 | 1.37601 | 0.10564 | 0.56618 | 0.05924 |
| 4 | 1.36212 | -0.05048 | 0.49277 | 0.01445 |
| 5 | 1.32187 | 0.01227 | 0.50205 | 0.04315 |
| 6 | 1.25696 | -0.00000 | 0.52141 | -0.02615 |
| 7 | 1.18499 | -0.00000 | 0.44184 | 0.00480 |
| 8 | 1.09099 | 0.00000 | 0.34934 | -0.00747 |
| 9 | 0.89656 | -0.00000 | 0.28502 | 0.00576 |
| 10 | 0.52315 | 0.00000 | 0.23897 | -0.00369 |
| 11 | 0. | | 0. | |

| | $L = 4.6L_d$ | | 89° Limb-dip | |
|---|---|---|---|---|
| $i$ | $\theta_i$ | $A_i$ | $\dot{\theta}_i$ | $\dot{A}_i$ |
| 1 | 1.55335 | 1.76665 | 0.24310 | 0.53787 |
| 2 | 1.54169 | -0.30696 | 0.34773 | 0.02550 |
| 3 | 1.50395 | 0.10793 | 0.62937 | -0.17751 |
| 4 | 1.45873 | -0.02584 | 0.79428 | -0.11530 |
| 5 | 1.43351 | 0.02400 | 0.59681 | -0.08482 |
| 6 | 1.39744 | -0.01244 | 0.31340 | 0.04053 |
| 7 | 1.29897 | -0.00000 | 0.21478 | 0.01374 |
| 8 | 1.14503 | 0.00000 | 0.19149 | -0.00006 |
| 9 | 0.92667 | -0.00000 | 0.03133 | 0.00547 |
| 10 | 0.55106 | 0.00000 | -0.05889 | -0.00232 |
| 11 | 0. | | 0. | |

REFERENCES

Anderson, E. M., 1951, The dynamics of faulting and dyke formation with applications to Britain: Edinburgh, Oliver and Boyd, Ltd., 2d ed. rev.

Billings, M. P., 1954, Structural geology: New York, Prentice-Hall, Inc., 2d ed.

Biot, M. A., 1961, Theory of folding of stratified viscoelastic media and its implications in tectonics and orogenesis: Geol. Soc. America Bull., v. 72, p. 1595-1620

Currie, J. B., Patnode, H. W., and Trump, R. P., 1962, Development of folds in sedimentary strata: Geol. Soc. America Bull., v. 73

de Sitter, L. U., 1956, Structural Geology: London, McGraw-Hill Book Co., Inc.

Dwight, H. B., 1947, Tables of integrals and other mathematical data: New York, The Macmillan Co., 2nd ed. rev.

Engeli, M., Ginsburg, T., Rutishauser, H., and Stiefel, E., 1959, Refined iterative methods for computation of the solution and the eigenvalues of self-adjoint boundary-value problems: Basle, Birkhäuser

Forsythe, G. E., and Wasow, W. R., 1960, Finite-difference methods for partial differential equations: New York, John Wiley and Sons, Inc.

Gibbs, J. W., 1961, The scientific papers of J. Willard Gibbs, v. I: New York, Dover Publications, Inc.

Goguel, J., 1948, Introduction à l 'étude mécanique des déformations de l 'écorce terrestre: Service Carte Géol. France Mém.

_____1952, Traité de Tectonique: Paris, Masson et Cie, Éditeurs

Griggs, D. T., 1940, Experimental flow of rocks under conditions favoring recrystallization: Geol. Soc. America Bull., v. 51, p. 1001-1022

Griggs, D. T., Turner, F. J., and Heard, H. C., 1960, Deformation of rocks at 500° to 800° C., chap. 4 in Rock deformation (A symposium): Geol. Soc. America Mem. 79, p. 39-104

Hafner, W., 1951, Stress distributions and faulting: Geol. Soc. America Bull., v. 62, p. 373-398

Hamming, R. W., 1962, Numerical methods for scientists and engineers: New York, McGraw-Hill Book Co., Inc.

Heard, H. C., 1963, Effect of large changes in strain rate in the experimental deformation of Yule marble: Jour. Geology, v. 71, no. 2, p. 162-195

Hills, E. S., 1953, Outlines of Structural Geology: London, Methuen and Co., Ltd., 3d ed. rev.

Hubbert, M. K., 1951, Mechanical basis for certain familiar geologic structures: Geol. Soc. America Bull., v. 62, p. 355-372

Jaeger, J. C., 1956, Elasticity, fracture and flow: London, Methuen and Co., Ltd.

Kienow, S., 1942, Grundzüge einer Theorie der Faltungs- und Schieferungsvorgänge: Berlin, Bornträger, Fortschritte der Geologie und Paleontologie, bd. XIV, h. 46, p. 1-129

Lanczos, C., 1956, Applied analysis: Englewood Cliffs, N.J., Prentice-Hall, Inc.

Modern Computing Methods, 1961: New York, Philosophical Library, Inc., 2d ed.

Nye, J. F., 1951, The flow of glaciers and ice-sheets as a problem in plasticity: Proc. Roy. Soc., series A, v. 207, p. 554-572

_____ 1952, The mechanics of glacier flow: Jour. Glaciology, v. 2, no. 12, p. 82-93

_____ 1957, The distribution of stress and velocity in glaciers and ice sheets: Proc. Roy. Soc., series A, v. 239, p. 113-133

Ode, H., 1957, Mechanical analysis of the dike pattern of the Spanish Peaks area, Colorado: Geol. Soc. America Bull., v. 68, p. 567-576

_____1960, Faulting as a velocity discontinuity in plastic deformation: chap. 11 in Rock deformation (A symposium), Geol. Soc. America Mem. 79, p. 293-321

Prescott, J., 1961, Applied elasticity: New York, Dover Publications, Inc.

Ramberg, H., 1960, Relationships between length of arc and thickness of ptygmatically folded veins: Am. Jour. Sci., v. 258, p. 36-46

_____1963, Fluid dynamics of viscous buckling applicable to folding of layered rocks: Bull. Amer. Assoc. Petr. Geol., v. 47, no. 3, p. 484-505

_____1963, Strain distribution and geometry of folds: Bull. Geol. Inst. Uppsala, v. XLII, p. 1-20

Ramsay, J. G., 1962, The geometry and mechanics of formation of "similar" type folds: Jour. Geology, v. 70, no. 3, p. 309-327

Rayleigh, J.W.S., 1945, The theory of sound, v. II: New York, Dover Publications, Inc.

Sanford, A. R., 1959, Analytical and experimental study of simple geologic structures: Geol. Soc. America Bull., v. 70, p. 19-52

Shaw, F. S., 1953, An introduction to relaxation methods: New York, Dover Publications, Inc.

Sokolnikoff, I. S., 1956, Mathematical theory of elasticity: New York, McGraw-Hill Book Co., Inc.

Timoshenko, S., 1955, Strength of materials, Pt. I, Elementary theory and problems: Toronto, D. Van Nostrand Co., Inc., 3d ed.

Turner, F. J., 1953, Nature and dynamic interpretation of deformation lamellae in calcite of three marbles: Am. Jour. Sci., v. 251, p. 276-298

Varnes, D. J., 1962, Analysis of plastic deformation according to von Mises' theory, with application to the South Silverton area, San Juan County, Colorado: U. S. Geol. Survey Professional Paper 378-B